Ref. Ares(2023)8520725 - 12/12/2023

HORIZON 2020

HORIZON 2020 RESEARCH AND INNOVATION FRAMEWORK PROGRAMME OF THE EUROPEAN ATOMIC ENERGY COMMUNITY

Nuclear Fission and Radiation Protection 2018 (NFRP-2018-4)

Project acronym:	**SANDA**
Project full title:	**Solving Challenges in Nuclear Data for the Safety of European Nuclear facilities**
Grant Agreement no.:	**H2020 Grant Agreement number: 847552**

Workpackage N°:	***WP5***
Identification N°:	***D5.8***
Type of document:	***Deliverable***
Title:	REPORT ON CRITICAL BENCHMARK C/E VALIDATION AND NUCLEAR DATA TRENDS
Dissemination Level:	
Reference:	
Status:	***VERSION 1***
Comments:	

	Name	Partner	Date	Signature
Prepared by:	N. Leclaire S. van der Marck	11, 19	27-02-2022	Nicolas LECLAIRE 2023.03.02 22:13:49 +01'00' S.C. van der Marck Digitally signed by S.C. van der Marck Date: 2023.03.05 21:25:32 +01'00'
WP leader:	R. Jacqmin	3		JACQMIN Robert 116318 Signature numérique de JACQMIN Robert 116318 Date : 2023.12.12 09:38:20 +01'00'
IP Co-ordinator:	E. González	1		Signed by GONZALEZ ROMERO ENRIQUE MIGUEL - DNI ***3708** at 12/12/2023 with a certificate emitted by AC Sector Público

SANDA Project D5.1: Report on critical benchmark C/E validation and nuclear data trends

N. Leclaire[1], S. van der Marck[2]

[1]*Institut de Radioprotection et de Sûreté Nucléaire (IRSN – PSN-RES), B17, 92262 Fontenay-aux-Roses Cedex (France).*

[2] *Nuclear Research and consultancy Group (NRG), P.O. Box 25, 1755 ZG Petten, Netherlands*

Contact: nicolas.leclaire@irsn.fr, Tel: +33 1 58 35 91 66.

Contact: vandermarck@nrg.eu, Tel: +31 6 22 45 53 48.

Contents

1. Introduction

The objective of this report is to give the main tendencies in terms of k_{eff} results for two sets of criticality benchmarks chosen by IRSN and NRG. These benchmarks are assumed to cover a wide range of cases representative of the use in criticality-safety in terms of fissile media and energy spectra. 182 benchmark cases were selected by IRSN, 576 by NRG and 120 are common to the two institutes. They were calculated with the MORET code by IRSN and with the MCNP code by NRG.

2. Description of codes used for the validation of nuclear data

2.1. IRSN MORET 5 code

MORET is a Monte Carlo transport code developed at IRSN, mainly for criticality safety calculations (only neutron tracks are simulated by MORET). It can be used either coupled with the deterministic APOLLO2 code (within the CRISTAL [Entringer 2022] criticality package) as an industrial calculation tool, or alone, in its continuous energy version, as a reference code like in this work. MORET 5 use nuclear data libraries in ACE format. For this work, the IRSN GAIA 1.1.2 [Haeck 2015] tool has been used to produce libraries. The 5.D.1 and 6.0 versions of the MORET code were used in this work [Jinaphanh 2016] [monange 2022].

Sensitivities profiles for k_{eff} were calculated with MORET 5 and 6. The theory behind this method, the iterated fission probability method, was documented by Kiedrowski [2009], while the implementation in MORET was documented [Jinaphanh2016].

2.2. NRG MCNP-6.2

Monte Carlo N-Particle (MCNP) is a general purpose Monte Carlo transport code developed at Los Alamos National Laboratory (LANL) in New Mexico, USA. Version 6 of the code was released in 2012 [Goorley 2012], and the most recent subversion, which was used for the calculations reported here, is version 6.2 [Werner 2018]. Since version 6 is a merger of the MCNPX code with MCNP-5, it can track many particle types over broad ranges of energies. For the present report, however, only neutron tracks were simulated, and only based on neutron data files (i.e. not based on models such as CGM). The neutron data files were created by processing the ENDF formatted files using NJOY version 2016 (see Section 3.2).

Sensitivity profiles for k_{eff} were calculated using MCNP-6.2 as well. The theory behind this method, the iterated fission probability method, was documented by Kiedrowski [2009], while the implementation in MCNP was documented somewhat later [Kiedrowski 2012].

3. Nuclear data used for the validation and processing tools

3.1. IRSN GAIA processing tool

The IRSN GAIA 1.1.2 [Haeck 2015] tool has been developed for processing ENDF files at the ACE format. This tool is largely based on NJOY code. GAIA generates automatically the NJOY input deck with a predefined sequence of modules and perform additional checking. In this work, we used the 2016.35 version of NJOY to generate the ENDF/B-VIII.0, JEFF-3.3, and JEFF-4t1 evaluations of nuclear data.

3.2. NRG NJOY2016

The ACE files used in the MCNP calculations reported here were all created by processing with NJOY [MacFarlane 2010]. The 2016 version used here was documented by Muir et al. [2018]. Subversion 2016.20 was used for libraries ENDF/B-VIII.0, JEFF-3.3 and JEFF-4t1. For JEFF-4t2, the newer subversion 2016.68 was used.

In this report also results obtained with JEF-2.2 data are given, because of the role of this library version still plays today. This older library JEF-2.2 was processed with an old version of NJOY, 'version 91' (because the newer versions of NJOY do not accept all ENDF formatted files of JEF-2.2). The JEF-2.2 results are listed for comparison purposes only.

4. Suites of selected experiments and methodology

The names of the experiments chosen for the intercomparison will follow the ICSBEP nomenclature. A first identifier is related to the type of fissile with its enrichment; a second identifier gives the physical form of the fissile; a third one gives the type of energy spectrum (FAST, EPITHERMAL or THERMAL), then the number of the experiment and the number of the case in the series of experiments.

For IRSN cases, the 3 first identifiers are collapsed in three letters. For instance, hmf1-1 standing for heu-met-fast-001-001 for a highly enriched metal sphere of uranium in fast energy spectrum (series 1 , case 1).

4.1. IRSN methodology

IRSN selected a set of about 200 benchmark cases that are assumed to be representative of most configurations and energy spectra useful for criticality safety. This selection of benchmarks has been used to test the versions of the JEFF-3.3, JEFF-4T1 and ENDF/B-VIII.0 evaluations of nuclear data. Fast benchmark cases with various reflectors were chosen to see the impact of the scattering cross sections of metals. Epithermal benchmark cases were also chosen to test uranium, plutonium and elements like iron in the resolved resonance and unresolved resonance ranges.
Finally, cases with suspected experimental biases and too large uncertainties were discarded from our selection of benchmark cases.

4.2. NRG methodology

NRG selected a number of benchmarks that each have several cases, so that a comparison can be made between cases within the same benchmark. This choice is rooted in the idea that each benchmark can have its own bias, but that this bias, or at least a large part of it, is shared by all the cases of that benchmark. The comparison of cases within the same benchmark is therefore a comparison that sidesteps the bias of the benchmark to a large extent. The benchmarks selected allow for such comparisons between cases with variation of, ideally, only one parameter, such as: lattice pitch, absorber concentration, reflector thickness, etc. Also, an attempt was made to identify benchmarks with a limited number of materials, so that it is easier to find out which nuclear data cause an effect in the calculations. Overall the objective was to test as much as possible the variation in spectrum conditions and fuel compositions that may be of interest to the nuclear community.

4.3. Experiments selected by IRSN and NRG

The list of experiments selected by IRSN and NRG is reported in Table 1. A short description of each series of experiments is given along with the benchmark $k_{eff,}$ its associated uncertainty and the Energy Average Lethargy of neutrons causing Fission (EALF). When the experiment is selected by one of the two companies, the box corresponding with the company is filled in green otherwise it is filled in red. Each experiment is identified through its collapsed ICSBEP identifier. All in all, there are 182 IRSN cases, 576 NRG cases and 120 cases in common.

Table 1. ***List of experiments selected by IRSN and NRG***

Selected case ICSBEP #	Description	Benchmark k_{eff}	Uncertainty	EALF (eV)	IRSN	NRG
hmf43-1	HEU cylinders axially reflected by steel	0.9995	0.0018	886000		
hmf44-1	HEU cylinders axially reflected by aluminum	0.9995	0.0019	885000		
hmf44-2		0.9995	0.0017	880000		
hmf44-3		0.9995	0.0019	869000		
hmf44-4		0.9995	0.0014	861000		
hmf44-5		0.9995	0.0015	859000		
hmf90-1	Two heterogeneous cylinders of highly enriched uranium, polyethylene, and aluminum with polyethylene reflector	0.9994	0.0007	8470		
hmf90-2		0.9993	0.0007	1420		
imf14-1	leu-met-fast-014 ZPR-9 assemblies 2 and 3: cylindrical assemblies of u metal and tungsten with aluminum reflectors	0.9958	0.0022	309000		
imf14-2		0.9927	0.0022	264000		
hci4-1	K-infinity experiments in intermediate neutron spectra for ^{235}U	1	0.004	143		
hcm1-1	Arrays of cans of highly enriched uranium dioxide reflected by polyethylene	1	0.0059	0.439		
hcm1-10		0.9979	0.0052	425		
hcm1-11		0.9983	0.0052	324		
hcm1-12		0.9972	0.0052	320		
hcm1-13		1.0032	0.0053	284		
hcm1-15		1.0083	0.005	35.1		
hcm1-16		1.0001	0.0046	35.6		
hcm1-17		0.9997	0.0046	31.2		
hcm1-18		1.0075	0.0046	28.8		
hcm1-19		1.0039	0.0047	71.9		
hcm1-2		1.0012	0.0059	0.438		
hcm1-20		1.006	0.0068	643		
hcm1-21		1.0026	0.0064	629		
hcm1-22		1.0013	0.0064	624		
hcm1-23		0.9995	0.0053	548		
hcm1-24		1.002	0.0053	534		
hcm1-29		0.9992	0.0052	548		
hcm1-5		0.9985	0.0056	1820		
hcm1-6		0.9953	0.0056	2140		
hcm1-7		0.9997	0.0038	2070		
hcm1-8		0.9984	0.0052	676		
hcm1-9		0.9983	0.0052	429		
hct21-1	Water reflected and moderated uniform lattice cores of aluminum clad uranium oxide and	1.0008	0.0029	0.242		
hct21-10		1.0018	0.0029	0.252		
hct21-100		1.0015	0.0016	0.0677		

Selected case ICSBEP #	Description	Benchmark k_{eff}	Uncertainty	EALF (eV)	IRSN	NRG
hct21-11	thorium oxide with and without boron poison	1.0008	0.0029	0.249		
hct21-12		1.0008	0.0029	0.246		
hct21-13		1.0008	0.0029	0.243		
hct21-14		1.0041	0.0025	0.226		
hct21-15		1.0046	0.0025	0.226		
hct21-16		1.0036	0.0025	0.223		
hct21-17		1.0024	0.0025	0.214		
hct21-18		1.0021	0.0025	0.208		
hct21-19		1.0015	0.0025	0.205		
hct21-2		1.0004	0.0024	0.189		
hct21-20		1.0016	0.0025	0.201		
hct21-21		1.0004	0.0025	0.199		
hct21-22		1.0014	0.0025	0.196		
hct21-23		1.0036	0.0024	0.252		
hct21-24		1.004	0.0024	0.252		
hct21-25		1.0025	0.0024	0.241		
hct21-26		1.0025	0.0024	0.235		
hct21-27		1.0019	0.0024	0.23		
hct21-28		1.0011	0.0024	0.225		
hct21-29		1.0018	0.0024	0.222		
hct21-3		1.0008	0.0018	0.101		
hct21-30		1.0011	0.0024	0.218		
hct21-31		1.0015	0.0024	0.216		
hct21-32		1.0026	0.0025	0.276		
hct21-33		1.0038	0.0025	0.272		
hct21-34		1.0035	0.0025	0.269		
hct21-35		1.0029	0.0025	0.266		
hct21-36		1.0037	0.0025	0.263		
hct21-37		1.0024	0.0025	0.259		
hct21-38		1.0028	0.0025	0.251		
hct21-39		1.0015	0.0025	0.248		
hct21-4		1.0023	0.0016	0.0677		
hct21-40		1.0018	0.0025	0.242		
hct21-41		1.0013	0.0025	0.238		
hct21-42		1.0001	0.0025	0.235		
hct21-43		1.0008	0.0025	0.234		
hct21-44		1.0035	0.003	0.291		
hct21-45		1.0033	0.003	0.289		
hct21-46		1.0026	0.003	0.286		
hct21-47		1.0026	0.003	0.276		
hct21-48		1.0021	0.003	0.268		
hct21-49		1.0016	0.003	0.263		
hct21-5		1.0015	0.0014	0.0535		

Selected case ICSBEP #	Description	Benchmark k_{eff}	Uncertainty	EALF (eV)	IRSN	NRG
hct21-50		1.0015	0.003	0.256		
hct21-51		1.0018	0.003	0.252		
hct21-52		1.0008	0.003	0.249		
hct21-53		1.0008	0.003	0.247		
hct21-54		1.0046	0.0018	0.111		
hct21-55		1.0049	0.0018	0.11		
hct21-56		1.004	0.0018	0.108		
hct21-57		1.0031	0.0018	0.107		
hct21-58		1.0028	0.0018	0.106		
hct21-59		1.0014	0.0018	0.104		
hct21-6		1.0038	0.0029	0.295		
hct21-60		1.0008	0.0018	0.103		
hct21-61		1.0008	0.0018	0.102		
hct21-62		1.0012	0.0018	0.102		
hct21-63		1.0039	0.002	0.12		
hct21-64		1.0048	0.002	0.12		
hct21-65		1.0033	0.002	0.118		
hct21-66		1.0035	0.002	0.117		
hct21-67		1.0026	0.002	0.115		
hct21-68		1.0021	0.002	0.113		
hct21-69		1.0008	0.002	0.111		
hct21-7		1.0033	0.0029	0.273		
hct21-70		1.0008	0.002	0.111		
hct21-71		1.0008	0.002	0.11		
hct21-72		1.0051	0.0018	0.131		
hct21-73		1.0049	0.0018	0.13		
hct21-74		1.0048	0.0018	0.129		
hct21-75		1.0038	0.0018	0.126		
hct21-76		1.0026	0.0018	0.123		
hct21-77		1.0024	0.0018	0.12		
hct21-78		1.0015	0.0018	0.119		
hct21-79		1.0008	0.0018	0.118		
hct21-8		1.0022	0.0029	0.266		
hct21-80		1.0017	0.0018	0.117		
hct21-81		1.0012	0.0018	0.117		
hct21-82		1.0055	0.0028	0.142		
hct21-83		1.0049	0.0028	0.141		
hct21-84		1.0042	0.0028	0.14		
hct21-85		1.0037	0.0028	0.136		
hct21-86		1.0034	0.0028	0.134		
hct21-87		1.0027	0.0028	0.13		
hct21-88		1.0016	0.0028	0.127		
hct21-89		1.0012	0.0028	0.125		

Selected case ICSBEP #	Description	Benchmark k_{eff}	Uncertainty	EALF (eV)	IRSN	NRG
hct21-9		1.0021	0.0029	0.259		
hct21-90		1.0008	0.0028	0.123		
hct21-91		1.0016	0.0028	0.122		
hct21-92		1.0008	0.0028	0.122		
hct21-93		1.0008	0.0028	0.121		
hct21-94		1.0026	0.0016	0.0697		
hct21-95		1.0021	0.0016	0.0694		
hct21-96		1.0021	0.0016	0.069		
hct21-97		1.0019	0.0016	0.0685		
hct21-98		1.0015	0.0016	0.0681		
hct21-99		1.001	0.0016	0.068		
hmf84-1	HEU metal cylinders with magnesium, titanium, aluminum, graphite, mild steel, nickel, copper, cobalt, molybdenum, natural uranium, tungsten, beryllium, aluminum oxide, molybdenum carbide, and polyethylene reflectors	0.9994	0.0019	856000		
hmf84-10		0.9993	0.0022	835000		
hmf84-11		0.9995	0.0019	167000		
hmf84-12		0.9994	0.002	862000		
hmf84-13		0.9994	0.0022	868000		
hmf84-14		0.9994	0.0019	789000		
hmf84-15		0.9995	0.0021	853000		
hmf84-16		0.9994	0.002	796000		
hmf84-17		0.9995	0.0019	845000		
hmf84-18		0.9995	0.0022	843000		
hmf84-19		0.9996	0.0019	869000		
hmf84-2		0.9994	0.0021	826000		
hmf84-20		0.9995	0.0025	833000		
hmf84-21		0.9995	0.0045	830000		
hmf84-22		0.9994	0.002	858000		
hmf84-23		0.9993	0.0024	501000		
hmf84-24		0.9996	0.0018	873000		
hmf84-25		0.9995	0.002	832000		
hmf84-26		0.9993	0.0022	766000		
hmf84-27		0.9994	0.002	750000		
hmf84-3		0.9993	0.0021	700000		
hmf84-4		0.9994	0.002	821000		
hmf84-5		0.9993	0.0021	813000		
hmf84-6		0.9994	0.0024	810000		
hmf84-7		0.9995	0.002	855000		
hmf84-8		0.9994	0.0034	794000		
hmf84-9		0.9993	0.0054	786000		
hmf1-1	Godiva	1	0.001	881000		
hmf11-1	U metal sphere - U(90%U5) - Diam=15.1 cm - Reflection CH_2 10 cm	0.9989	0.0015	30200		

Selected case ICSBEP #	Description	Benchmark k_{eff}	Uncertainty	EALF (eV)	IRSN	NRG
hmf13-1	U metal sphere - U(90%U5) - Diam=16.7 cm – Steel reflector 3.65 cm	0.999	0.0015	832000		
hmf15-1	U metal cylinder - U(96%U5) - Diam=20 cm – No reflector	0.9996	0.0017	894000		
hmf18-1	U metal sphere - U(90%U5) ; Diam=18.4 cm – No reflector	1	0.0014	868000		
hmf19-1	U metal sphere - U(90%U5) ; Diam=18.3 cm - Reflection Graphite 3.45cm	1	0.0028	797000		
hmf20-1	U metal sphere - U(90%U5) ; Diam=16.7 cm - Reflection CH_2 1.45cm	1	0.0028	471000		
hmf21-1	U metal sphere - U(90%U5) ; Diam=15.1 cm – Steel reflection 9.70cm	1	0.0024	796000		
hmf22-1	U metal sphere - U(90.4%U5) - Diam=8.35 cm – Duralumin reflector (Fe, Al, Cu) 2.9cm	1	0.0019	836000		
hmf28-1	U metal sphere - U(93,2 % U5) ; Diam = 6.11 cm – Reflection Unat	1	0.003	838000		
hmf3-10	U metal sphere - U(93.5%U5) – Reflection Unat, tungsten, nickel	1	0.005	577000		
hmf3-11	U metal sphere - U(93.5%U5) – Reflection Unat, tungsten, nickel	1	0.005	551000		
hmf3-12	U metal sphere - U(93.5%U5) – Reflection Unat, tungsten, nickel	1	0.003	697000		
hmf32-1	U metal sphere - U(93.9 % U5) ; Diam = 6.3 à 7.8 cm – Reflection Unat	1	0.0016	857000		
hmf32-2	U metal sphere - U(93.9 % U5) ; Diam = 6.3 à 7.8 cm – Reflection Unat	1	0.0027	859000		
hmf3-8	ORALLOY reflected by WC	1	0.005	695000		
hmf38-1	HEU+DU reflected and moderated by Be and BeO	0.9999	0.0007	250000		
hmf3-9	U metal sphere - U(93.5%U5) – Reflection Unat, tungsten, nickel	1	0.005	634000		
hmf4.-1	U metal sphere - U(97.7%U5) - Diam=13.1 cm – Water reflection 27 cm	0.9985		33800		

Selected case ICSBEP #	Description	Benchmark k_{eff}	Uncertainty	EALF (eV)	IRSN	NRG
hmf41-3	U metal sphere - U(93.9% U5) ; Diam=12.84 à 14.77 cm – Graphite reflection (5.1 à 20.3 cm) ou Beryllium	1.0006	0.0029	774000		
hmf57-2	Sphères and cylinders of U(93.2%U5) reflected by lead (9 à 17 cm)	1	0.0023	836000		
hmf60-1	Zpr-9 assembly 4: a cylindrical assembly of u metal (93% ^{235}U) and tungsten with aluminum reflectors	0.9955	0.0024	223000		
hmf63-1	Cylinders of U(93.5%U5) reflected by lid (1.27 cm or 2.54 cm)	0.9993	0.004	710000		
hmf65-1	Cylinders of U(95.8%U5) diameter 20 cm non reflected	0.9995	0.0013	893000		
hmf67-1	Zpr-9 assemblies 5 and 6: HEU (93% 235u) cylindrical cores with tungsten, graphite, and aluminum diluents with a dense aluminum reflector	0.9959	0.0024	118000		
hmf67-2		0.9938	0.0024	209000		
hmf70-1	Zpr-9 assemblies 7, 8 and 9: cylindrical cores with HEU (93% ^{235}U), tungsten, and aluminum or aluminum oxide with a dense aluminum, aluminum oxide, or beryllium oxide reflector	1.0005	0.0013	72650		
hmf7-10	Unreflected, CH_2 moderated	0.9981	0.0012	27300		
hmf7-31	Unreflected, plexiglas moderated	0.9996	0.0022			
hmf7-32	Unreflected, teflon moderated	0.9941	0.0012	773000		
hmf79-1	Five titanium-reflected heu cylinders	0.9996	0.0015	884000		
hmf79-2		0.9996	0.0014	879000		
hmf79-3		0.9996	0.0015	869000		
hmf79-4		0.9996	0.0014	860000		
hmf79-5		0.9996	0.0015	859000		
hmf8-1	Sphere of U metal - U(90%U5) - Diam=20.3 cm – Non reflected	0.9989	0.0016	870000		
hmf85-1	Highly enriched uranium metal spheres surrounded by copper, cast iron, nickel, nickel-copper-zinc alloy, thorium, tungsten alloy, or zinc reflectors	0.9998	0.0029	769000		
hmf85-2		0.9997	0.0031	701000		
hmf85-3		0.9995	0.0046	777000		
hmf85-4		0.9996	0.0029	782000		
hmf85-5		0.9995	0.0024	816000		
hmf85-6		0.9997	0.0029	739000		

Selected case ICSBEP #	Description	Benchmark k_{eff}	Uncertainty	EALF (eV)	IRSN	NRG
hmi1-1	HEU-met-inter-001 the uranium/iron benchmark assembly: a 235U(93%)/iron cylinder reflected by stainless steel	0.9966	0.0026	31760		
hmi6-1	The initial set of ZEUS experiments: intermediate-spectrum critical assemblies with a graphite-HEU core surrounded by a copper reflector	0.9977	0.0008	4440		
hmi6-2		1.0001	0.0008	9450		
hmi6-3		1.0015	0.0008	22800		
hmi6-4		1.0016	0.0008	80800		
hmm2-1	Spherical assembly of ^{235}U(90%) with central area of polyethylene and 12.85-cm polyethylene reflector	1	0.0037	1380		
hmm3-1	Spherical assembly of ^{235}U(90%) with central area of polyethylene and 15.85-cm polyethylene reflector	1	0.0038	1380		
hmt11-1	Arrays of plates of uranium (93% enriched) aluminium alloy, water-moderated and water-reflected	1	0.00096	0.121		
hmt11-10		1	0.00051	0.0719		
hmt11-11		1	0.00051	0.0694		
hmt11-12		1	0.00051	0.0701		
hmt11-13		1	0.00051	0.0674		
hmt11-14		1	0.00051	0.0657		
hmt11-15		1	0.00051	0.0645		
hmt11-16		1	0.00051	0.0638		
hmt11-17		1	0.00051	0.0636		
hmt11-18		1	0.00051	0.0712		
hmt11-19		1	0.00051	0.0707		
hmt11-2		1	0.00096	0.123		
hmt11-20		1	0.00051	0.0702		
hmt11-21		1	0.00051	0.0698		
hmt11-22		1	0.00054	0.0824		
hmt11-23		1	0.0006	0.0628		
hmt11-24		1	0.0006	0.0625		
hmt11-25		1	0.0007	0.0587		
hmt11-26		1	0.0007	0.0589		
hmt11-27		1	0.00079	0.0564		
hmt11-28		1	0.00079	0.0563		
hmt11-29		1	0.00079	0.056		
hmt11-3		1	0.00054	0.0785		
hmt11-30		1	0.00079	0.056		
hmt11-31		1	0.00051	0.0694		
hmt11-32		1	0.00051	0.0693		

Selected case ICSBEP #	Description	Benchmark k_{eff}	Uncertainty	EALF (eV)	IRSN	NRG
hmt11-33		1	0.00051	0.0692		
hmt11-34		1	0.00051	0.0693		
hmt11-35		1	0.00169	0.175		
hmt11-36		1	0.00169	0.173		
hmt11-37		1	0.0005	0.109		
hmt11-38		1	0.0006	0.0893		
hmt11-39		1	0.0006	0.0911		
hmt11-4		1	0.00054	0.0802		
hmt11-40		1	0.00084	0.0797		
hmt11-41		1	0.00097	0.0743		
hmt11-42		1	0.0006	0.0888		
hmt11-43		1	0.0006	0.0902		
hmt11-5		1	0.00051	0.0649		
hmt11-6		1	0.0006	0.0585		
hmt11-7		1	0.0006	0.0585		
hmt11-8		1	0.0006	0.0583		
hmt11-9		1	0.0006	0.0582		
hst1-1	Cylinders of HEU	1.0004	0.006	0.0814		
hst14-1	Uranium nitrate solution (70g U/l) with gadolinium	1	0.0028	0.0461		
hst14-2		1	0.0052	0.0477		
hst14-3		1	0.0087	0.0498		
hst15-1	Uranium nitrate solution (100g U/l) with gadolinium	1	0.0032	0.0577		
hst15-2		1	0.0034	0.056		
hst15-3		1	0.0068	0.063		
hst15-4		1	0.0069	0.061		
hst15-5		1	0.0089	0.0656		
hst16-1	Uranium nitrate solution (150g U/l) with gadolinium	1	0.0036	0.0784		
hst16-2		1	0.0069	0.0825		
hst16-3		1	0.0079	0.0915		
hst17-1	Uranium nitrate solution (200g U/l) with gadolinium	1	0.0028	0.0974		
hst17-2		1	0.004	0.108		
hst17-3		1	0.0036	0.101		
hst17-4		1	0.0047	0.105		
hst17-5		1	0.0058	0.111		
hst17-6		1	0.0055	0.127		
hst17-7		1	0.0057	0.118		
hst17-8		1	0.0067	0.135		
hst18-1	Uranium nitrate solution (300 g U/l) with gadolinium	1	0.0034	0.159		
hst18-10		1	0.0057	0.274		
hst18-11		1	0.0059	0.244		
hst18-12		1	0.0065	0.272		
hst18-2		1	0.0046	0.185		
hst18-3		1	0.0042	0.169		

Selected case ICSBEP #	Description	Benchmark k_{eff}	Uncertainty	EALF (eV)	IRSN	NRG
hst18-4		1	0.0044	0.178		
hst18-5		1	0.0046	0.222		
hst18-6		1	0.0045	0.202		
hst18-7		1	0.0058	0.199		
hst18-8		1	0.0056	0.242		
hst18-9		1	0.0056	0.219		
hst19-1	Uranium nitrate solution (400 g U/l) with gadolinium	1	0.0041	0.309		
hst19-2		1	0.0041	0.289		
hst19-3		1	0.0067	0.345		
hst20-1	HEU moderated by D_2O	0.9966	0.0116	1.34		
hst20-5	HEU moderated by D_2O	0.9959	0.0077	0.0589		
hst25-1	Uranium nitrate solutions with gadolinium	1.0002	0.0025	0.0406		
hst25-10		1.0003	0.0043	0.0708		
hst25-11		1.0002	0.0045	0.0715		
hst25-12		1.0002	0.0045	0.0877		
hst25-13		1.0009	0.0047	0.0888		
hst25-14		1.0008	0.0053	0.118		
hst25-15		1.0002	0.0058	0.112		
hst25-16		1	0.0049	0.184		
hst25-17		1	0.0055	0.17		
hst25-18		1	0.0061	0.161		
hst25-2		1.0007	0.0025	0.0406		
hst25-3		1.0002	0.0064	0.0428		
hst25-4		1.0003	0.0027	0.0415		
hst25-5		1.0013	0.003	0.0488		
hst25-6		1.0002	0.0067	0.043		
hst25-7		1.0009	0.0073	0.0473		
hst25-8		1	0.0067	0.0487		
hst25-9		1.0002	0.0065	0.0553		
hst27-9	Uranium (89% ^{235}U) nitrate solution with central boron carbide or cadmium absorber rod	1	0.0039	0.075		
hst4-1	HEU reflected and moderated by D_2O	1	0.0033			
hst4-3	HEU reflected and moderated by D_2O	1	0.0039	2.67		
hst4-6	HEU reflected and moderated by D_2O	1	0.0059	0.197		
hst46-1	HEU reflected by C and Be	1.0011	0.0029	0.0371		
hst49-1	Highly enriched uranyl nitrate solution containing cadmium	1.0012	0.0026	0.312		

Selected case ICSBEP #	Description	Benchmark k_{eff}	Uncertainty	EALF (eV)	IRSN	NRG
hst49-12	Highly enriched uranyl nitrate solution cadmium	1.0012	0.0021	0.617		
hst6-1	Boron-poisoned highly enriched uranyl nitrate solution	0.9973	0.005	0.207		
hst7-1	Concrete reflected arrays of highly enriched solutions of uranyl nitrate	1	0.0035	0.0474		
ici1-1	K-infinity measurements with enriched uranium mixed with thorium and polyethylene (kbr-18, kbr-19, kbr-20, and kbr-21 assemblies)	0.969	0.005	177000		
ici1-2		0.98	0.003	29700		
ici1-3		1.014	0.006	100		
ici1-4		0.964	0.012	9.949		
imf6-1	Ieu-met-fast-006 duralumin-reflected spherical assembly of ^{235}U(36%) 1 1	1	0.0023	639000		
lct10-1	Water-moderated $U(4.31)O_2$ fuel rods reflected by two lead, uranium, or steel walls	1	0.0021	0.136		
lct10-10		1	0.0021	0.135		
lct10-11		1	0.0021	0.133		
lct10-12		1	0.0021	0.13		
lct10-13		1	0.0021	0.127		
lct10-14		1	0.0028	0.376		
lct10-15		1	0.0028	0.361		
lct10-16		1	0.0028	0.351		
lct10-17		1	0.0028	0.341		
lct10-18		1	0.0028	0.335		
lct10-19		1	0.0028	0.327		
lct10-2		1	0.0021	0.13		
lct10-20		1	0.0028	0.36		
lct10-21		1	0.0028	0.349		
lct10-22		1	0.0028	0.335		
lct10-23		1	0.0028	0.326		
lct10-24		1	0.0028	0.821		
lct10-25		1	0.0028	0.747		
lct10-26		1	0.0028	0.688		
lct10-27		1	0.0028	0.641		
lct10-28		1	0.0028	0.596		
lct10-29		1	0.0031	0.112		
lct10-3		1	0.0021	0.128		
lct10-30		1	0.0031	0.0111		
lct10-4		1	0.0021	0.126		
lct10-5		1	0.0021	0.487		
lct10-6		1	0.0021	0.349		
lct10-7		1	0.0021	0.268		

Selected case ICSBEP #	Description	Benchmark k_{eff}	Uncertainty	EALF (eV)	IRSN	NRG
lct10-8		1	0.0021	0.232		
lct10-9		1	0.0021	0.141		
lct16-1	Water-moderated rectangular clusters of $U(2.35)O_2$ fuel rods (2.032-cm pitch) separated by steel, boral, copper, cadmium, aluminum, or zircaloy-4 plates	1	0.0031	0.0111		
lct16-10		1	0.0031	0.114		
lct16-11		1	0.0031	0.113		
lct16-12		1	0.0031	0.114		
lct16-13		1	0.0031	0.112		
lct16-14		1	0.0031	0.112		
lct16-15		1	0.0031	0.112		
lct16-16		1	0.0031	0.112		
lct16-17		1	0.0031	0.112		
lct16-18		1	0.0031	0.113		
lct16-19		1	0.0031	0.114		
lct16-2		1	0.0031	0.112		
lct16-20		1	0.0031	0.114		
lct16-21		1	0.0031	0.113		
lct16-22		1	0.0031	0.113		
lct16-23		1	0.0031	0.113		
lct16-24		1	0.0031	0.113		
lct16-25		1	0.0031	0.113		
lct16-26		1	0.0031	0.0111		
lct16-27		1	0.0031	0.0111		
lct16-28		1	0.0031	0.011		
lct16-29		1	0.0031	0.0111		
lct16-3		1	0.0031	0.0109		
lct16-30		1	0.0031	0.011		
lct16-31		1	0.0031	0.115		
lct16-32		1	0.0031	0.113		
lct16-4		1	0.0031	0.113		
lct16-5		1	0.0031	0.112		
lct16-6		1	0.0031	0.113		
lct16-7		1	0.0031	0.113		
lct16-8		1	0.0031	0.114		
lct16-9		1	0.0031	0.113		
lct17-1	Water-moderated $U(2.35)O_2$ fuel rods reflected by two lead, uranium, or steel walls	1	0.0031	0.115		
lct17-10		1	0.0031	0.117		
lct17-11		1	0.0031	0.115		
lct17-12		1	0.0031	0.113		
lct17-13		1	0.0031	0.111		
lct17-14		1	0.0031	0.11		
lct17-15		1	0.0028	0.218		
lct17-16		1	0.0028	0.21		
lct17-17		1	0.0028	0.204		

Selected case ICSBEP #	Description	Benchmark k_{eff}	Uncertainty	EALF (eV)	IRSN	NRG
lct17-18		1	0.0028	0.202		
lct17-19		1	0.0028	0.199		
lct17-2		1	0.0031	0.113		
lct17-20		1	0.0028	0.196		
lct17-21		1	0.0028	0.194		
lct17-22		1	0.0028	0.194		
lct17-23		1	0.0028	0.208		
lct17-24		1	0.0028	0.202		
lct17-25		1	0.0028	0.192		
lct17-26		1	0.0028	0.519		
lct17-27		1	0.0028	0.437		
lct17-28			0.0028	0.378		
lct17-29			0.0028	0.333		
lct17-3		1	0.0031	0.111		
lct17-4		1	0.0031	0.268		
lct17-5		1	0.0031	0.232		
lct17-6		1	0.0031	0.216		
lct17-7		1	0.0031	0.204		
lct17-8		1	0.0031	0.166		
lct17-9		1	0.0031	0.131		
lct27-1	Water-moderated and lead-reflected 4.738-wt.%-enriched uranium dioxide rod arrays	1.0014	0.0015	0.146		
lct27-2		1.0014	0.0012	0.138		
lct27-3		1.0014	0.0015	0.132		
lct27-4		1.0014	0.0015	0.125		
lct29-1	Water-moderated and water-reflected 4.738-wt.%-enriched uranium dioxide rod arrays surrounded by hafnium plates	1	0.001	0.149		
lct29-11	Water-moderated and water-reflected 4.738-wt.%-enriched uranium dioxide rod arrays surrounded by hafnium plates	1	0.0007	0.139		

Selected case ICSBEP #	Description	Benchmark k_{eff}	Uncertainty	EALF (eV)	IRSN	NRG
lct29-12	Water-moderated and water-reflected 4.738-wt.%-enriched uranium dioxide rod arrays surrounded by hafnium plates	1	0.0007	0.138		
lct29-8	Water-moderated and water-reflected 4.738-wt.%-enriched uranium dioxide rod arrays surrounded by hafnium plates	1	0.0014	0.145		
lct34-17	Four 4.738-wt.%-enriched uranium dioxide rod assemblies contained in cadmium, borated stainless steel, or boral square canisters, water-moderated and -reflected	1	0.0053	0.184		
lct34-18		1	0.0053	0.178		
lct34-19		1	0.0053	0.173		
lct34-20		1	0.0053	0.169		
lct34-21		1	0.0047	0.165		
lct34-22		1	0.0047	0.162		
lct34-23		1	0.0047	0.159		
lct34-24		1	0.0047	0.156		
lct34-25		1	0.0047	0.154		
lct34-26		1	0.0047	0.151		
lct40-1	UO_2 rods in water reflected by Pb	1	0.0039	0.167		
lct40-10	Four 4.738-wt.%-enriched uranium dioxide rod assemblies contained in borated stainless steel or boral square canisters, water moderated and reflected by lead or steel	1	0.0046	0.165		
lct40-2	Four 4.738-wt.%-enriched uranium dioxide rod assemblies contained in borated stainless steel or boral square canisters, water moderated and reflected by lead or steel	1	0.0041	0.192		
lct40-4	Four 4.738-wt.%-enriched uranium dioxide rod assemblies contained in borated stainless steel or boral square canisters, water moderated and reflected by lead or steel	1	0.0041	0.177		

Selected case ICSBEP #	Description	Benchmark k_{eff}	Uncertainty	EALF (eV)	IRSN	NRG
lct40-8	Four 4.738-wt.%-enriched uranium dioxide rod assemblies contained in borated stainless steel or boral square canisters, water moderated and reflected by lead or steel	1	0.0044	0.161		
lct49-1	Powder of $U(5)O_2$ lowly moderated - MARACAS	1	0.0034	2.49		
lct50-1	149Sm solution tank in the middle of water-moderated 4.738-wt.%-enriched uranium dioxide rod arrays	1.0004	0.001	0.238		
lct50-10		1.0004	0.001	0.227		
lct50-11		1.0004	0.001	0.253		
lct50-12		1.0004	0.001	0.237		
lct50-13		1.0004	0.001	0.233		
lct50-14		1.0004	0.001	0.244		
lct50-15		1.0004	0.001	0.242		
lct50-16		1.0004	0.001	0.248		
lct50-17		1.0004	0.001	0.246		
lct50-18		1.0004	0.001	0.245		
lct50-2		1.0004	0.001	0.226		
lct50-3		1.0004	0.001	0.247		
lct50-4		1.0004	0.001	0.235		
lct50-5		1.0004	0.001	0.265		
lct50-6		1.0004	0.001	0.254		
lct50-7		1.0004	0.001	0.249		
lct50-8		1.0004	0.001	0.244		
lct50-9		1.0004	0.001	0.23		
lct5-1	Critical experiments with low-enriched uranium dioxide fuel rods in water containing dissolved gadolinium	1	0.0023	0.175		
lct5-10		1	0.0028	2.12		
lct5-11		1	0.0043	2.14		
lct5-12		1	0.0066	4.24		
lct5-13		1	0.0064	5.48		
lct5-14		1	0.002	0.169		
lct5-15		1	0.002	0.198		
lct5-16		1	0.0032	0.442		
lct5-2		1	0.0021	0.195		
lct52-1	Uranium dioxide (4.738-wt.%-enriched) fuel rod arrays moderated and reflected by gadolinium nitrate solution	1.0003	0.0023	0.523		
lct52-2		1.0003	0.0036	0.19		
lct52-3		1.0003	0.0034	0.0946		
lct52-4		1.0003	0.0023	0.525		
lct52-5		1.0003	0.0036	0.191		
lct52-6		1.0003	0.0034	0.0959		
lct5-3		1	0.0029	0.281		

Selected case ICSBEP #	Description	Benchmark k_{eff}	Uncertainty	EALF (eV)	IRSN	NRG
lct5-4	Critical experiments with low-enriched uranium dioxide fuel rods in water containing dissolved gadolinium	1	0.0025	0.291		
lct5-5		1	0.0047	0.811		
lct5-6		1	0.0042	1.01		
lct5-7		1	0.0043	1.3		
lct5-8		1	0.0021	1.72		
lct5-9		1	0.004	1.96		
lct7-1	UO_2 rods in water	1	0.0014	0.287		
lct71-1	Tight lattice pitch experiments LEU	1	0.00076	0.948		
lct71-4	Tight lattice pitch experiments LEU	1	0.0008	1.06		
lct7-2	UO_2 rods in water	1	0.0008	0.124		
lct7-3	UO_2 rods in water	1	0.0007	0.0784		
lct7-4	UO_2 rods in water	1	0.0008	0.276		
lct7-5	UO_2 rods in water	1	0.0014	0.114		
lct7-7	UO_2 rods in water	1	0.0007	0.316		
lct7-8	UO_2 rods in water	1	0.0014	0.169		
lct9-1	Water-moderated rectangular clusters of $U(4.31)O_2$ separated by steel, boral, copper, cadmium, aluminum, or zircaloy-4 plates	1	0.0021	0.13		
lct9-10		1	0.0021	0.13		
lct9-11		1	0.0021	0.129		
lct9-12		1	0.0021	0.13		
lct9-13		1	0.0021	0.129		
lct9-14		1	0.0021	0.131		
lct9-15		1	0.0021	0.13		
lct9-16		1	0.0021	0.131		
lct9-17		1	0.0021	0.13		
lct9-18		1	0.0021	0.131		
lct9-19		1	0.0021	0.13		
lct9-2		1	0.0021	0.129		
lct9-20		1	0.0021	0.131		
lct9-21		1	0.0021	0.13		
lct9-22		1	0.0021	0.131		
lct9-23		1	0.0021	0.13		
lct9-24		1	0.0021	0.129		
lct9-25		1	0.0021	0.129		
lct9-26		1	0.0021	0.129		
lct9-27		1	0.0021	0.129		
lct9-3		1	0.0021	0.13		
lct9-4		1	0.0021	0.129		
lct9-5		1	0.0021	0.131		
lct9-6		1	0.0021	0.13		
lct9-7		1	0.0021	0.131		
lct9-8		1	0.0021	0.13		
lct9-9		1	0.0021	0.131		
lmsct3-1		0.9978	0.0008	0.135		

Selected case ICSBEP #	Description	Benchmark k_{eff}	Uncertainty	EALF (eV)	IRSN	NRG
lmsct3-10	Stacy: a 60-cm-diameter tank containing 5%-enriched UO_2 fuel rods (1.5-cm square lattice pitch) in 6%-enriched uranyl nitrate solutions	0.9998	0.0008	0.129		
lmsct3-11		0.9998	0.0008	0.13		
lmsct3-12		0.9999	0.0008	0.134		
lmsct3-13		0.9999	0.0008	0.141		
lmsct3-14		0.9999	0.0008	0.151		
lmsct3-15		0.9998	0.0008	0.165		
lmsct3-2		0.9968	0.0008	0.134		
lmsct3-3		0.9972	0.0008	0.134		
lmsct3-4		0.9976	0.0008	0.135		
lmsct3-5		0.9981	0.0008	0.138		
lmsct3-6		0.9989	0.0008	0.143		
lmsct3-7		0.9984	0.0008	0.152		
lmsct3-8		0.9993	0.0008	0.164		
lmsct3-9		0.9998	0.0008	0.128		
lmsct5-1	Stacy: a 60-cm-diameter water-reflected tank containing 5%-enriched UO_2 fuel rods (1.5-cm square lattice pitch) in 6%-enriched uranyl nitrate solutions poisoned with pseudo-fission-product elements	1	0.0007			
lmsct5-10		0.9998	0.0007	0.135		
lmsct5-11		0.9999	0.0007	0.135		
lmsct5-12		0.9999	0.0007	0.135		
lmsct5-2		1.0001	0.0007	0.132		
lmsct5-2		1.0001	0.0007	0.132		
lmsct5-3		0.9999	0.0007	0.134		
lmsct5-4		1	0.0007	0.134		
lmsct5-5		1	0.0007	0.134		
lmsct5-6		1	0.0007	0.134		
lmsct5-7		0.9999	0.0007	0.134		
lmsct5-8		0.9999	0.0007	0.135		
lmsct5-9		0.9999	0.0007	0.135		
lmsct6-1	Stacy: a 60-cm-diameter tank containing 5%-enriched UO_2 fuel rods (1.5-cm square lattice pitch) in 6%-enriched uranyl nitrate solutions poisoned with gadolinium, unreflected and water-reflected	0.9999	0.0008	0.131		
lmsct6-10		0.9994	0.0016	0.153		
lmsct6-2		1	0.001	0.135		
lmsct6-3		1.0001	0.0013	0.138		
lmsct6-4		1.0001	0.0014	0.142		
lmsct6-5		1.0001	0.0016	0.145		
lmsct6-6		0.9975	0.0008	0.138		
lmsct6-7		0.998	0.001	0.142		
lmsct6-8		0.9985	0.0013	0.146		
lmsct6-9		0.9983	0.0014	0.15		
lmt4-1	Triangular lattices of 2.49 cm diameter leu (4.948) rods in water	0.9998	0.0017	1.24		
lmt4-2		0.9978	0.0018	1.17		
lmt4-3		0.9993	0.0009	0.839		
lmt4-4		0.9972	0.001	0.791		
lmt4-5		0.9983	0.001	0.625		
lmt4-6		0.997	0.001	0.597		

Selected case ICSBEP #	Description	Benchmark k_{eff}	Uncertainty	EALF (eV)	IRSN	NRG
lmt4-7		0.9984	0.0018	0.46		
lmt4-8		0.9968	0.0019	0.446		
lmt7-1	Water-moderated and water-reflected 0.30 in. Diameter U(4.95) metal rods in square-pitched arrays	0.9983	0.0114	0.673		
lmt7-2		0.9976	0.0068	0.332		
lmt7-3		0.9974	0.0031	0.207		
lmt7-4		0.9974	0.0006	0.157		
lmt7-5		0.9972	0.0028	0.121		
lmt7-6		0.9967	0.0053	0.102		
mct001-1	Water-reflected mixed plutonium-uranium oxide (20 wt.% Pu) pins	1	0.0025	1.07		
mct001-2		1	0.0026	0.292		
mct001-3		1	0.0032	0.174		
mct001-4		1	0.0039	0.12		
mct003-1	Rectangular arrays of water-moderated uo2-6.6 wt.% PuO_2 fuel rods	1.0028	0.00723	0.922		
mct003-2		1.0019	0.00587	0.559		
mct003-3		1	0.00538	0.663		
mct003-4		1.0027	0.00311	0.192		
mct003-5		1.0049	0.00267	0.159		
mct003-6		1	0.00229	0.103		
mct004.c10	Critical arrays of mixed plutonium-uranium fuel rods with water-to-fuel volume ratios ranging from 2.4 to 5.6	1	0.0051	0.082		
mct004.c11		1	0.0051	0.0916		
mct004-1		1	0.0046	0.149		
mct004-2		1	0.0046	0.148		
mct004-3		1	0.0046	0.147		
mct004-4		1	0.0039	0.123		
mct004-5		1	0.0039	0.122		
mct004-6		1	0.0039	0.121		
mct004-7		1	0.004	0.0951		
mct004-8		1	0.004	0.0948		
mct004-9		1	0.004	0.0944		
mmm1-1	Bfs-97, -99, -101 assemblies: critical experiments with heterogeneous compositions of plutonium, depleted-uranium dioxide, and polyethylene	1.001	0.0029	355000		
mmm1-2		1.0011	0.0026	71500		
mmm1-3		1.0016	0.0031	5660		
mmm1-4		1.0011	0.0027	2790		
mmm1-5		1.0018	0.0028	5550		
mmm1-6		1.0009	0.0028	5760		
mmm1-7		1.0012	0.0026	2510		
mmm1-8		1.0023	0.0022	21600		
mmm1-9		1.0021	0.0021	5960		
pmf10-1	Plutonium metal sphere (phase d, 4.9% ^{240}Pu) – Unat reflection	1	0.0018	1240000		
pmf1-1	Jezebel	1	0.00129	1330000		

Selected case ICSBEP #	Description	Benchmark k_{eff}	Uncertainty	EALF (eV)	IRSN	NRG
pmf11-1	Pu metal sphere phase α- 5.18% ^{240}Pu - Diam=8.24 cm – Water reflection 25cm	1	0.001	108000		
pmf14-1	Nickel reflected array of plutonium rods Pu(97.6%PU9) reflected by nickel (> 30 cm)	1.0037	0.0031	846000		
pmf18-1	Sphere of Pu metal (phase d, 4.9% ^{240}Pu) – Beryllium reflection	1	0.003	943000		
pmf19-1	Sphere of Pu metal (9% 240Pu) – Beryllium reflection	0.9992	0.0015	800000		
pmf2-1	Jezebel Pu metal sphere, phase d - 20.1% ^{240}Pu - Diam=13.3 cm – Non reflected	1	0.002	1330000		
pmf22-1	Pu metal sphere phase d- 1.8% ^{240}Pu - Diam=13.34 cm – Non reflected	1	0.0021	1310000		
pmf23-1	Pu metal sphere phase d- 1.8% ^{240}Pu - Diam=12 cm – Graphite reflection 2.35cm	1	0.002	1210000		
pmf24-1	Pu metal sphere phase d- 1.8% ^{240}Pu - Diam=12 cm - CH_2 reflection 1.55cm	1	0.002	699000		
pmf25-1	Pu metal sphere phase d- 1.8% ^{240}Pu - Diam=12 cm – Steel reflection 1.55cm	1	0.002	1270000		
pmf26-1	Pu metal sphere phase d- 1.8% ^{240}Pu - Diam=10.7 cm – Steel reflection 11.9cm	1	0.0024	1160000		
pmf27-1	Pu metal sphere phase d- 9% ^{240}Pu - Diam=10.7 cm - CH_2 reflection 5.58cm	1	0.0022	90200		
pmf28-1	Pu metal sphere phase d- 9% ^{240}Pu - Diam=10.7 cm – Steel reflection 19.65cm	1	0.0022	1120000		
pmf29-1	Pu metal sphere phase a- 10% ^{240}Pu - Diam=10.7 cm – Non reflected	1	0.002	1330000		
pmf30-1	Pu metal sphere phase a- 10% ^{240}Pu - Diam=9.32 cm – Graphite reflection 4.49cm	1	0.0021	1210000		
pmf31-1	Pu metal sphere phase a- 10% ^{240}Pu - Diam=9.32 cm - CH_2 reflection 3.69cm	1	0.0021	223000		
pmf32-1	Pu metal sphere phase α- 10% ^{240}Pu - Diam=9.32 cm – Steel reflection 4.49cm	1	0.002	1250000		

Selected case ICSBEP #	Description	Benchmark k_{eff}	Uncertainty	EALF (eV)	IRSN	NRG
pmf38-1	Pu metal sphere (phase α - 6% ^{240}Pu) – Diam = 7.6 cm) – Beryllium reflection (1.5 cm)	0.9983	0.0019			
pmf39-1	Spherical assembly o f ^{239}Pu(d, 98%) with a 4.25-cm duralumin re flector	1	0.0022	1230000		
pmf40-1	Pu metal sphere (phase d, 98% ^{239}Pu) - Diam = 6 cm – copper 1.6 cm	1	0.0038	1190000		
pmf44-4	Pu metal sphere (phase d, 5.1% ^{240}Pu) – reflection beryllium, graphite, aluminium, iron, molybdenum and polyethylene	0.9977	0.0021	235000		
pmf45-1	Critical experiments performed for LAMPRE	1	0.0047	935000		
pmf45-2		1	0.0046	973000		
pmf45-3		1	0.0044	1010000		
pmf45-4		1	0.0046	975000		
pmf45-5		1	0.0045	1010000		
pmf45-6		1	0.0049	898000		
pmf45-7		1	0.005	833000		
pmf5-1	Pu metal sphere (phase d, 4.9% ^{240}Pu) – Diam=5.08 cm – Tungsten reflection	1	0.0013	1090000		
pmf6-1	Pu metal sphere (phase d, 4.8% ^{240}Pu) – Diam=4.53 cm – Unat reflection	1	0.003	1150000		
pmf8-2	Pu metal sphere (phase d, 5.1% ^{240}Pu) – Diam=5.31 cm – Thorium reflection	1	0.0006	1110000		
pmf9-1	Benchmark critical experiment of a plutonium sphere reflected by aluminum	1	0.0027	1220000		
pst1-1	Pu Solution containing gadolinium	1	0.005	0.0885		
pst12-1	19% 240Pu solution in water reflected 130 x 130 x 100 cm cubic tank	1	0.0043	0.0478		
pst18-1	Water-reflected 24-inch diameter cylinder of plutonium (42.9% ^{240}Pu) nitrate solution	1	0.0034	0.0569		
pst28-1	Water-reflected annular cylinders (50/30 cm diam.) containing plutonium (3% ^{240}Pu) nitrate solutions	0.9994	0.0012	0.106		
pst30-1	1.5% ^{240}Pu solution in 50 x 20 cm annular cylinders	1	0.00143	0.054		

Selected case ICSBEP #	Description	Benchmark k_{eff}	Uncertainty	EALF (eV)	IRSN	NRG
pst32-1	9.95% ^{240}Pu solution in 50 x 20 cm annular cylinders	1	0.00198	0.087		
pst34-1	Plutonium (8.3 wt.% ^{240}Pu) nitrate solution with gadolinium in water-reflected 24-inch diameter cylinder	1	0.0062	0.147		
pst34-10		1	0.0052	1.94		
pst34-11		1	0.0048	2.08		
pst34-12		1	0.0042	2.28		
pst34-13		1	0.0043	2.47		
pst34-14		1	0.0044	2.63		
pst34-15		1	0.0042	2.73		
pst34-2		1	0.0044	0.176		
pst34-3		1	0.004	0.205		
pst34-4		1	0.0039	0.231		
pst34-5		1	0.004	0.258		
pst34-6		1	0.0042	0.282		
pst34-7		1	0.0057	1.56		
pst34-8		1	0.0055	1.66		
pst34-9		1	0.0052	1.76		

5. C/E results and analysis

5.1. Uranium cases

5.1.1. IRSN results

5.1.1.1. Fast cases

The results of selected cases involving highly enriched uranium and various reflectors are reported in Figure 1. There is a general good agreement between the calculated k_{eff} and the benchmark one. Most C-E results lie within 2σ uncertainty margins of experimental uncertainties.

The three nuclear data evaluations do not lead to significant discrepancy for high enriched uranium. However, for some reflectors, discrepancies can be explained by the nuclear data evaluation of the reflector's element since k_{eff} is sensitive to this element (see Table 2). For hmf3-12 where a nickel reflector surrounds the sphere of uranium we can see a strong overestimation of JEFF-4.0T1, which is due to the new evaluation of nickel. A quick look at Figure 2 shows how this configuration is sensitive to the elastic scattering cross section of ^{58}Ni.

Table 2. Comparison JEFF-33/JEFF-4.0T1 – HMF systems

Selected case ICSBEP #	JEFF-33	JEFF-4.0T1	σ_{MC}	Element of the reflector	JEFF-3.3 replaced by JEFF-4.0T1 for element	C-E (pcm)
hmf3-12	1.00541	1.03611	0.0002	Nickel (20 cm)	1.03585	3585
hmf22-1	0.99746	1.00528	0.0002	Aluminum (3.9 cm)	1.00585	585
hmf70-1	1.01093	1.00787	0.0002	Tungsten	1.00529	529

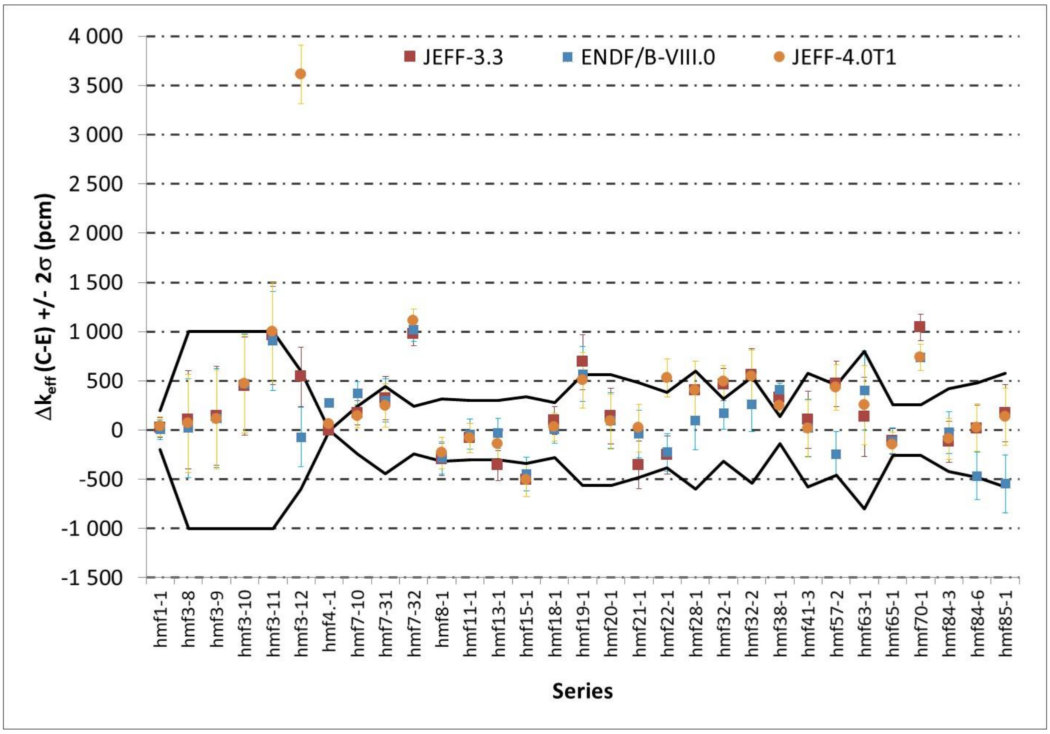

Figure 1. C-E results for highly enriched uranium cases.

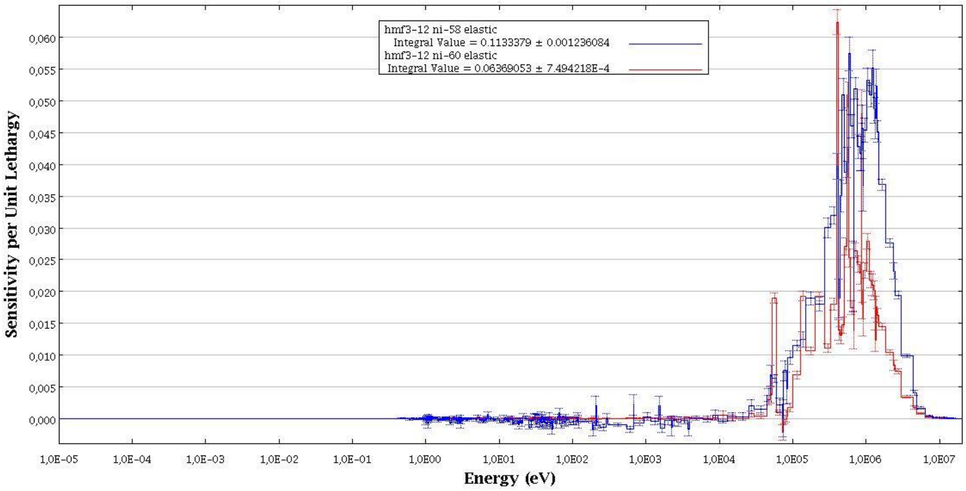

Figure 2. Sensitivity profile of k_{eff} to the scattering cross section of ^{58}Ni

5.1.1.2. Thermal cases

The results of cases involving highly enriched uranium in solutions are provided in Figure 3. A quite good agreement between the calculated k_{eff} and the benchmark k_{eff} is obtained whatever the library. All C-E results are comprised in the experimental uncertainty margins at the 2σ level, except hst46-1 and at a lesser extent, hst6-1 and hst7-1. However, for some cases, the results significantly differ between the three nuclear data evaluations. That is the case particularly for hst4 and hst20 series.

The k_{eff} difference between JEFF-3.3 and JEFF-4.0T1 for hst20-1 and hst4-3 benchmarks is mainly due to the cross sections of ^{16}O which differ between both evaluations (see Table 3).

Table 3. Comparison JEFF-33/JEFF-4.0T1 – hst systems

Selected case ICSBEP #	JEFF-33	JEFF-4.0T1	ENDF/B-VIII.0	σ_{MC}	Element to be changed	JEFF-3.3 replaced by JEFF-4.0T1 for element
hst4-3	0.99541	0.99183	0.99010	0.00020	^{16}O	0.99010
hst20-1	1.00034	0.99524	0.99445	0.00020	^{16}O	0.99459

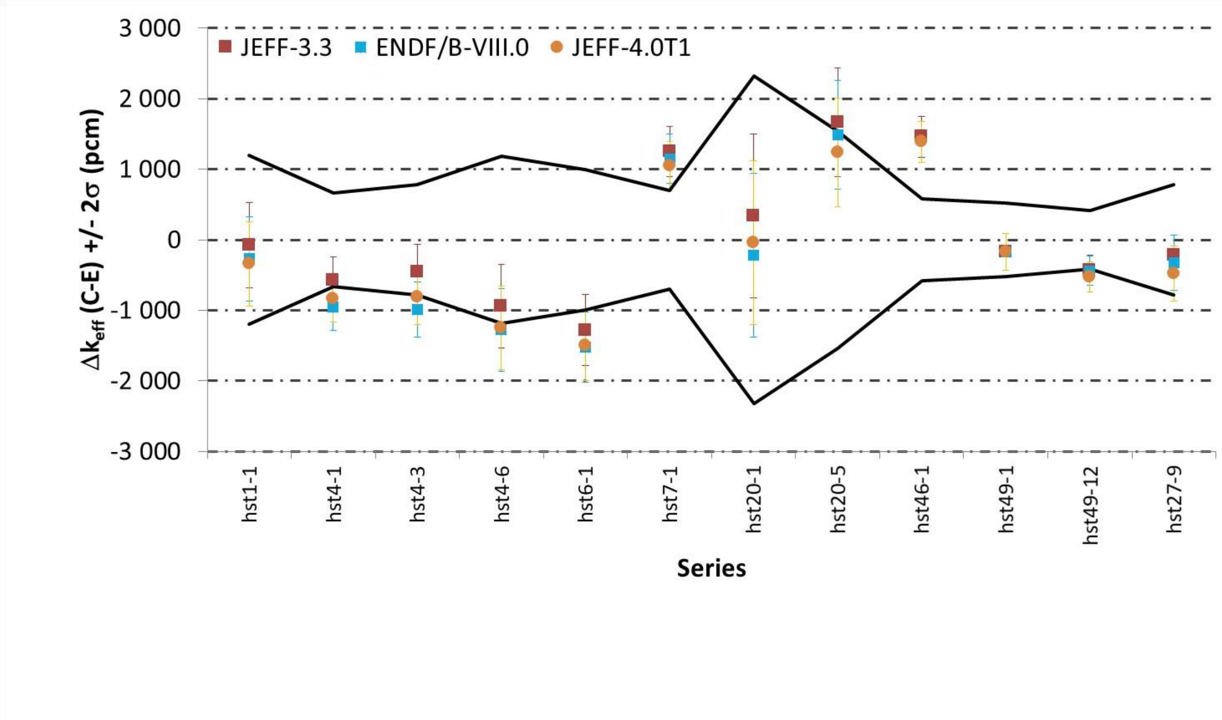

Figure 3. C-E results for solutions with highly enriched uranium.

The results of cases involving lattices of UO_2 rods are provided in Figure 4. A quite good agreement between the calculated k_{eff} and the benchmark k_{eff} is obtained whatever the library, except for lct27. All C-E results are comprised in the experimental uncertainty margins at the 2σ level.

However, for most cases, there is significant discrepancy between libraries, which is mainly due to the new evaluation of ^{16}O, ^{235}U, ^{238}U and to the new TSL of water.

For lct27 series, the ENDF/B-VIII.0 evaluation of lead leads to far better results. Moreover, we can see that there is a tendency to increase k_{eff} with the gap between the assembly and the lead reflector. It can be linked to the sensitivity of k_{eff} to the scattering cross sections of ^{207}Pb provided with on Figure 5.

Table 4. Comparison JEFF-33/JEFF-4.0T1 – lct systems

Selected case ICSBEP #	JEFF-33	JEFF-4.0T1	ENDF/B-VIII.0	σ_{MC}	Element to be changed	JEFF-3.3 replaced by other evaluation for element
lct7-4	0.99782	1.00063	0.99970	0.00020	^{16}O, ^{235}U, ^{238}U and hydrogen in water	1.00032 (JEFF-4.0T1)
lct27-1	1.00874	1.00689	1.00134	0.00020	Lead	1.00258 (ENDF/B-VIII.0)
lct34-23	1.00392	1.00138	1.00121	0.00020	^{16}O, ^{235}U, ^{238}U and hydrogen in water	1.00136 (JEFF-4.0T1)

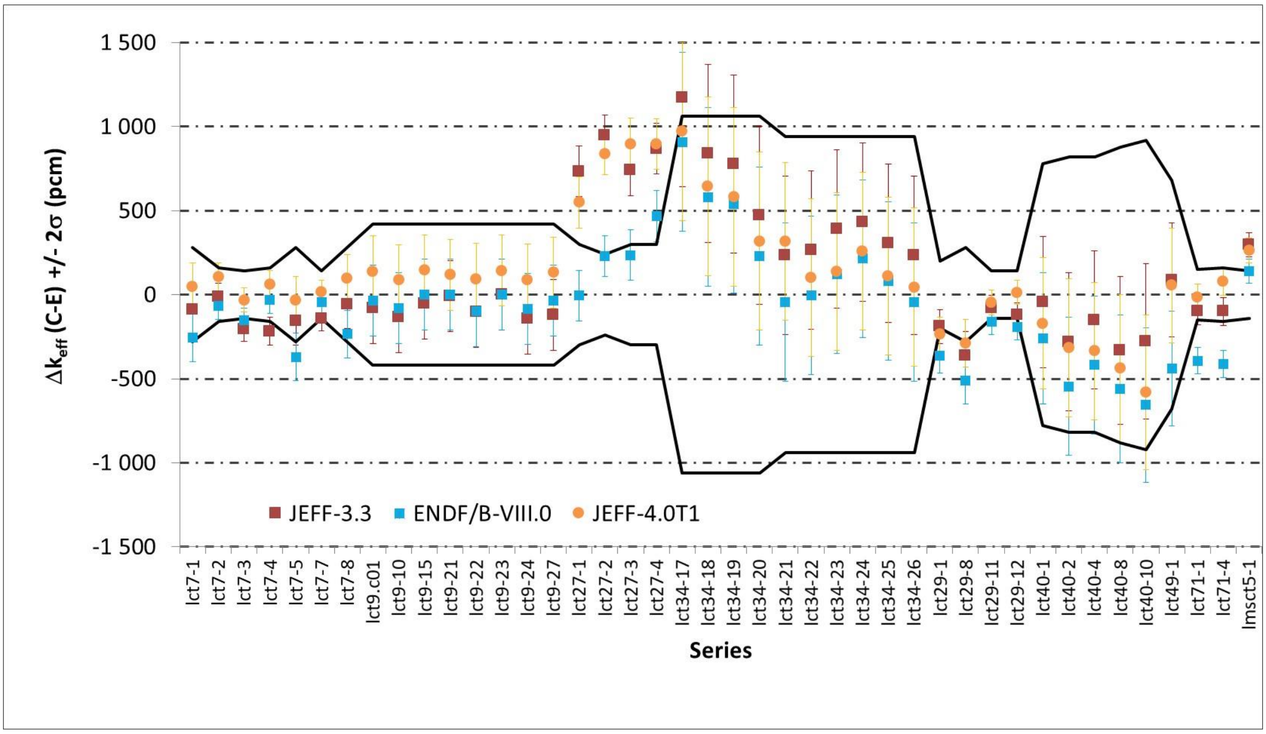

Figure 4. C-E results for experiments with lattices of UO_2 rods in water.

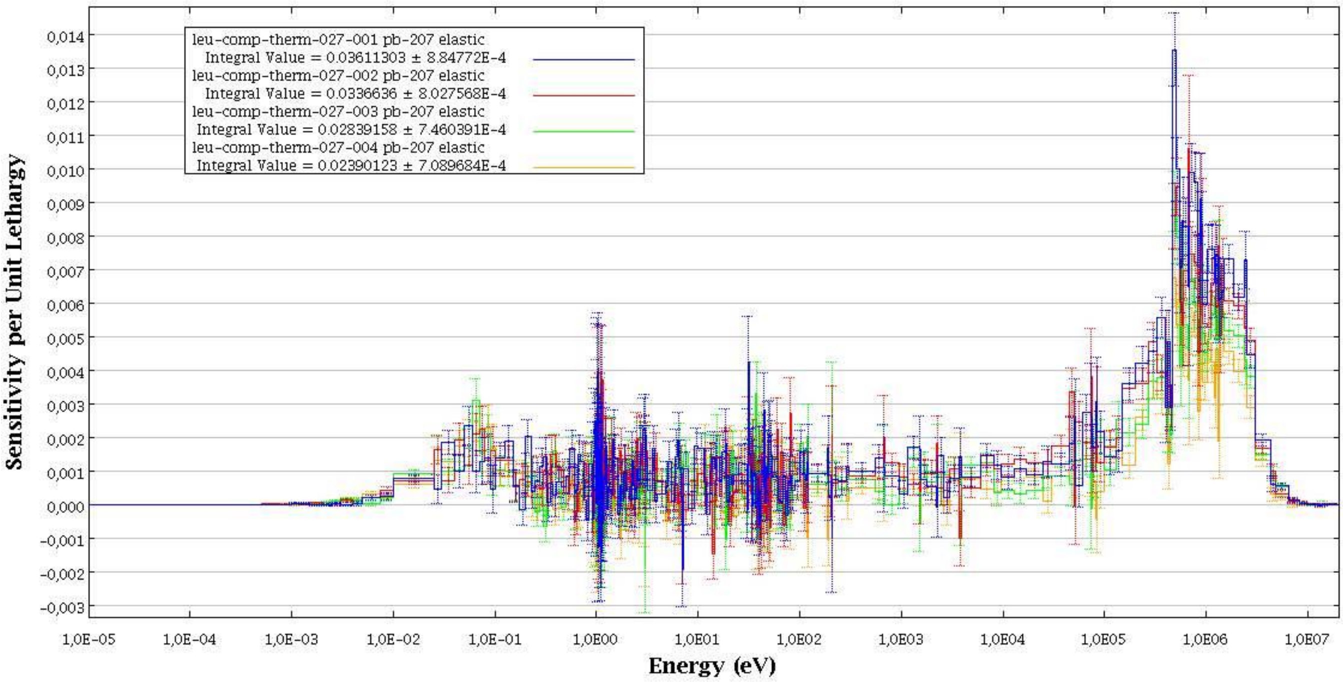

Figure 5. Sensitivity profile of k_{eff} to scattering cross sections of ^{207}Pb.

5.1.1.3. Focus on 235U (IRSN)

A focus on benchmark results with uranium in various energy ranges is done in Figure 6.

The main discrepancies between the benchmark k_{eff} and the calculated one are observed for the epithermal energy spectrum (hci4, hmi1, hmi6) and also for hmf70.

Concerning hci4, the k_{eff} difference between ENDF/B-VIII.0 and the other evaluations comes from the evaluation of ^{235}U. The ENDF/B-VIII.0 results are closer to the benchmark k_{eff}.

Regarding hmi1, the k_{eff} difference between nuclear data evaluations mainly comes from the evaluation of ^{56}Fe. The ENDF/B-VIII.0 results are closer to the benchmark k_{eff}.

Concerning hmi6 series, the JEFF-33 and JEFF-4T1 evaluations of copper and ^{235}U lead to results that are more consistent with the benchmark k_{eff} than the ENDF/B-VIII.0 evaluation.

The large overestimation of hmf7-32 with all libraries is strongly improved using the JEFF-4T2 evaluation of nuclear data. The new F-19 is mainly responsible for this improvement.

The impacts on k_{eff} of isotopes can be seen in Table 5.

Sensitivity profiles to the scattering cross section of ^{56}Fe for hmi1 are reported on Figure 8.

Sensitivity profiles to the scattering and capture cross sections of ^{63}Cu and fission cross section of ^{235}U for hmi6 are reported on Figure 9 and on Figure 10.

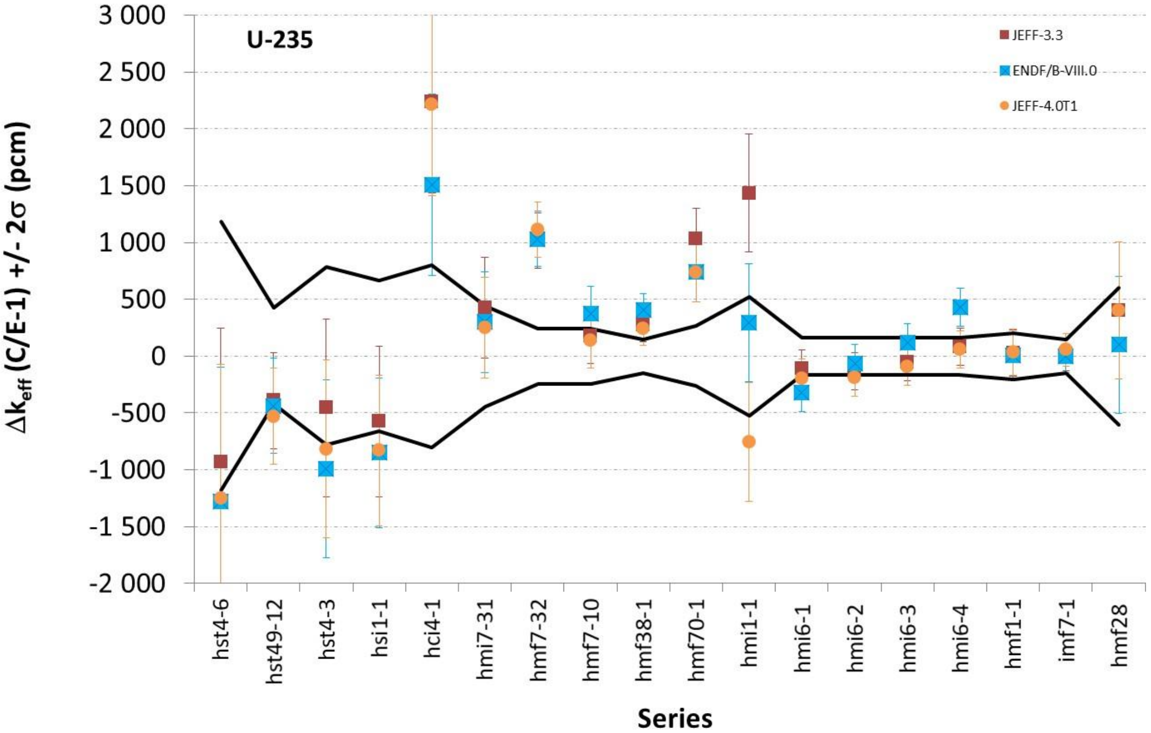

Figure 6. C-E results for experiments with uranium.

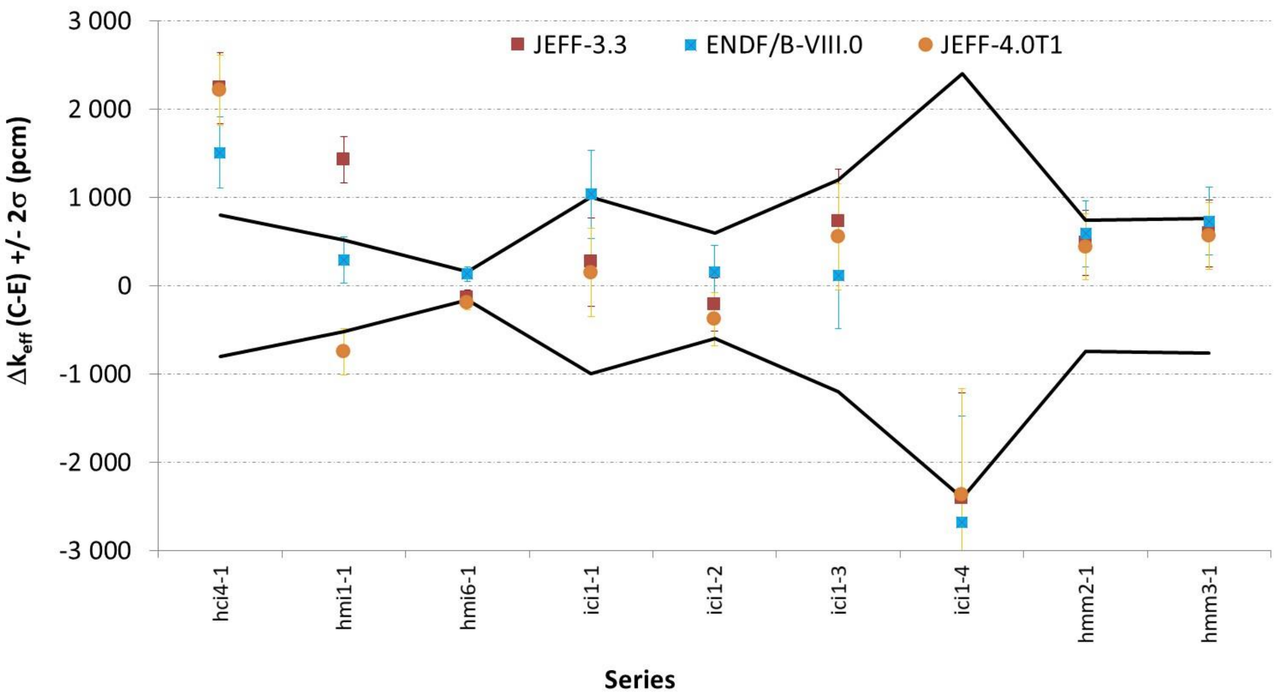

Figure 7. C-E results for experiments with uranium.

Table 5. Comparison JEFF-33/ENDF/B-VIII.0 –experiments with uranium

Selected case ICSBEP #	Experimental k_{eff}	JEFF-33	ENDF/B-VIII.0	σ_{MC}	Element to be changed	JEFF-3.3 replaced by ENDF/B-VIII.0 for element
hmi1-1	0.9966 ± 0.0026	1.01086	0.99882	0.00020	^{56}Fe	0.99804
ici1-1	0.9690 ± 0.0050	0.97188	0.97930	0.00020	^{235}U+^{238}U + ^{56}Fe	0.97880
hci4-1	1.0000 ± 0.0040	1.02239	1.01576	0.00020	^{235}U	1.01634
hmi6-1	0.9946 ± 0.0003	0.99659	0.99448	0.00020	Cu + ^{235}U + ^{238}U	0.99554
hmi6-2	0.9985 ± 0.0003	0.99876	0.99944	0.00020	Cu + ^{235}U + ^{238}U	0.99995
hmi6-3	1.0023 ± 0.0003	1.00097	1.00272	0.00020	Cu + ^{235}U + ^{238}U	1.00356
hmi6-4	1.0064 ± 0.0003	1.00243	1.00591	0.00020	Cu + ^{235}U + ^{238}U	1.00660

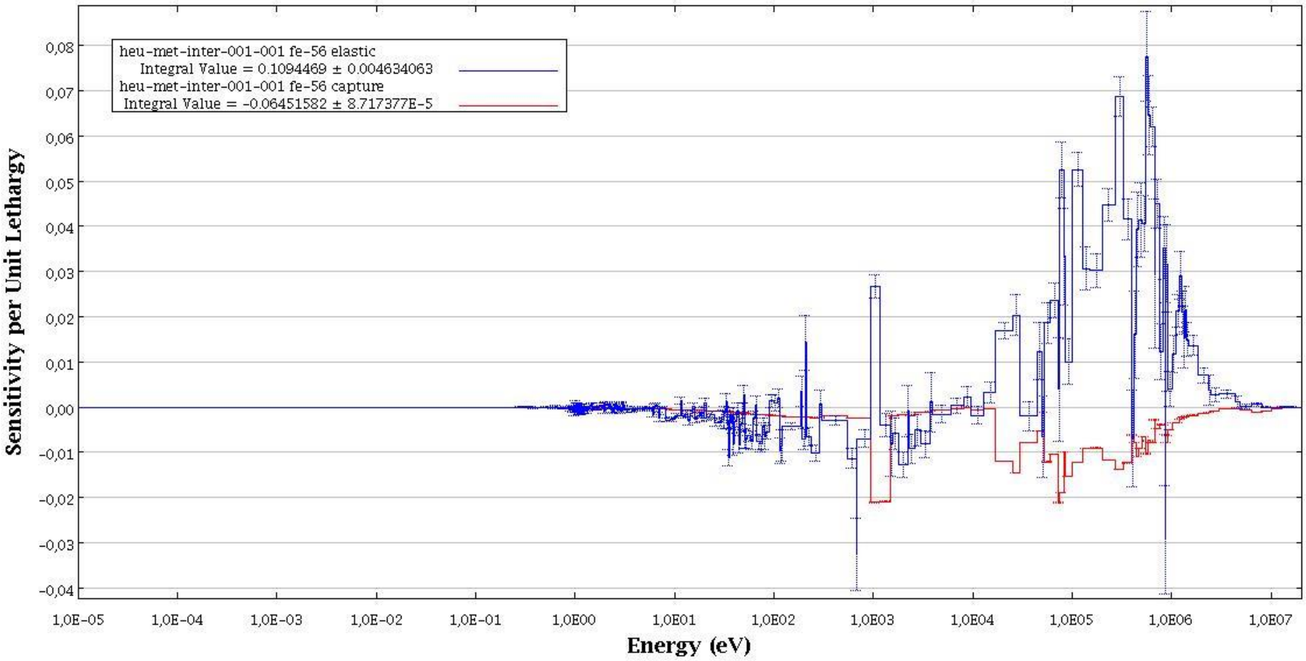

Figure 8. Sensitivity profile for hmi1-1 experiment – ^{56}Fe elastic and ^{56}Fe capture

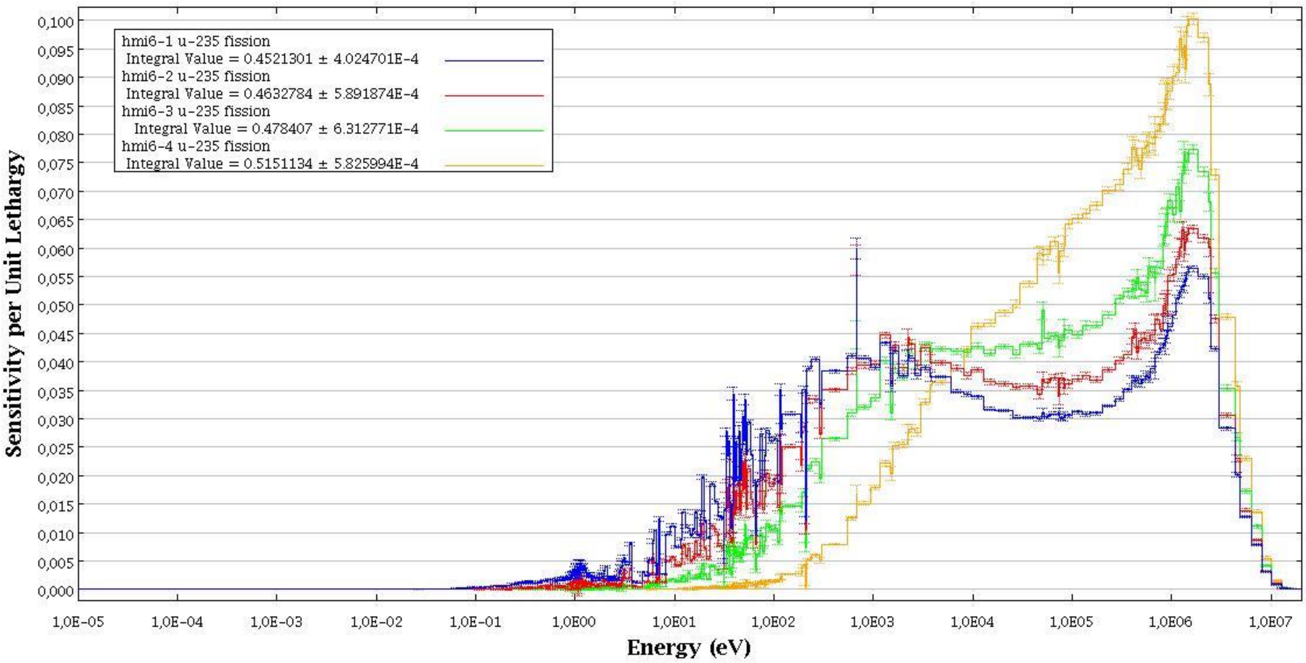

Figure 9. Sensitivity profile for hmi6 experiment – ^{235}U fission

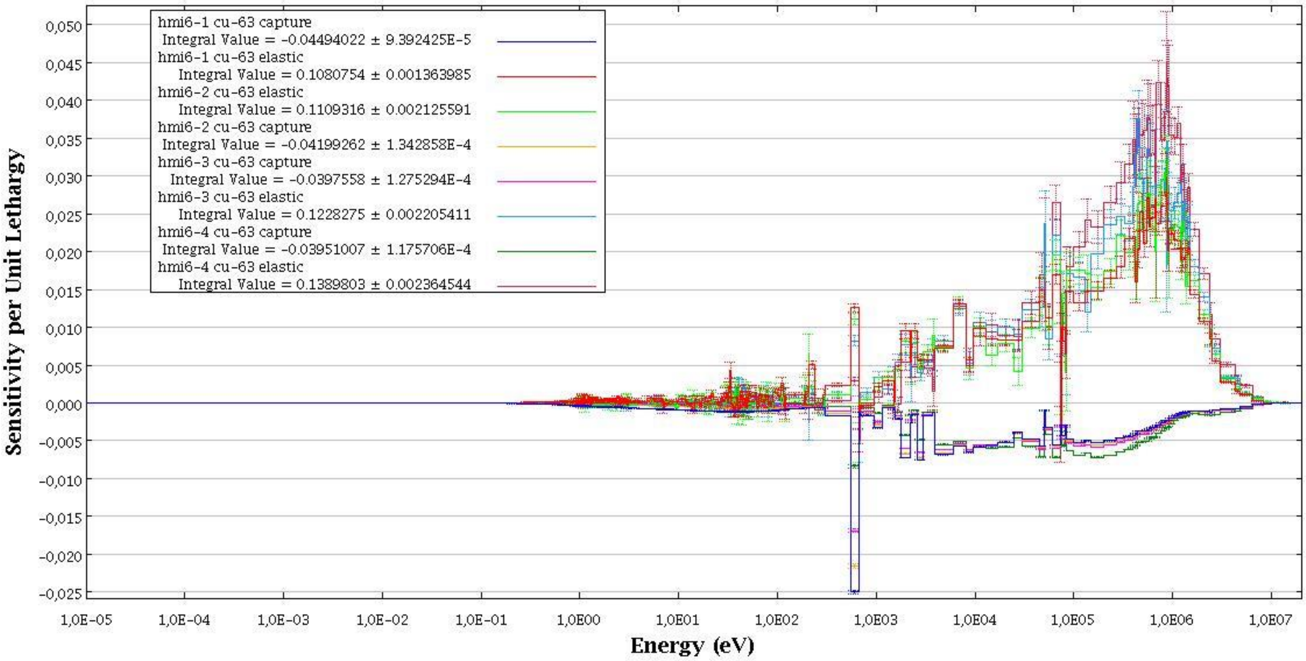

Figure 10. Sensitivity profile for hmi6 experiment – ^{63}Cu elastic and capture

5.1.2. NRG results

5.1.2.1. Fast cases

Benchmarks with (almost) only HEU

The results for cases with a fast neutron spectrum and almost only HEU are shown in Figure 11. The benchmark models for hmf1 (Godiva, simple model), hmf18, hmf51, hmf81 (Grotesque, simple model), and hmf100 (ORSphere, simple model) only contain HEU and no other materials. In some of these benchmark models, the HEU does contain certain levels of impurities. The benchmark models of hmf8, and hmf15 contain small amounts of other materials, such as steel.

It can be seen from the Figure that most libraries, with the exception of JEF-2.2, have a similar performance for these fast spectrum benchmarks with only HEU. When plotted as in Figure 11 there is no indication why k_{eff} is overestimated for some benchmarks and underestimated for others, even though in all these benchmarks almost only HEU is used.

In Figure 12 the same results are shown as a function of the energy that corresponds to the average lethargy causing fission (EALF). In this Figure there appears to be an approximate correlation between the C/E values and EALF. The sensitivities of a selection of these benchmarks to several cross sections is shown in Figure 13. The sensitivity to capture and fission are rather similar for all selected cases, but there seems to be differences in the sensitivity to elastic and inelastic scattering, although the statistical accuracy of the calculations is not always good enough to draw conclusions.

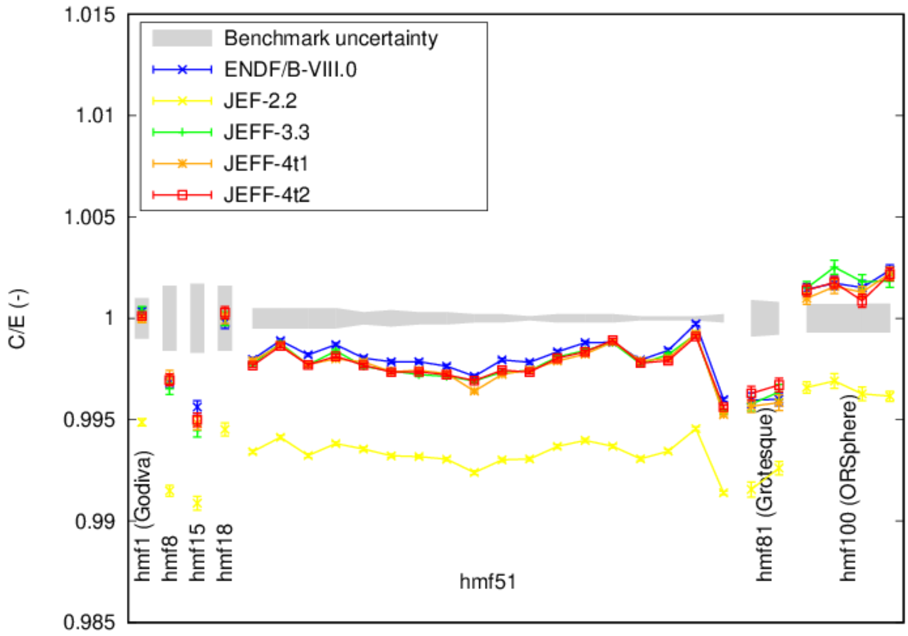

Figure 11. C/E results for fast spectrum benchmarks with almost only HEU.

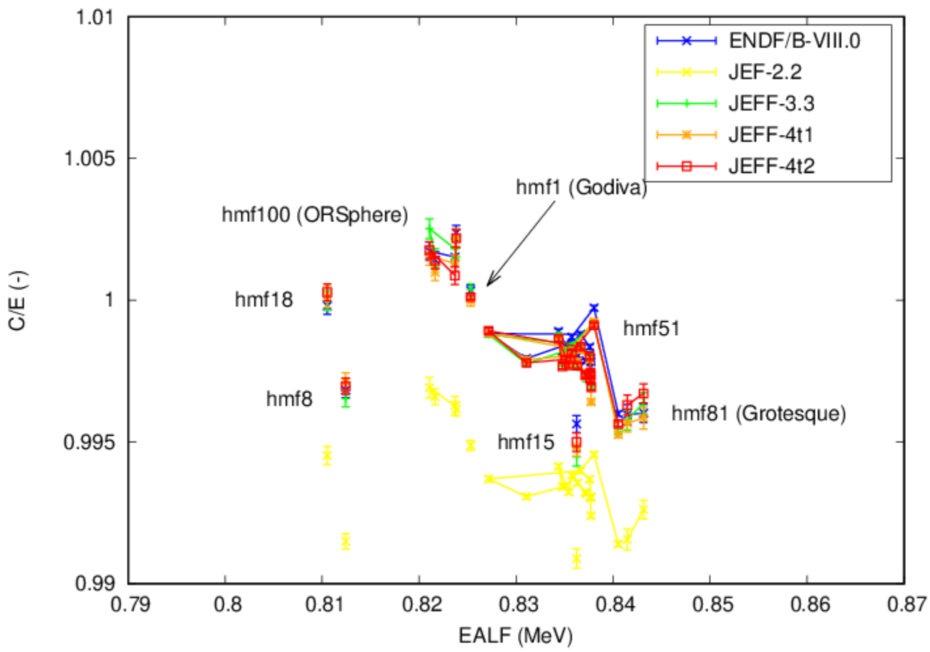

Figure 12. C/E results for fast spectrum benchmarks with almost only HEU, as a function of the energy that corresponds to the average lethargy causing fission (EALF).

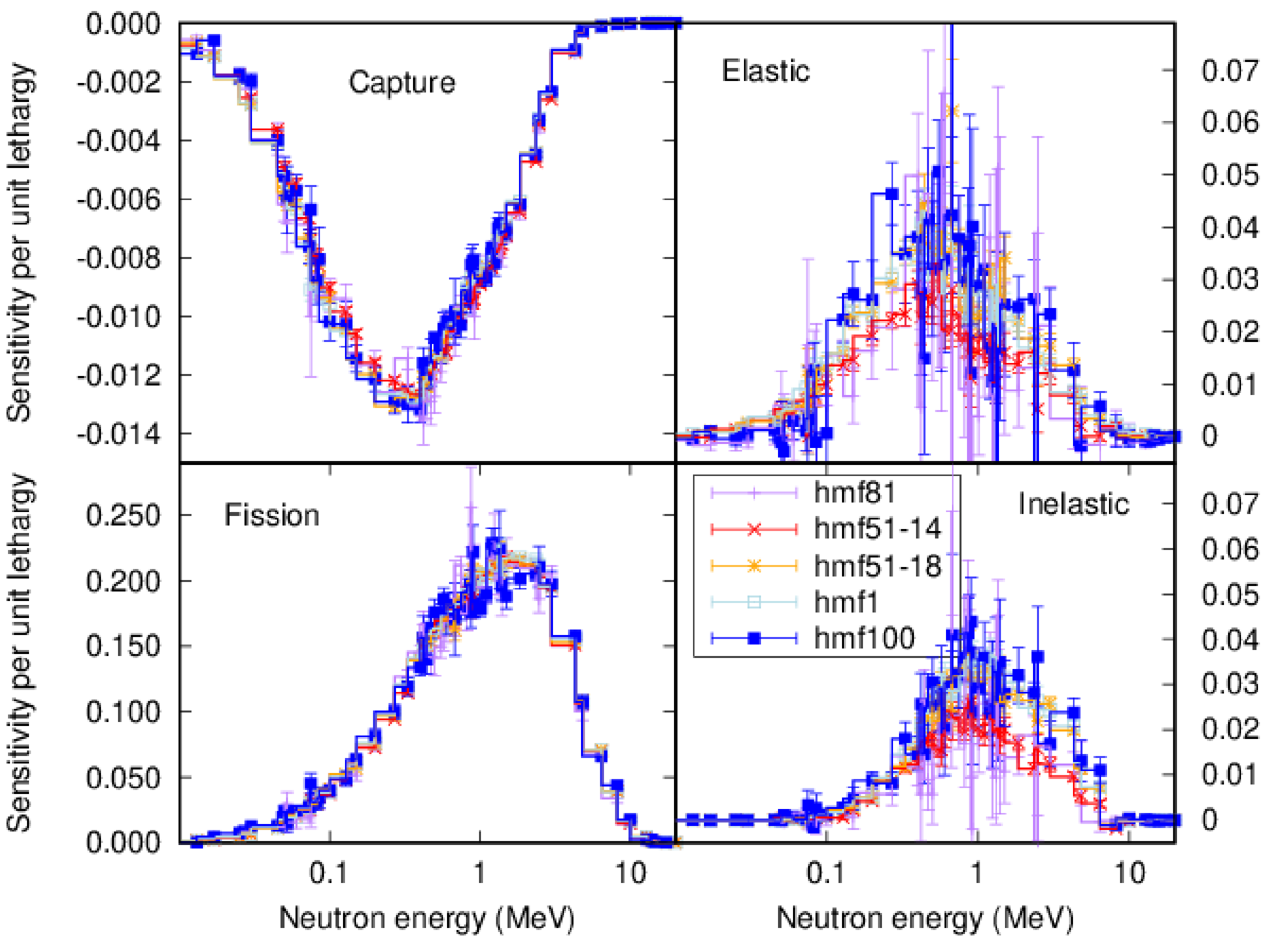

Figure 13. Sensitivity of several hmf benchmark cases to capture, fission, elastic and (n,n') cross sections of ^{235}U.

Benchmarks with HEU and U-nat or U-dep reflector

A next category of benchmarks is benchmarks with mostly HEU in combination with a natural or depleted uranium reflector. In other words, there is still (almost) only uranium, but now in different enrichments. The results for hmf14, hmf28 and hmf32 are shown in Figure 14. The various versions of JEFF, with the exception of JEF-2.2, perform similarly. The results for ENDF/B-VIII.0 are slightly lower.

The results for hmf32 do not show a monotonous trend, even though the radius of the HEU sphere increases from left to right in the Figure, with the thickness of the natural uranium reflector decreasing.

There are also hmf3 results for HEU with a depleted uranium reflector, see later (Figure 51).

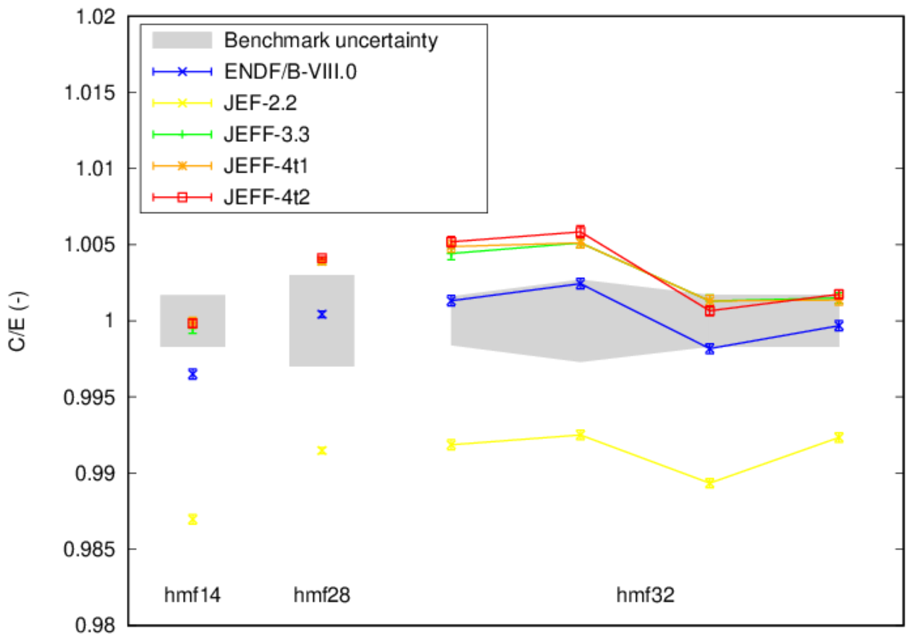

Figure 14. C/E results for benchmarks with HEU and a U-nat or U-dep reflector.

Benchmarks with IEU

Continuing with benchmarks that contain (almost) only uranium, there is also a category of benchmarks with intermediate enriched uranium. In the case of imf2 (16% enriched uranium cylinder with a natural uranium cylinder around it) and imf3 (a bare sphere of 36% enriched uranium), the benchmark models contain only uranium. The benchmark models of imf1 ('Jemima') and imf7 ('Big Ten') also contain small parts of other materials.

The results are shown in Figure 15. The same results are also shown in Figure 16 as a function of EALF. In the latter Figure also the benchmarks with HEU and a U-nat or U-dep reflector have been included. In other words, Figure 16 contains the results of benchmarks with sizable contributions from both U-235 and U-238, whereas Figure 12 contains the results for benchmarks with contributions mostly from U-235 only. It is noticeable that for Figure 12 there appears to be a trend of C/E with EALF, but for Figure 16 a similarly clear trend is not visible.

Overall there is quite reasonable agreement between calculated and benchmark values for all libraries except JEF-2.2, for which all calculated values are low for fast spectrum benchmarks with (almost) only uranium.

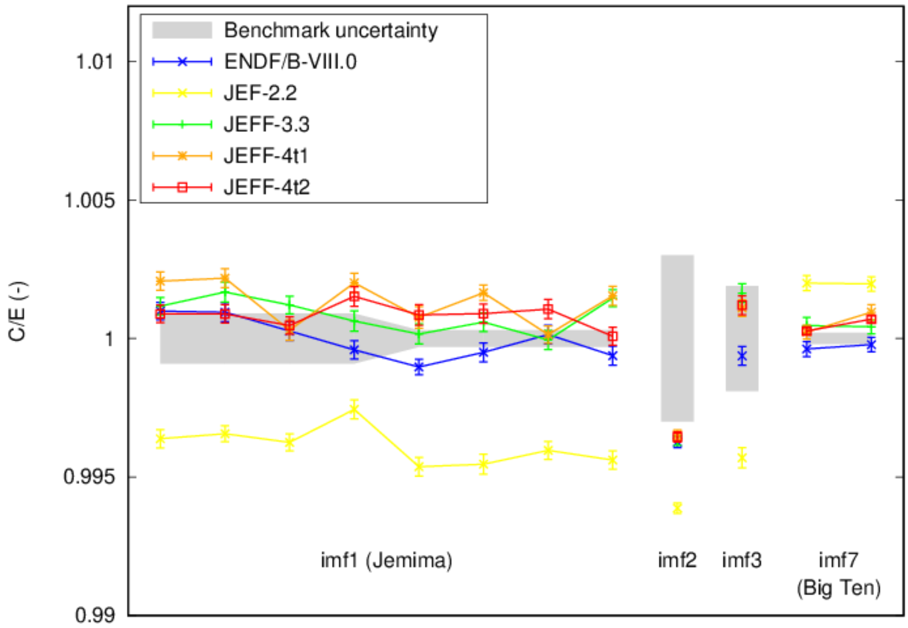

Figure 15. C/E results for IEU benchmarks with (almost) only uranium.

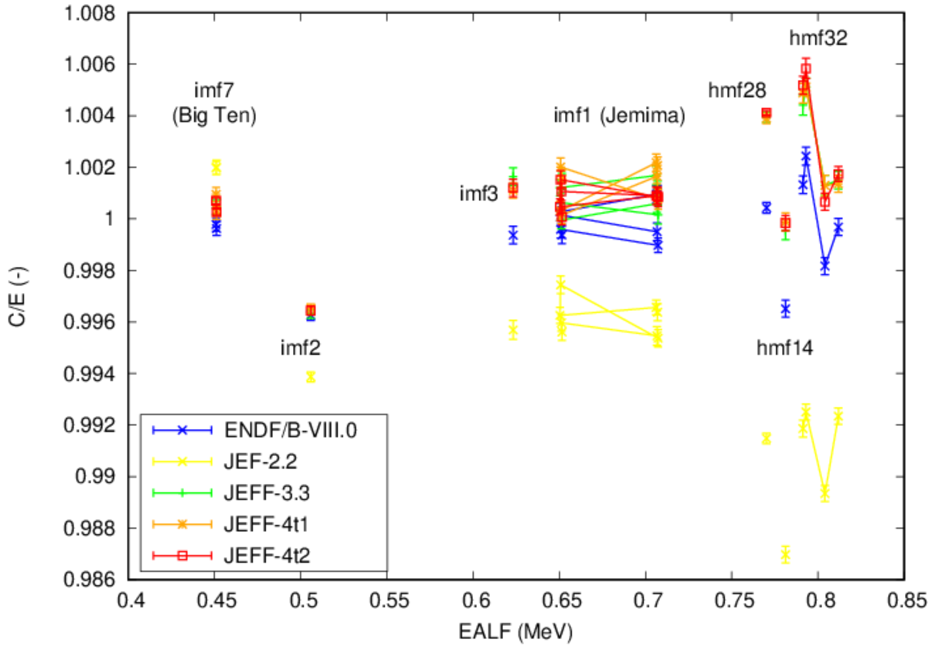

Figure 16. C/E results for IEU benchmarks with (almost) only uranium as a function of EALF. Also included are benchmarks with HEU and a U-nat or U-dep reflector.

5.1.2.2. Thermal cases

Benchmarks were selected that contain almost only uranium and water. In the case of lmt4 and lmt7 there is indeed only uranium and water, and in both cases the pitch of the lattice was varied, thereby varying the spectrum. The results for these two benchmarks are shown in Figure 17. It is clear from the Figure that for some libraries, most obviously for JEF-2.2, there is a clear trend of C/E with varying pitch. For the latest test version, JEFF-4t2, this trend has been mitigated; only for lmt7 there still is a downward slope in the Figure. In Figure 18 the sensitivity of selected cases to the capture and fission cross section of ^{235}U are shown.

In lct6, a benchmark with uranium and water and a small amount of aluminium, there is also variation of the pitch of the lattice. It can be seen from the results in Figure 19 that for some libraries, notably JEFF-3.3 and JEFF-4t1, there is a trend with the pitch of the lattice. For ENDF/B-VIII.0 and JEFF-4t2 there is no significant trend visible for this benchmark. A possible reason why there still is a visible trend for lmt7 in Figure 17 is that the range of pitch variation is wider, leading to a wider range of spectrum conditions in lmt7 compared to lct6. The spectra of both benchmarks are shown in Figure 20. While the peak at high energies is roughly similar for both benchmarks, but the height of the thermal peak varies more for lmt7. There is also a stark difference in the epithermal part of the spectrum, where case 6 of lmt7 has much lower values. The sensitivity to the capture cross section is similar for lmt4, lmt7, but lmt7 has a wider range of sensitivity to the fission cross section (Figure 18).

Also for lct7, a benchmark with similarities to lct6, there is a pitch variation. In this case there is no clear trend of the C/E results with the pitch. The range of spectrum conditions is shown in Figure 22, also compared to those in lmt7. Again the range of spectrum variation is greater in lmt7: the most thermalized case of lmt7 is almost reproduced by lct7, with lct7-1 being somewhat more thermalized. The case with the fastest spectrum of lct7 also approaches the spectrum of the case with the hardest spectrum in lmt7, with the lmt7 case having the harder spectrum. Several sensitivity profiles for lct7 case-1 and case-4 are shown in Figure 23. It is clear that there are differences in sensitivity in the thermal part of the spectrum for the ^{235}U fission cross section as well as the capture cross sections for ^{235,238}U and ^{1}H. Also evident are differences in sensitivity in the fast part of the spectrum to the elastic ^{1}H cross section and the fission and (n,n') ^{238}U cross sections. Finally there is also a clear difference in sensitivity to the ^{238}U capture cross section in the epithermal range

Lct39 is a benchmark with the same experimental device and the same rods, not with in each case a number of lattice positions left empty. The results shown in Figure 24 indicate no clear trends in the first 10 cases, but for cases 11 to 17 (at the right of the Figure) there is a slight upward trend for most libraries. These trends are, for most libraries, larger than the statistical uncertainty, which is shown in Figure 25. The difference between these cases is that a pattern of empty positions is located near the edge of the array for case 11, and then moves more and more towards the centre of the array; in case 17 it is almost at the centre. It was checked that the spectrum differences in the fuel (the average over all fuel rods) are very small between these cases, so it is at present not understood what causes the observed slight trend in C/E.

Another set of benchmarks is lct71 and lct72, again from the same experimental facility as lct7 and lct39. These benchmarks are called 'low moderated' and 'under-moderated' respectively. The results show differences in C/E for the two pitch values used in these two benchmarks, see Figure 26. The spectrum conditions in these benchmarks are compared to lmt7 in Figure 27: the spectrum in lct71 is harder than the hardest one from lmt7. So one could say that a combination of lct7 and lct71, possibly combined with lct39 and lct72 covers an even wider range of spectrum conditions than lmt7. The advantage of lmt7 is that one can compare results within one benchmark, avoiding to a large extent the issue of benchmark bias. Several sensitivity profiles for lct71 case-1 and lct72 case-1 are shown in Figure 28. Similar differences can be seen as in Figure 23: differences in sensitivity in the thermal part of the spectrum for the ^{235}U fission cross section as well as the capture cross sections for ^{235,238}U and ^{1}H. Also evident are differences in sensitivity in the fast part of the spectrum to the elastic ^{1}H cross section and the fission and (n,n') ^{238}U cross sections. Finally, there is also a clear difference in sensitivity to the ^{238}U capture cross section in the epithermal range.

There are also solution benchmarks with a limited number of materials. In Figure 29 the results for solution benchmarks lst3, lst4, lst7, lst16, lst17, lst20, and lst21 are shown. The benchmark models contain mostly uranyl nitrate solutions and a limited amount of vessel and support material. In spite of the similarity between these benchmarks, there are marked differences in C/E between them for all libraries. The spectrum in some of these benchmarks is plotted in Figure 30, the spectra in the others are similar. Also plotted is the spectrum in the most thermalized case of lmt7, for comparison. Clearly the spectrum in the solution benchmarks is softer, as expected. Sensitivity profiles for lst4-1 and lst16-1 are shown in Figure 31. These cases were selected because their C/E results are rather different. The sensitivity profiles are rather similar on the other hand, with the most clear difference being the ^{1}H capture cross section in the thermal range and, to a much smaller degree, the ^{235}U fission cross section in the thermal range.

Finally, there is also an HEU benchmark, hmt11, with a thermal spectrum and a limited number of other materials than uranium and water. The results for this benchmark are shown in Figure 32. The trend with variation of the pitch in this benchmark is rather pronounced for some libraries, but less so for others. A comparison of the spectrum in this benchmark with the spectrum in lmt7 is given in Figure 33. It shows that the most thermalized spectrum in hmt11 roughly matches that of lmt7, but also that the hardest spectrum in hmt11 is not as hard as in lmt7. The sensitivity of cases 1 and 9 of hmt11 to ^{235}U and ^{1}H cross sections is shown in Figure 34. It is interesting to note that the sensitivity of these cases with very different pitch to the ^{235}U capture cross section is similar, but to the ^{1}H cross section is quite different. Also, the sensitivity to the ^{235}U fission cross section is different for these two cases.

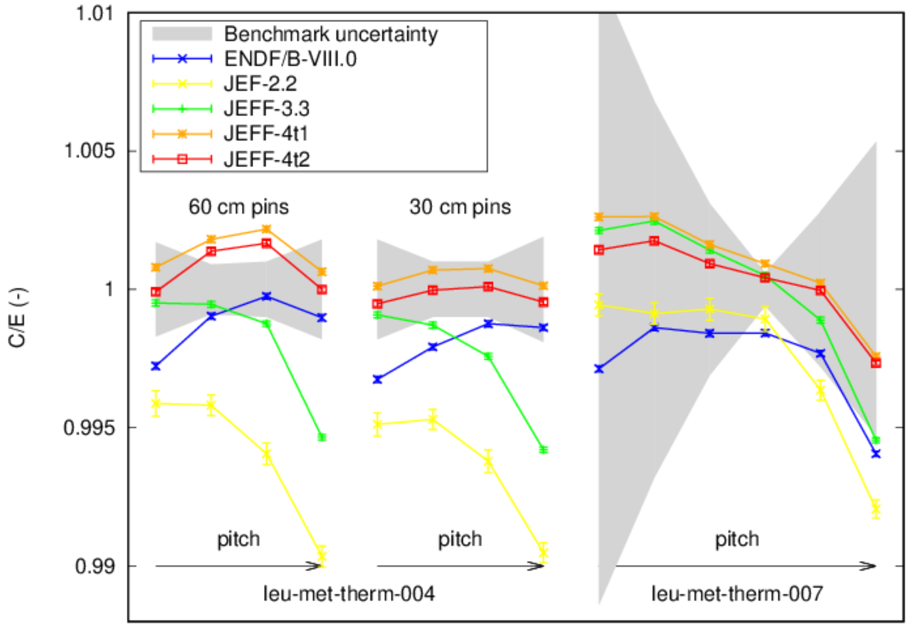

Figure 17. C/E results for lmt4 and lmt7: benchmarks with only water and uranium.

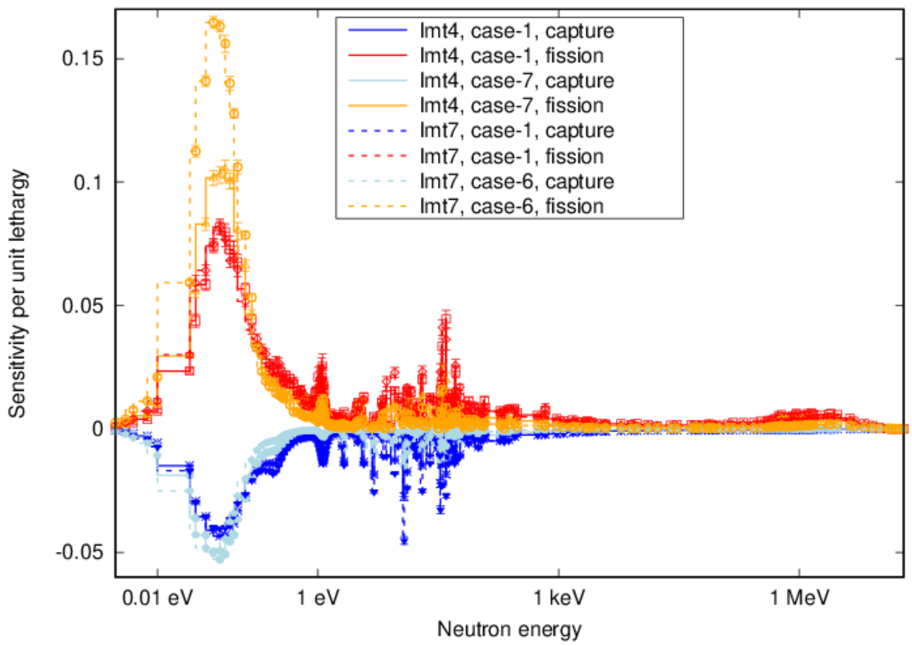

Figure 18. Sensitivity of lmt-4 and lmt7 to the capture and fission cross section of ^{235}U.

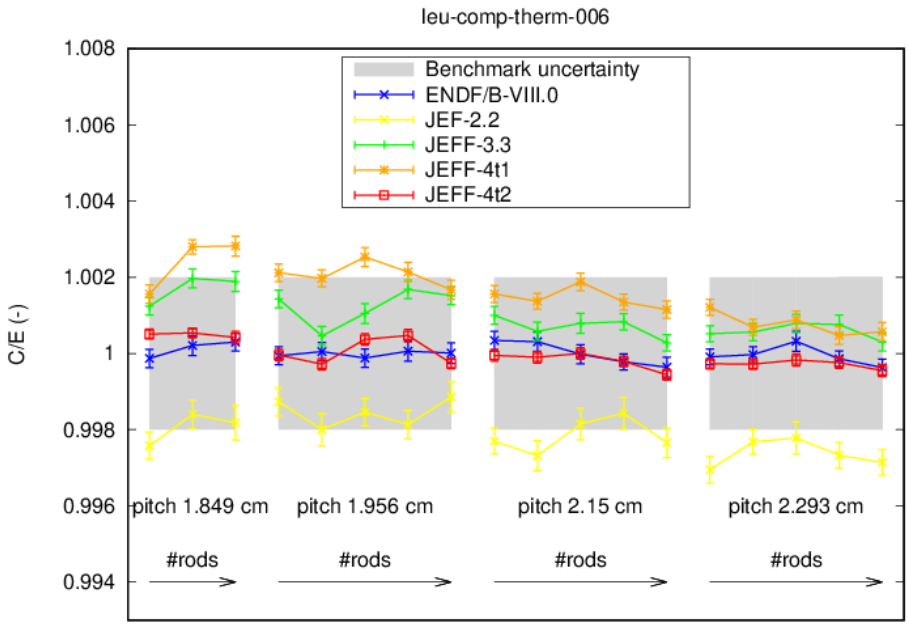

Figure 19. C/E results for lct6, a benchmark with mostly water and uranium.

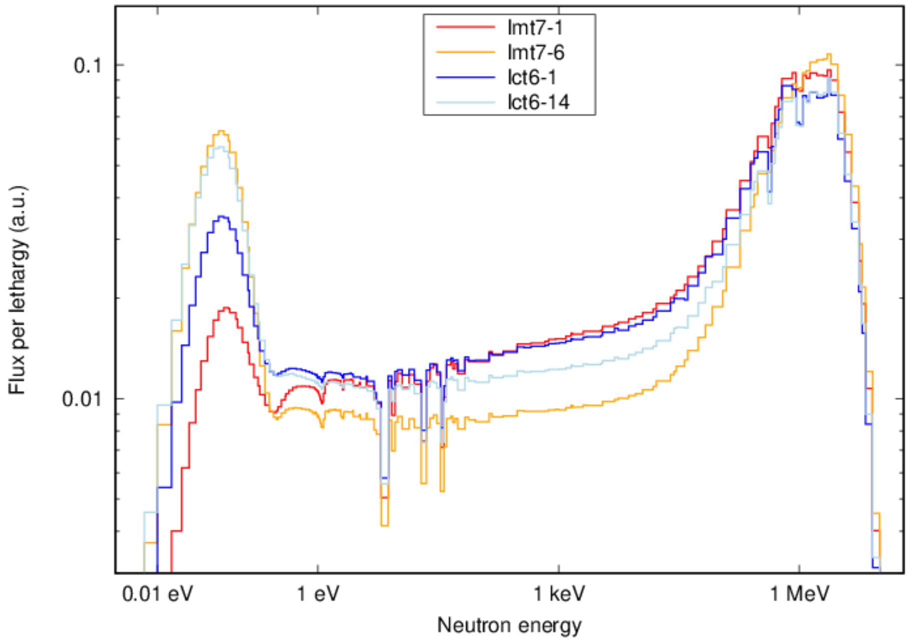

Figure 20. The spectra in the fuel for two cases of lmt7 and two cases of lct6.

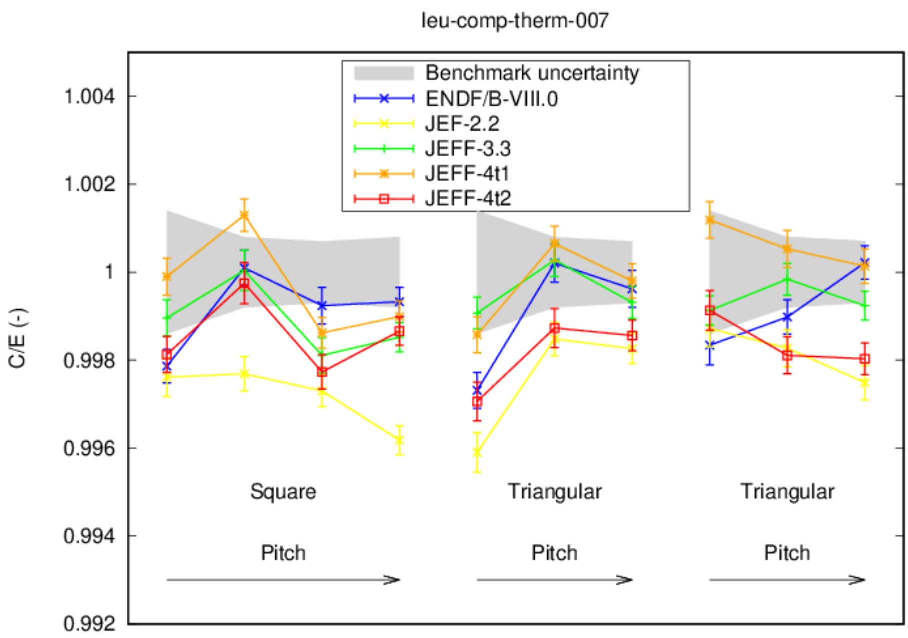

Figure 21. C/E results for lct7, a benchmark with mostly water and uranium.

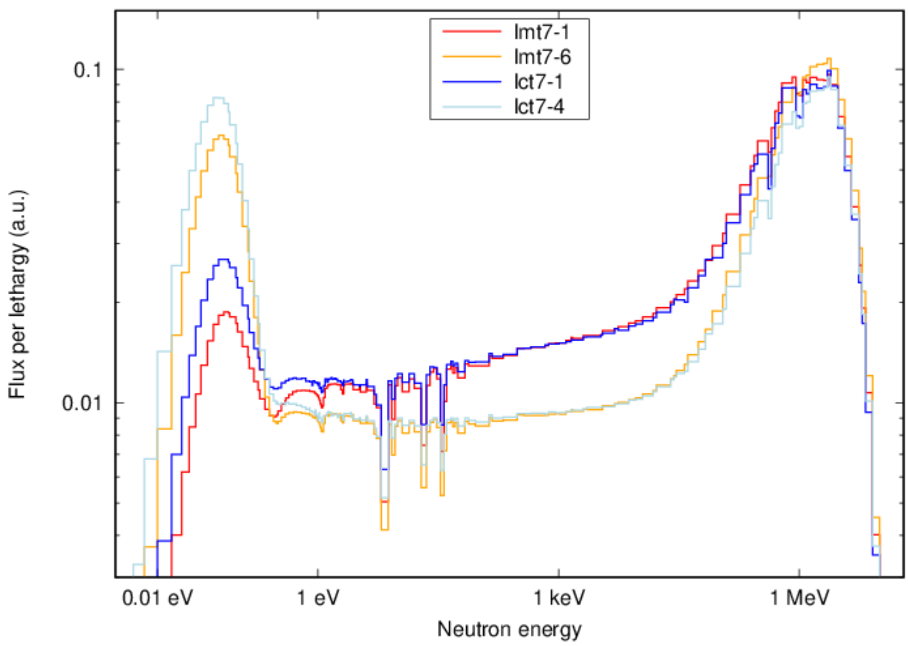

Figure 22. The spectra in the fuel for two cases of lmt7 and two cases of lct7.

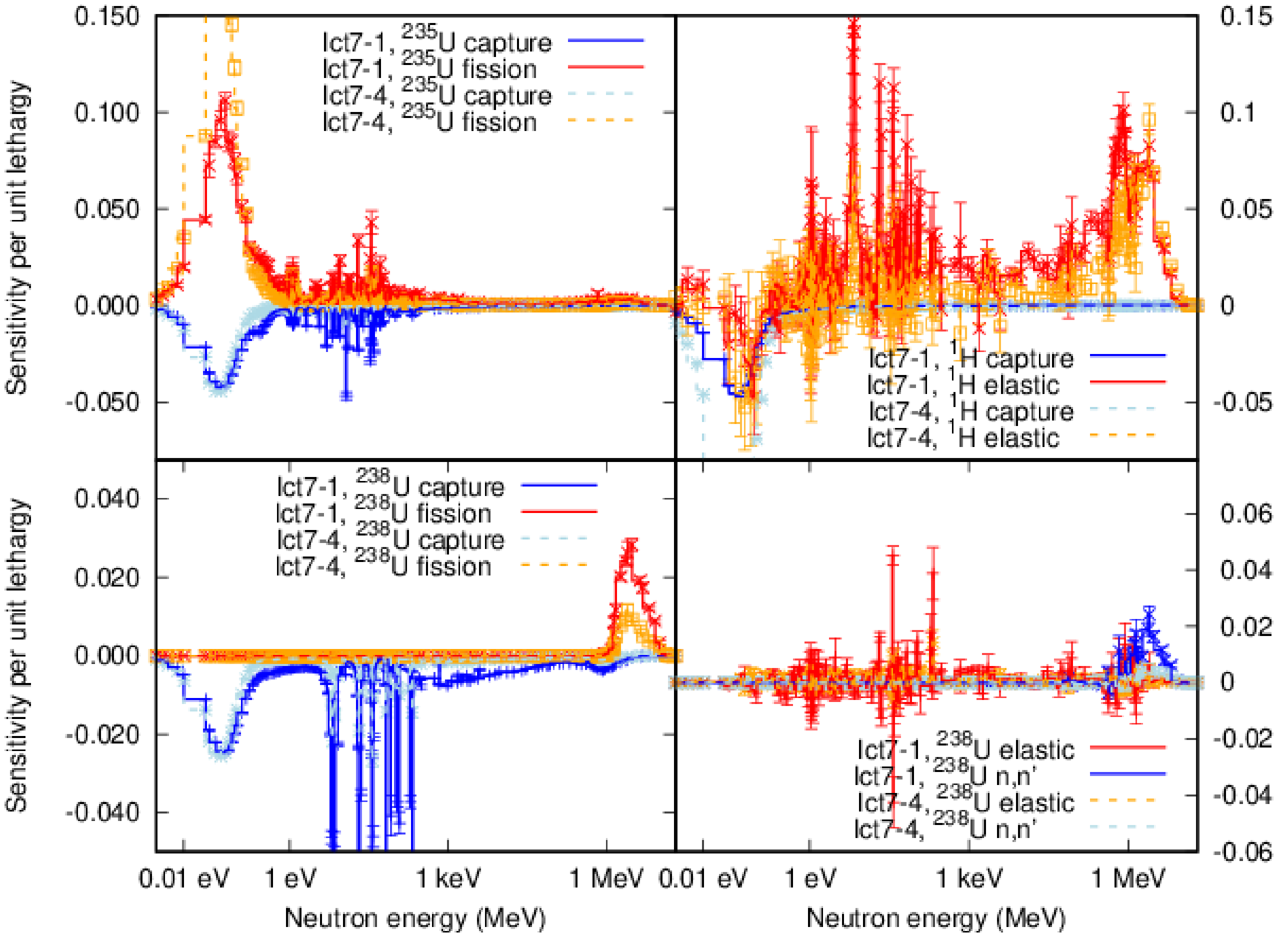

Figure 23. The sensitivity of lct7, cases 1 and 4, to several cross sections of ^{235,238}U and ^{1}H.

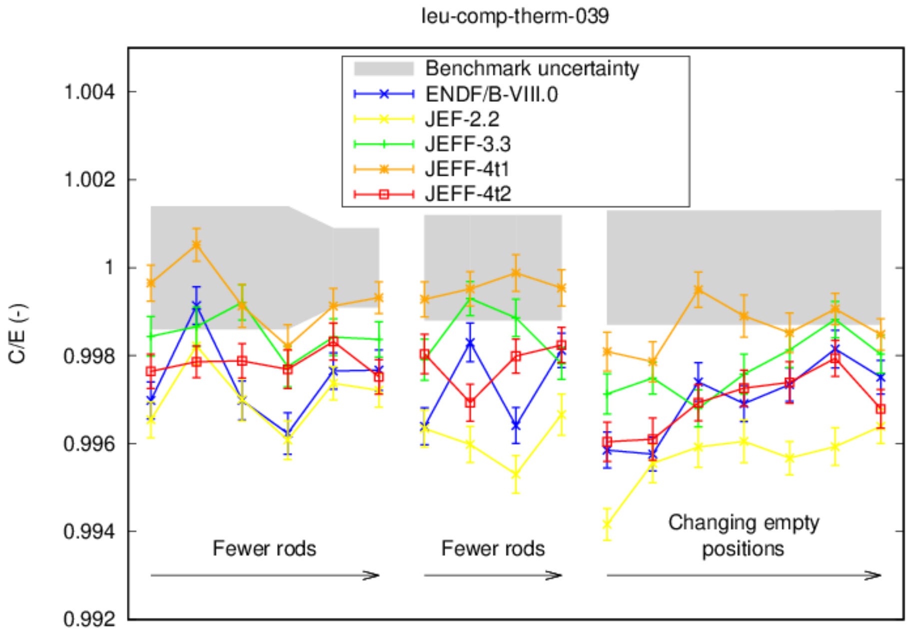

Figure 24. C/E results for lct39, a benchmark with mostly water and uranium.

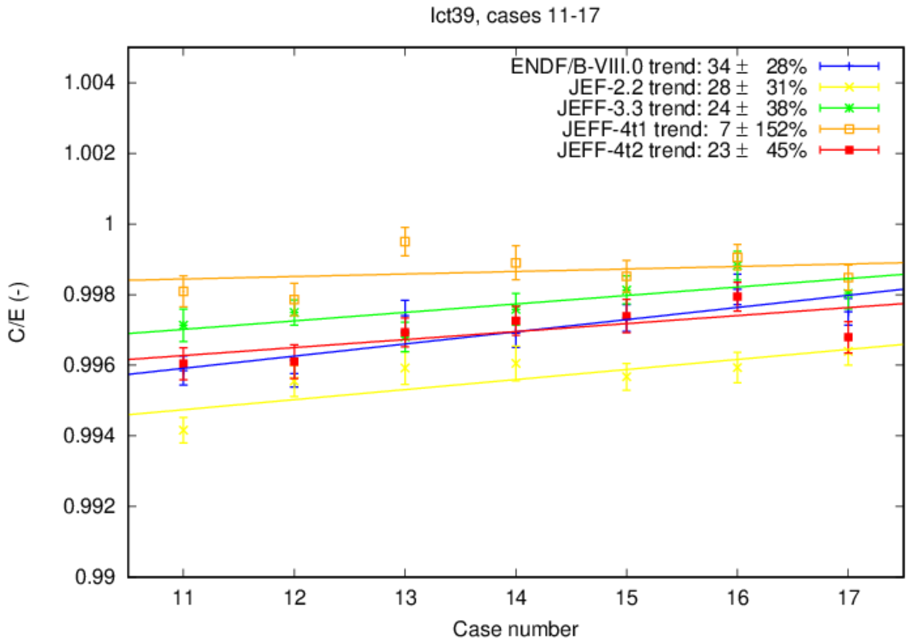

Figure 25. C/E results for lct39, cases 11-17. In case 11 the pattern of empty lattice positions is located at the edge of the core, and for higher case numbers the pattern is moved more and more towards the centre of the core.

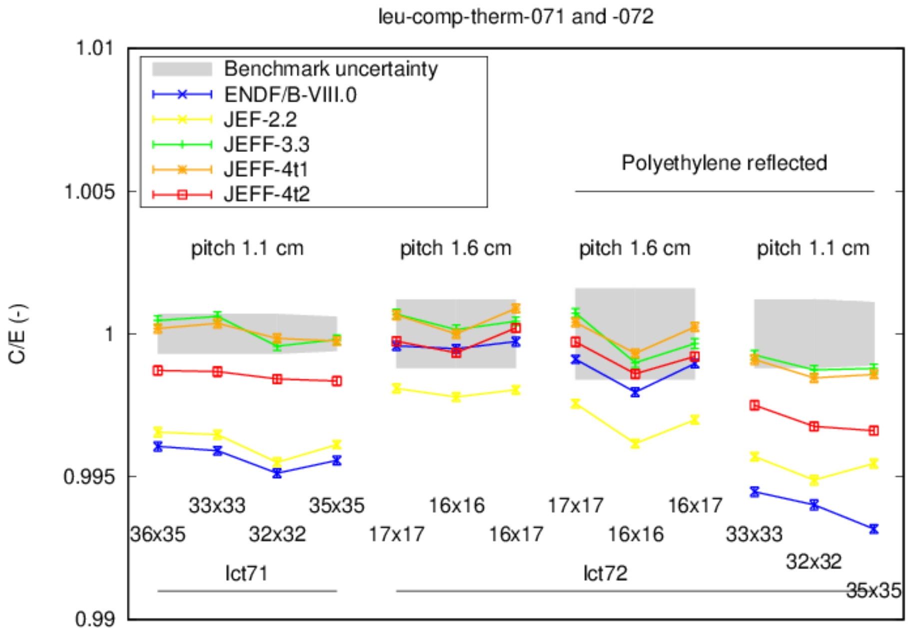

Figure 26. C/E results for lct71 and lct72, benchmarks with mostly water and uranium.

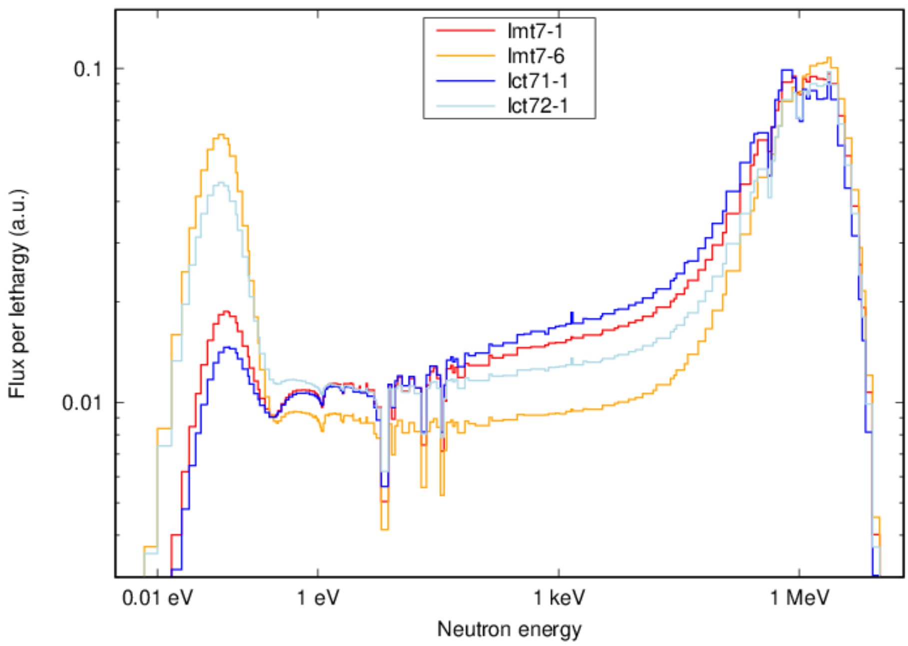

Figure 27. The spectra in the fuel for two cases of lmt7, one case of lct71 and one case of lct72.

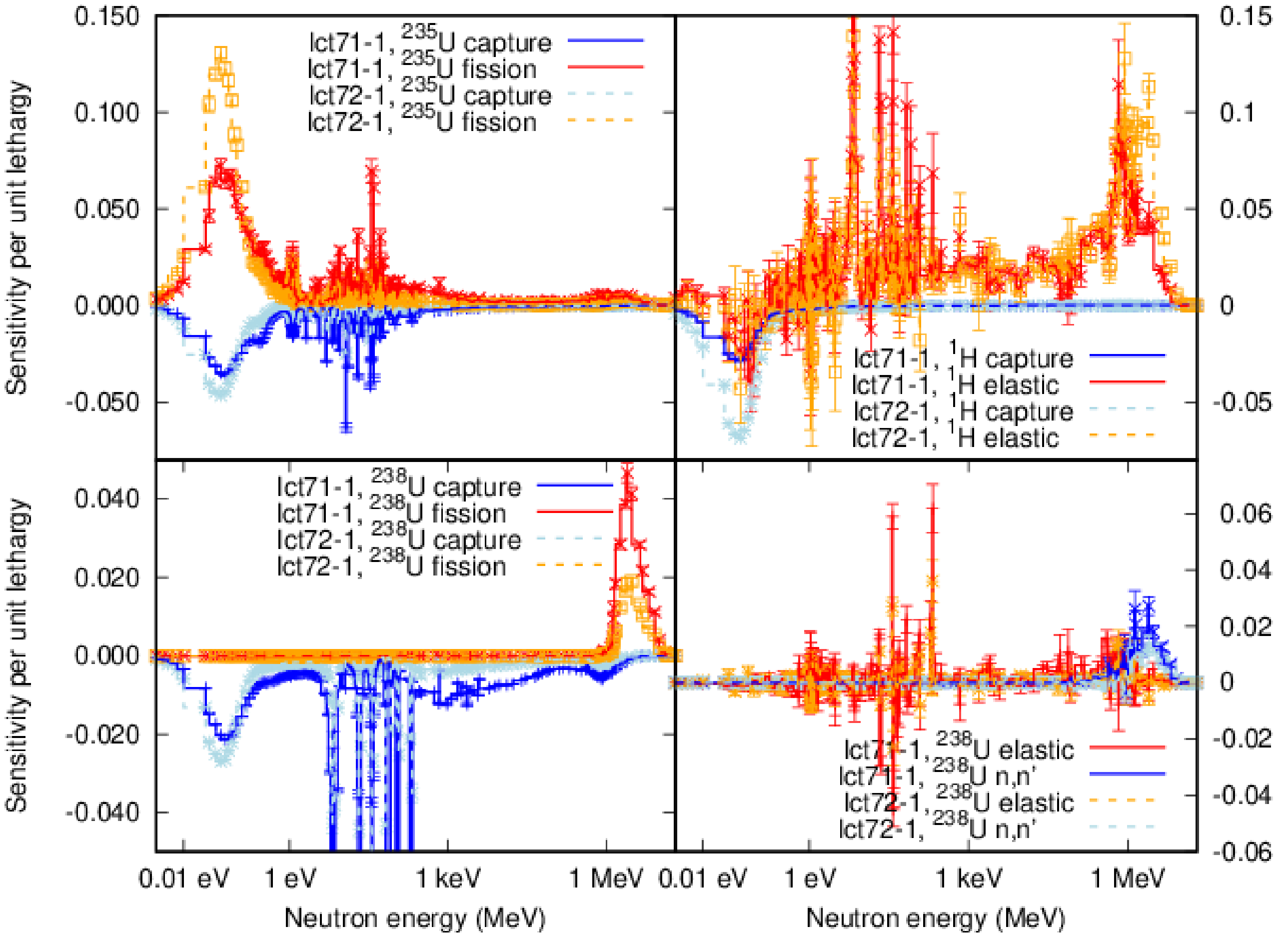

Figure 28. The sensitivity of lct71-1 and lct72-1 to several cross sections of $^{235,238}U$ and ^{1}H.

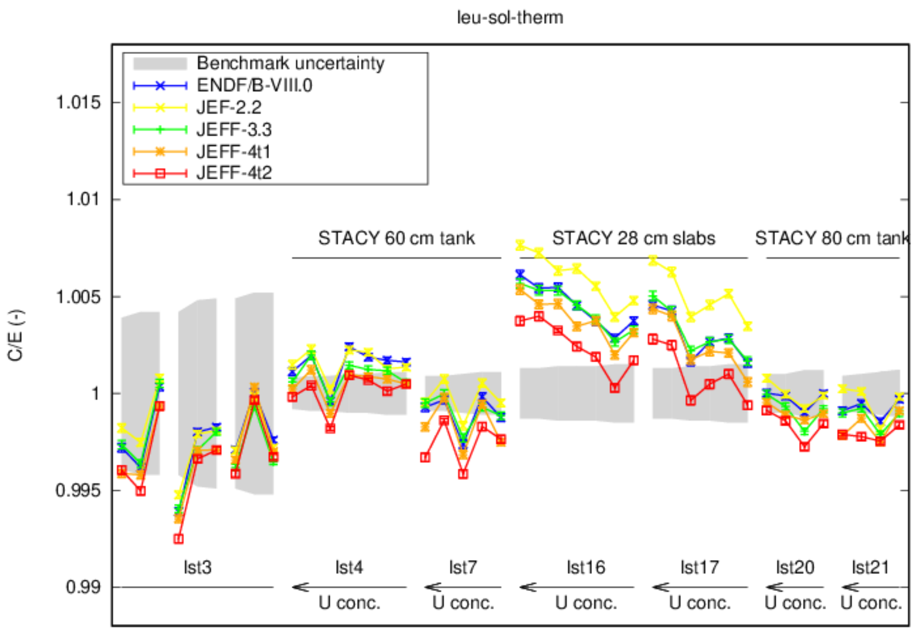

Figure 29. C/E results for several leu-sol-therm benchmarks with only uranium and uranyl nitrate solution.

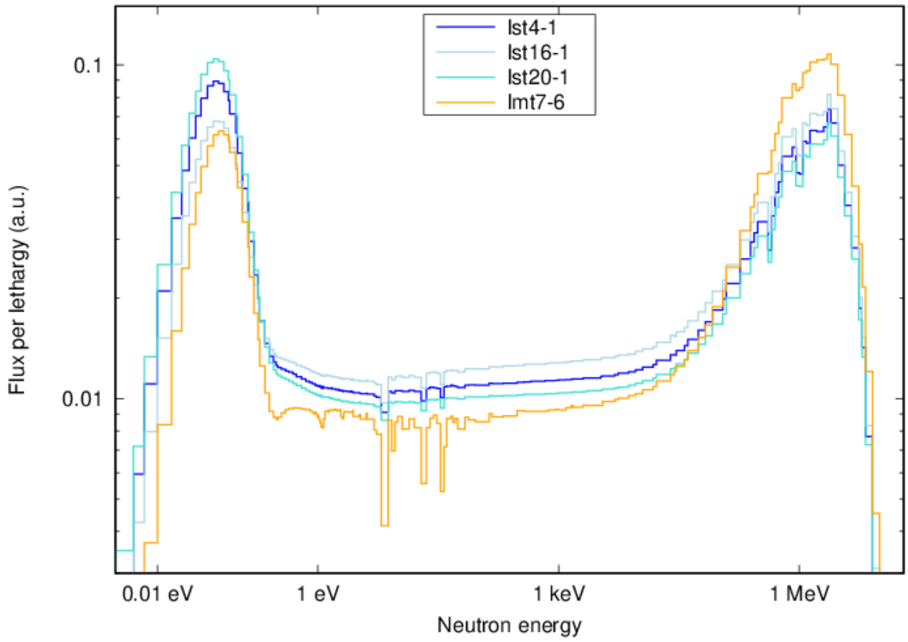

Figure 30. The spectra in the fuel for lst4, lst16, and lst20, compared to the spectrum in the most thermalized case of lmt7.

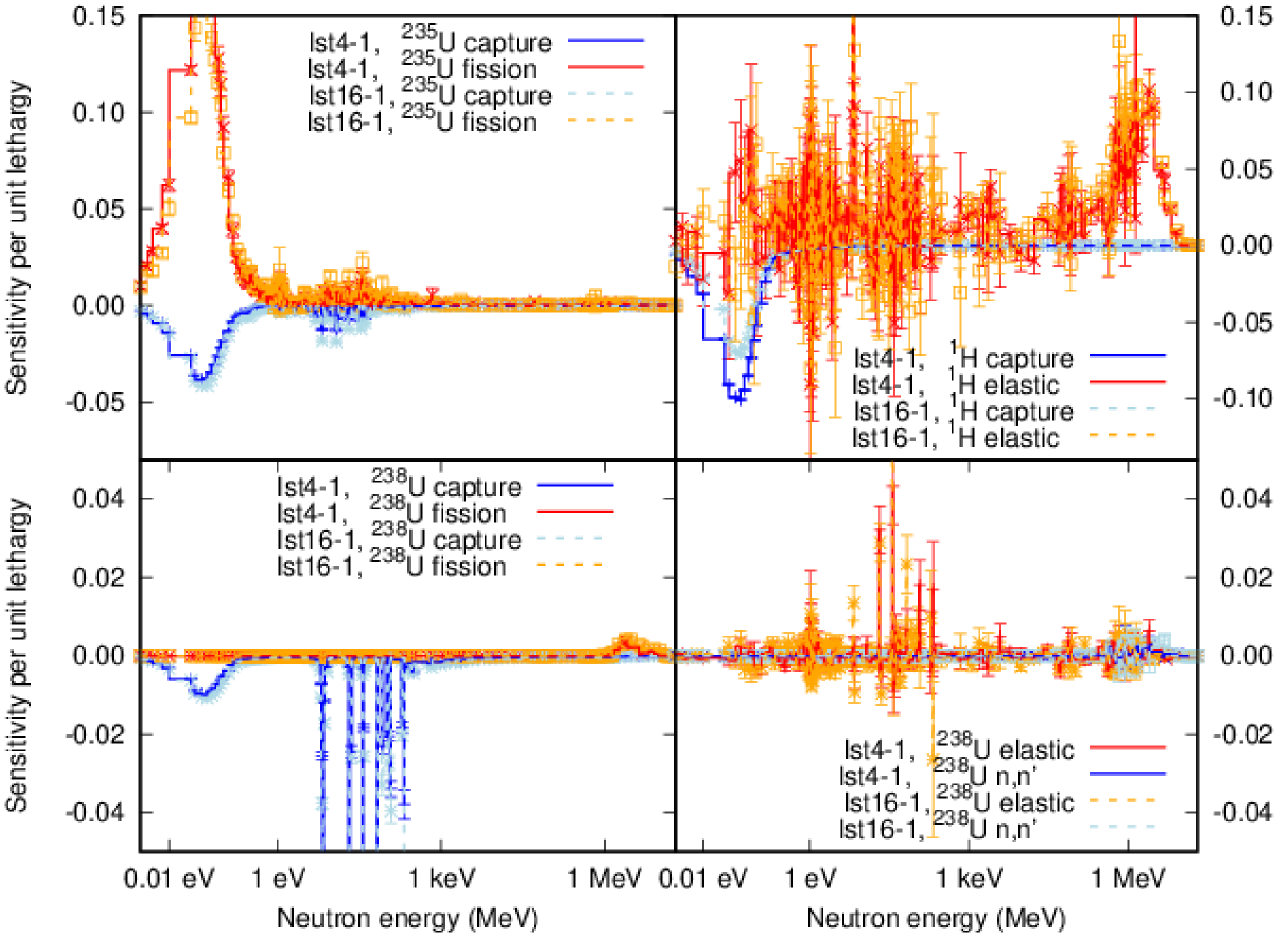

Figure 31. The sensitivity of lst4-1 and lst16-1 to several cross sections of ^{235,238}U and ^{1}H.

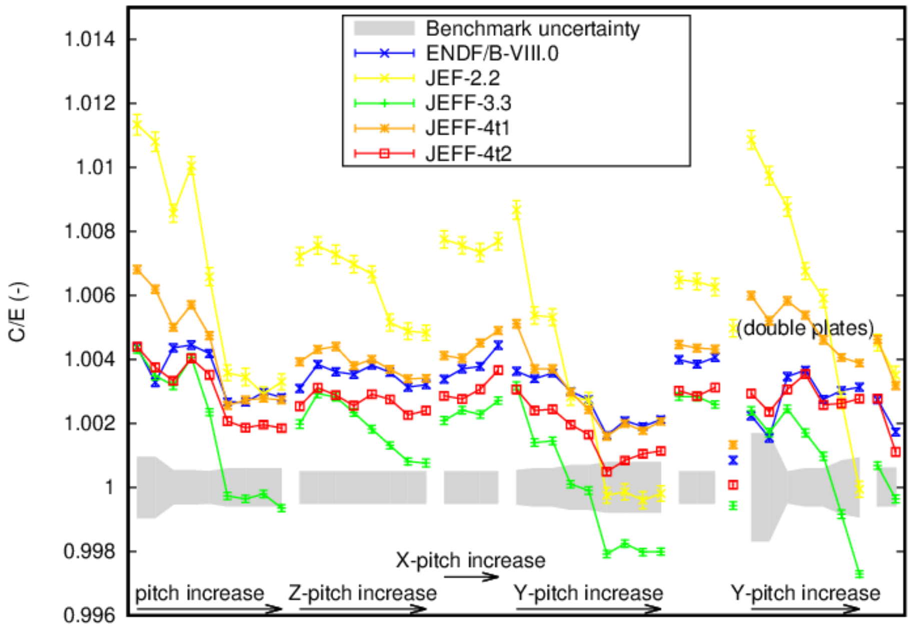

Figure 32. C/E results for hmt11, a benchmark with almost only water, uranium and a limited amount of polyethylene.

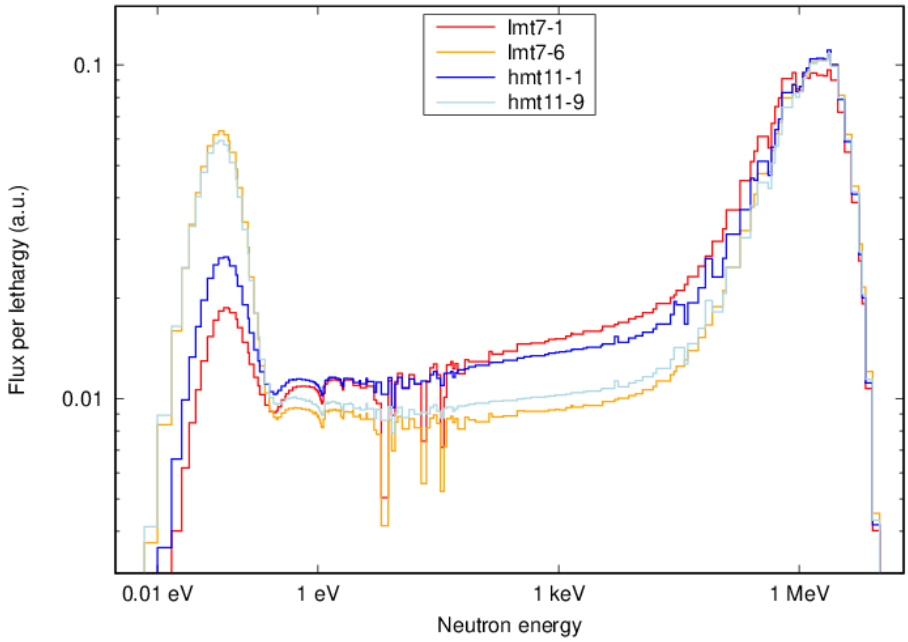

Figure 33. The spectrum in the fuel for two cases of hmt11 and two cases of lmt7.

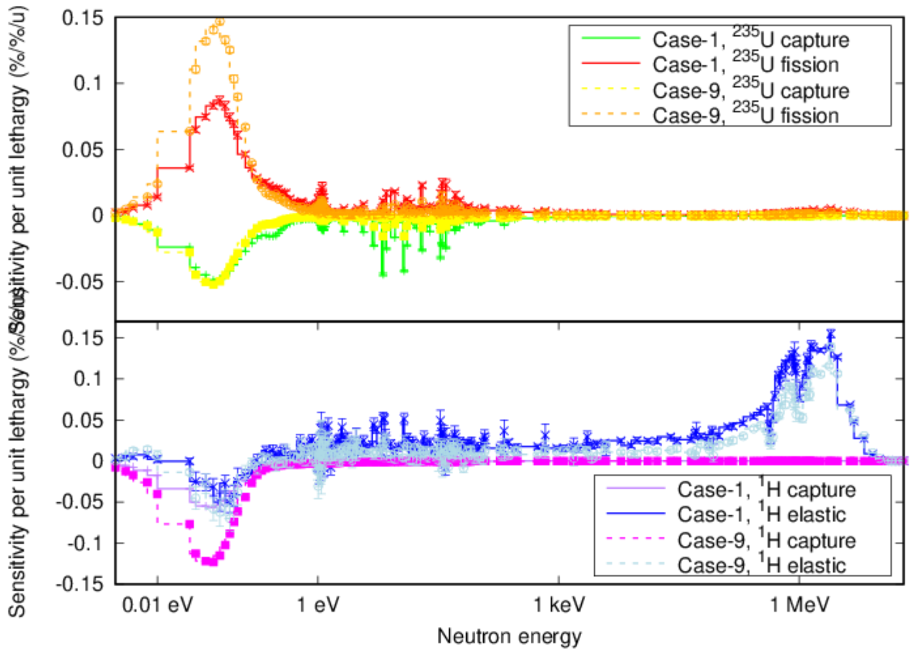

Figure 34. The sensitivity of hmt11 cases 1 and 9 to several ^{235}U and ^{1}H cross sections.

5.1.2.3. Mixed spectrum cases

Also investigated was the benchmark heu-comp-mixed-001, which has a wide variety of spectrum conditions. It consists of arrays of cans with uranium oxide reflected by polyethylene. There were four can types, of which the third and fourth contained alcohol as moderator. In some cases, there was no material in between the cans, in other cases there was Plexiglas between top and bottom layers of cans ('2D moderator'), while in the remaining cases there was Plexiglas between the cans in all directions ('3d moderator').

The results for hcm1 are shown in Figure 35. The results depend quite a bit on the case, in the same way for all libraries. In Figure 36 the same results are plotted as a function of the 'percentage thermal fission'. Also in this

Figure is a line to guide the eye, showing that in the intermediate region the C/E results are systematically lower than on either side of the Figure. The neutron spectrum of some of these cases is shown in Figure 37. The sensitivity to ^{235}U and ^{1}H cross sections are shown in Figure 38 and Figure 39 respectively. Next to some clear and expected differences, it is noticeable that for the case with the hardest spectrum, case-25, the sensitivities are different in the intermediate energy range, around 1 keV.

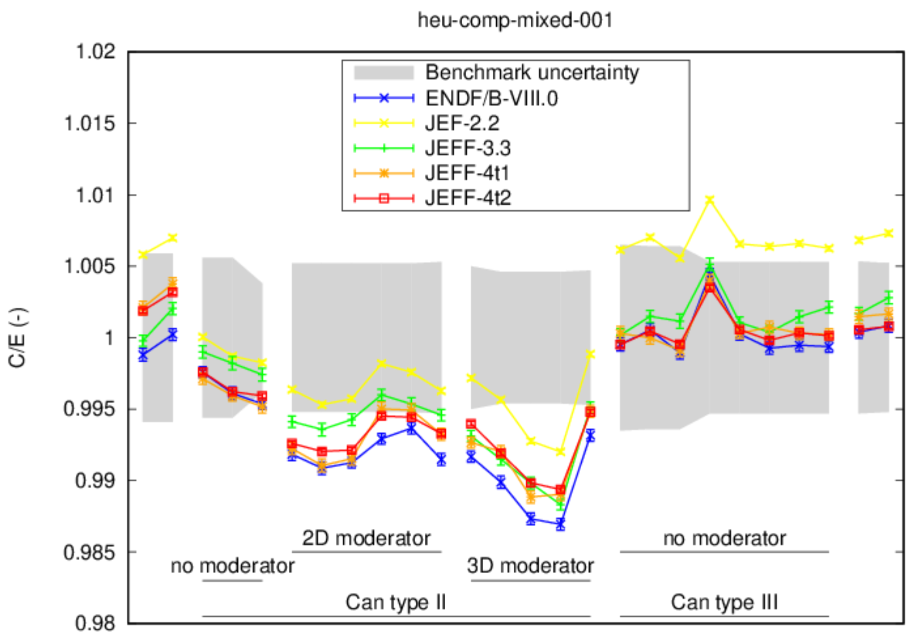

Figure 35. C/E results for hcm1, a benchmark with a wide range of spectrum conditions.

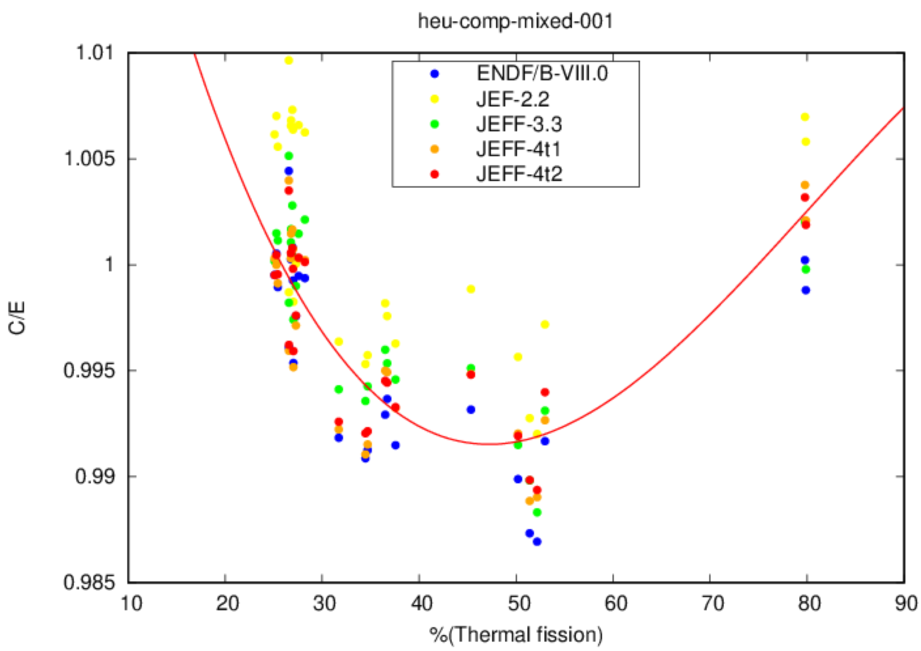

Figure 36. C/E results for hcm1 as a function of the percentage of fission that is caused by thermal neutrons.

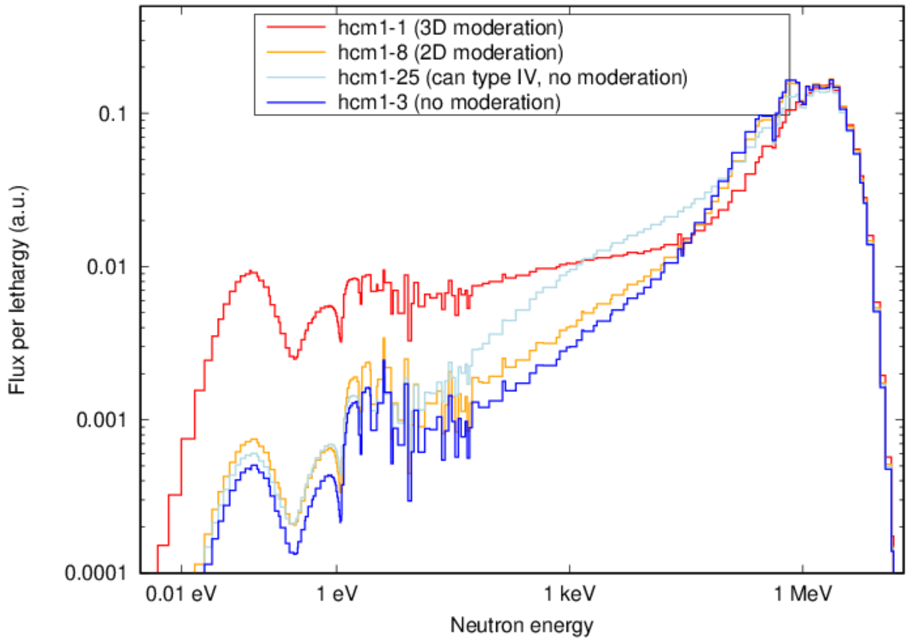

Figure 37. The spectrum for several cases of hcm1.

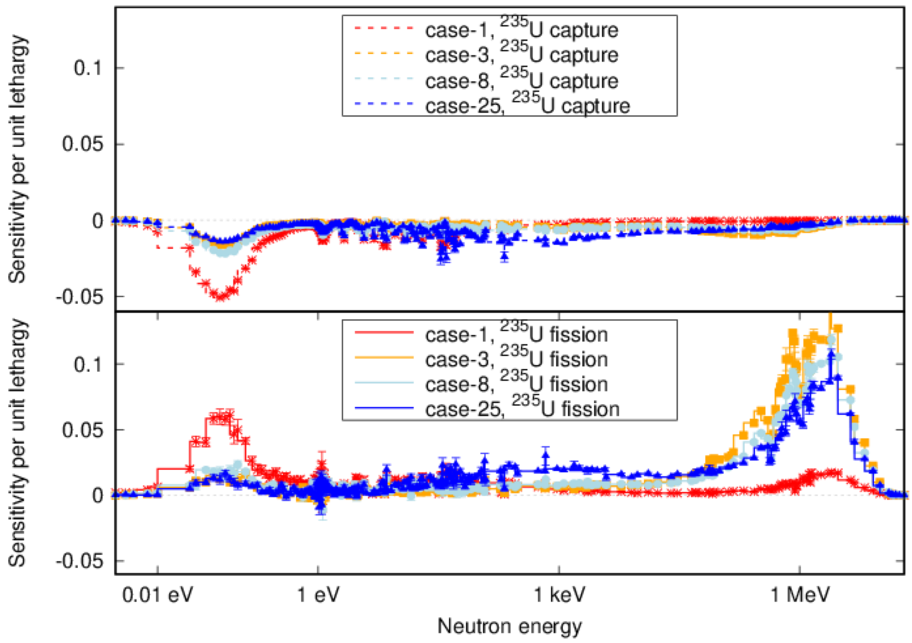

Figure 38. The sensitivity of four hcm1 cases to the capture and fission cross sections of ^{235}U.

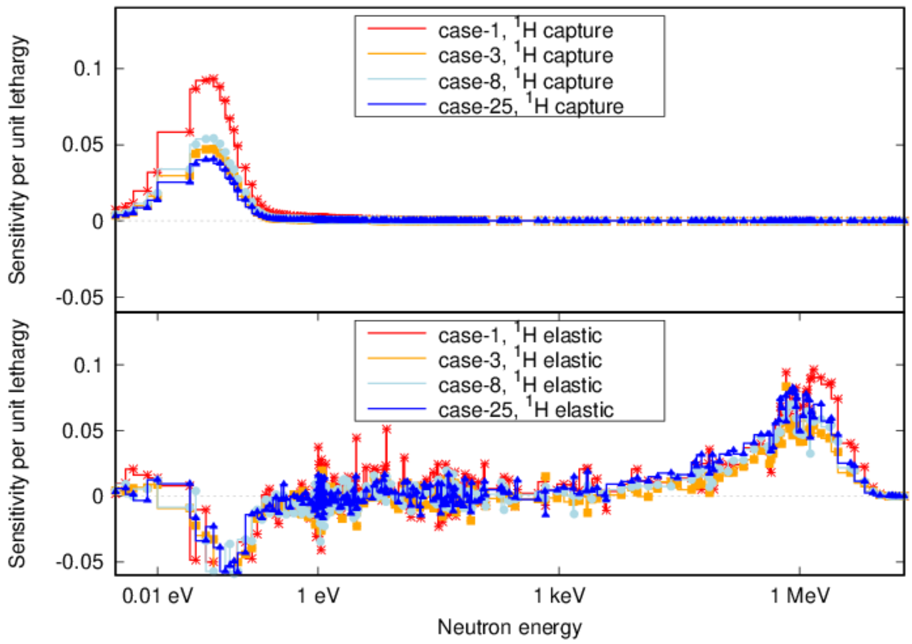

Figure 39. The sensitivity of four hcm1 cases to the capture and elastic cross sections of ^{1}H.

5.2. Plutonium cases

5.2.1. IRSN results

5.2.1.1. Fast cases

The results of selected cases involving plutonium in fast energy spectrum with various reflectors are reported in Figure 40. There is a general good agreement between the calculated k_{eff} and the benchmark one. C-E results lie within 2σ uncertainty margins of experimental uncertainties, except for pmf14-1 where a nickel reflector surrounds the sphere of plutonium. In this case, we can see a strong overestimation of JEFF-4.0T1, which is due to the evaluation of nickel.

The three nuclear data evaluations do not lead to significant discrepancy for pmf1 for which the plutonium sphere is unreflected. However, for some reflectors, discrepancies can be explained by the nuclear data evaluation of the reflector's element since k_{eff} is sensitive to this element (see Table 6 and Figure 41).

Table 6 Comparison JEFF-33/JEFF-4.0T1 – pmf systems

Selected case ICSBEP #	JEFF-33	JEFF-4.0T1	σ_{MC}	Element of the reflector (thickness)	JEFF-3.3 replaced by JEFF-4.0T1 for element
pmf5-1	1.00047	1.00410	0.00020	Tungsten (4.7 cm)	1.00296
pmf14-1	1.00302	1.02468	0.00020	Nickel (29.6 cm)	1.02402
pmf26-1	0.99679	1.00197	0.00020	^{56}Fe (11.9 cm)	1.00193
pmf28-1	0.99874	1.00414	0.00020	^{56}Fe (20 cm)	1.00467
pmf32-1	0.99658	0.99991	0.00020	^{56}Fe (4.5 cm)	0.99948
pmf44-4	0.9997	1.00442	0.00020	Aluminum (1 cm)	1.00478

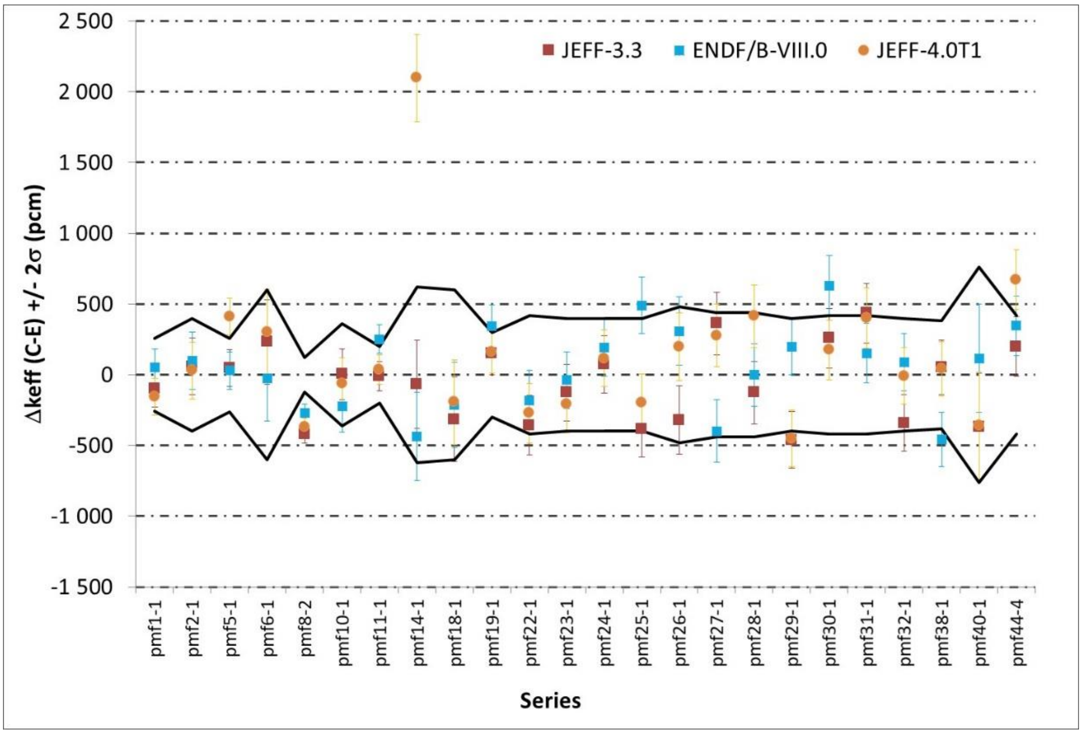

Figure 40. C-E results for metal systems with plutonium.

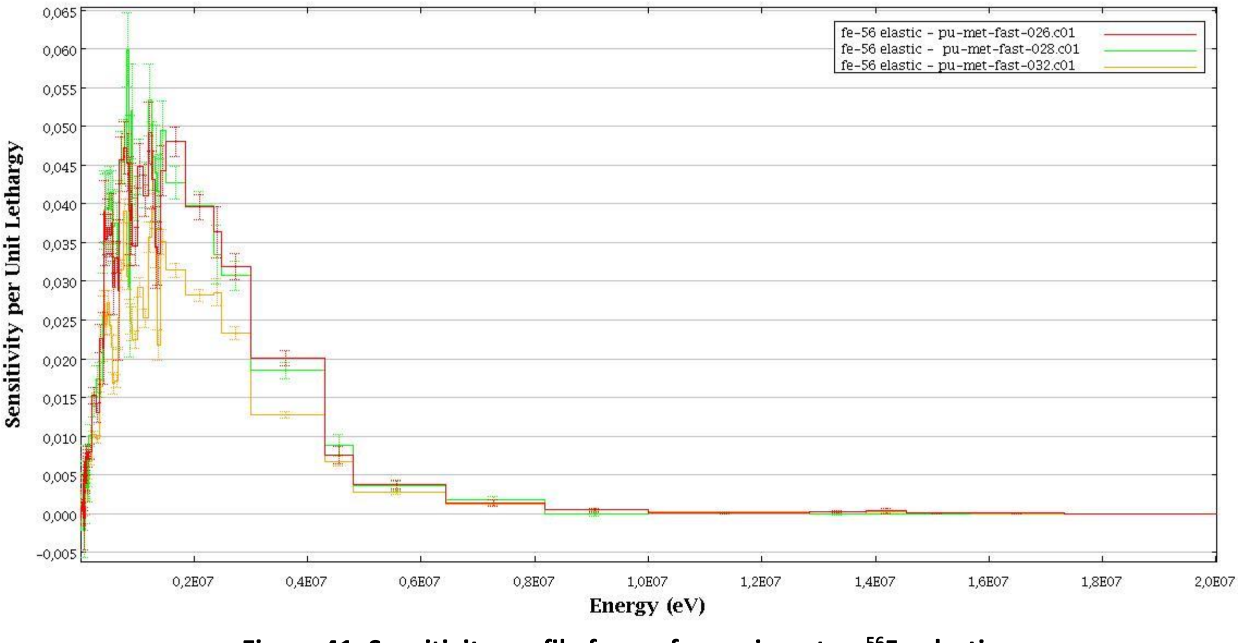

Figure 41. Sensitivity profile for pmf experiments – ^{56}Fe elastic

5.2.1.2. Thermal cases

The results of selected cases involving plutonium solutions are reported in Figure 42.
There is a general good agreement between the calculation k_{eff} and the benchmark k_{eff} (except for pst32-1) since the C-E stands within the 2σ level of experimental uncertainties.

The effect of nuclear data evaluation is quite limited except for pst12-1 and pst18-1, where we can see a difference between JEFF-33 and JEFF-4T1 nuclear data evaluations. The JEFF-4.0T1 evaluations of ^{16}O and ^{240}Pu are responsible for the decrease in k_{eff}. The k_{eff} decrease is even more significant for pst18 since the content in ^{240}Pu is higher.

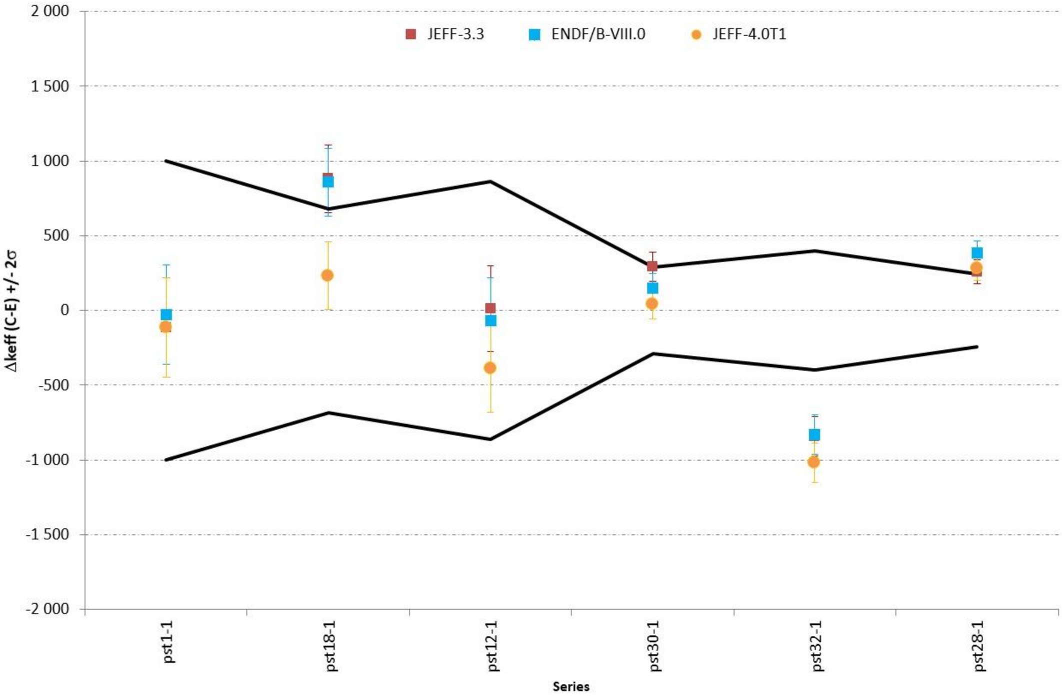

Figure 42. C-E results for solutions with plutonium.

5.2.2. NRG results

For cases with plutonium there are no results based on JEFF-4t2 available due to a problem with the ^{239}Pu ACE file (the MCNP run would crash with a segmentation fault).

Results for a range of fast spectrum cases are shown in **Erreur ! Source du renvoi introuvable.**. These results are mostly for simple benchmark, consisting of a plutonium sphere or cylinder, with or without a reflector. For almost all cases the results are within the range of the benchmark uncertainty or close to it. The most notable exceptions are JEFF-4t1 results for cases with Ni (e.g. pmf5) or Al (pmf-5) in the reflector. This was also seen for uranium benchmark with such reflectors. Other exceptions are JEF-2.2 results for cases with uranium reflectors (pmf6, pmf10, pmf20, and pmf41).

The benchmark series pmf44 has five different reflectors. Results for this benchmark are shown in **Figure *44***. Also here the cases with an aluminium reflector has a high result for JEFF-4t1. Benchmark series pmf45, **Figure *45***, has several cases with Ni and Fe reflectors. As seen before, the JEFF-4t1 results for the cases with Ni reflectors deviate substantially from the benchmark values.

One thermal spectrum benchmark with plutonium is presented in this section: pu-sol-therm-034, a plutonium nitrate solution with a varying amount of gadolinium. The results in **Figure *46*** show that for most libraries the results are within, or close to, the experimental uncertainty range. The results exhibit a slight trend with the gadolinium concentration. This trend is visible for both levels of plutonium concentration in the solution. For most libraries this trend is downward with increasing Gd concentration, but for JEFF-3.3 the trend is upwards.

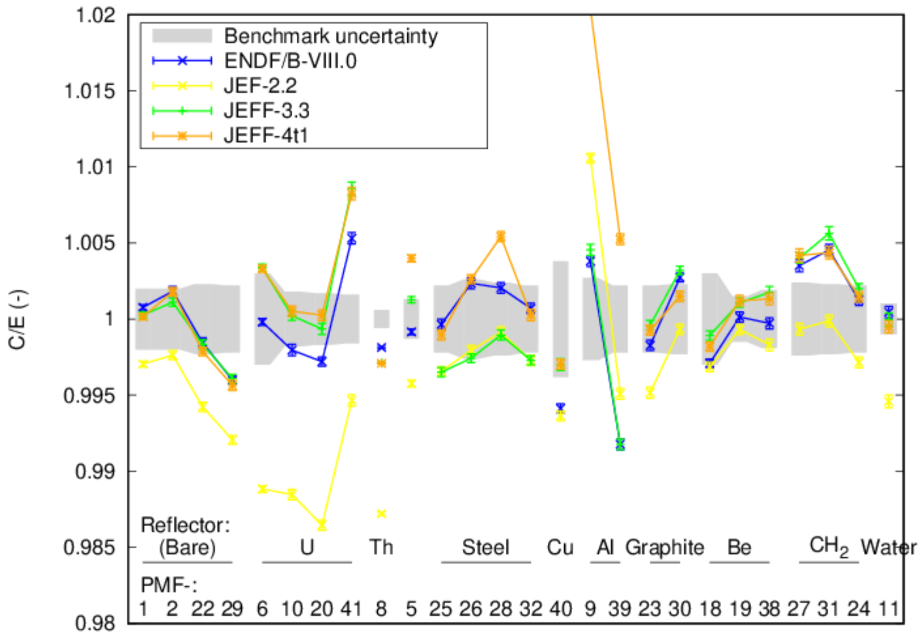

Figure 43. C/E results for pu-met-fast benchmarks. On the left of the Figure are four benchmarks with bare uranium spheres, all the other benchmarks consist of a uranium sphere with a reflector around it. The number of the benchmark is indicated at the bottom, e.g. the three left-most benchmarks are pmf1, pmf2, and pmf22.

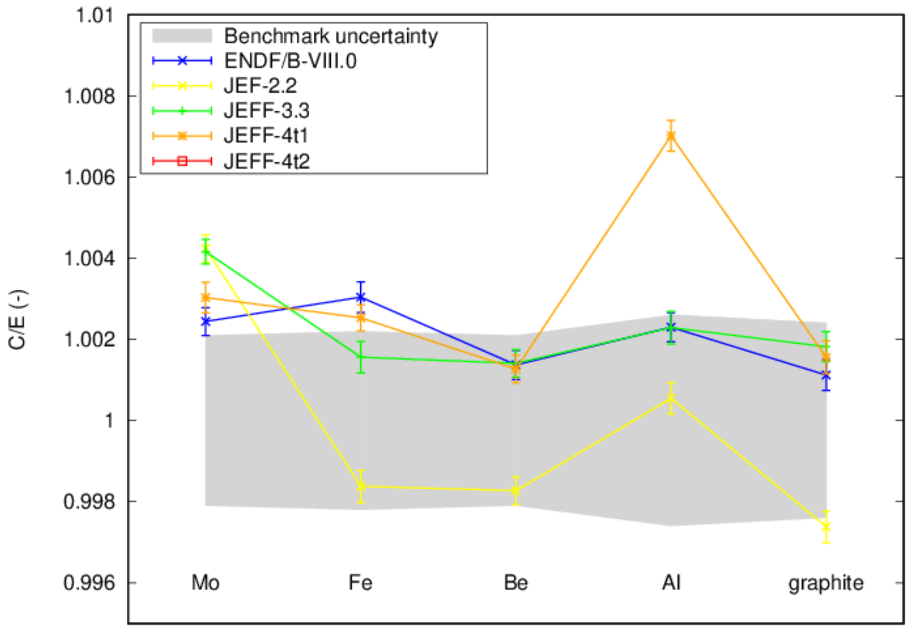

Figure 44. C/E results for pmf44, a plutonium sphere with five different reflectors.

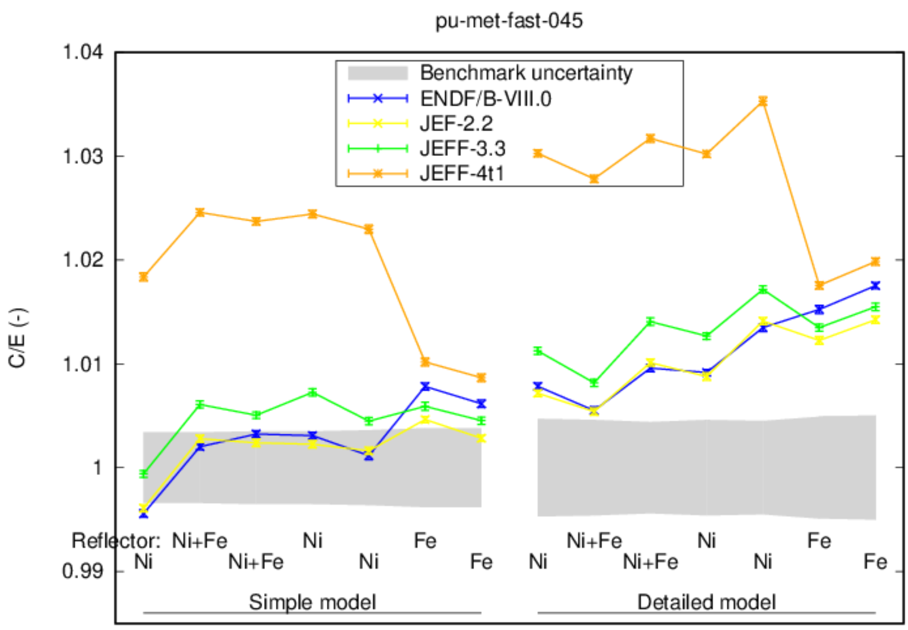

Figure 45. C/E results for pmf45, based on the Los Alamos Molten Plutonium reactor (LAMPRE).

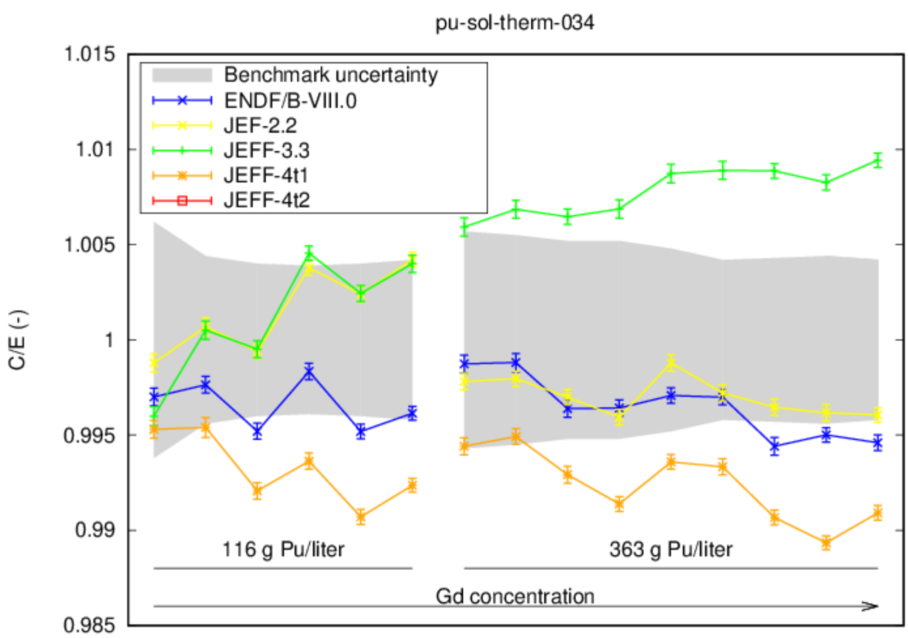

Figure 46. C/E results for pst34, a plutonium nitrate solution with gadolinium.

5.3. Mixed Uranium-plutonium cases

5.3.1. IRSN results

The results of selected cases involving mixed uranium and plutonium lattices of rods are reported in Figure 47. All k_{eff} results are in good agreement with the benchmark k_{eff}. There is a general good agreement between the calculation k_{eff} and the benchmark k_{eff} since the C-E stands within the 2σ level of experimental uncertainties.

No significant effect of the nuclear data evaluation can be pointed out.

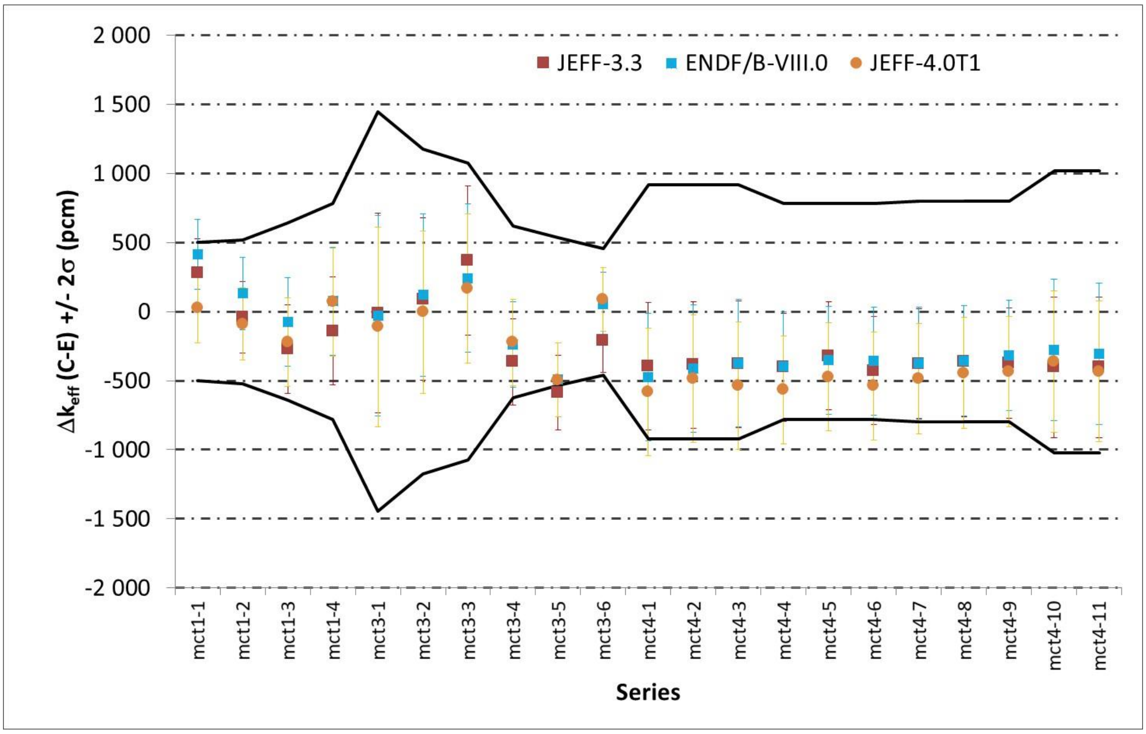

Figure 47. C-E results for mixed uranium and plutonium lattices of rods.

5.3.2. NRG results

No NRG results are presented for this category.

5.4. U233

5.4.1. IRSN results

The results of selected cases involving U233 in fast energy spectrum are reported in Figure 48.
The results of selected cases involving U233 in epithermal energy spectrum are reported in Figure 49.
The results of selected cases involving U233 in thermal energy spectrum are reported in Figure 50.

There is a general good agreement between the calculation k_{eff} and the benchmark k_{eff} for the fast energy range since the C-E stands within the 2σ level of experimental uncertainties. Results with JEFF-4T1 are consistent with the ones using JEFF-3.3 except for U233-MET-FAST-004-001 and 002 (tungsten reflector).

There is a tendency to largely under-estimate k_{eff} for experiments in the epithermal energy range. Moreover, the JEFF-4T1 results are consistent with the JEFF-3.3 and ENDF/B-VIII.0 results.

There is a general good agreement between the calculation k_{eff} and the benchmark k_{eff} for the thermal energy range since the C-E stands within the 2σ level of experimental uncertainties. Results using JEFF-4T1 are generally in slightly better agreement with results using ENDF/B-VIII.0 than with results using JEFF-3.3.

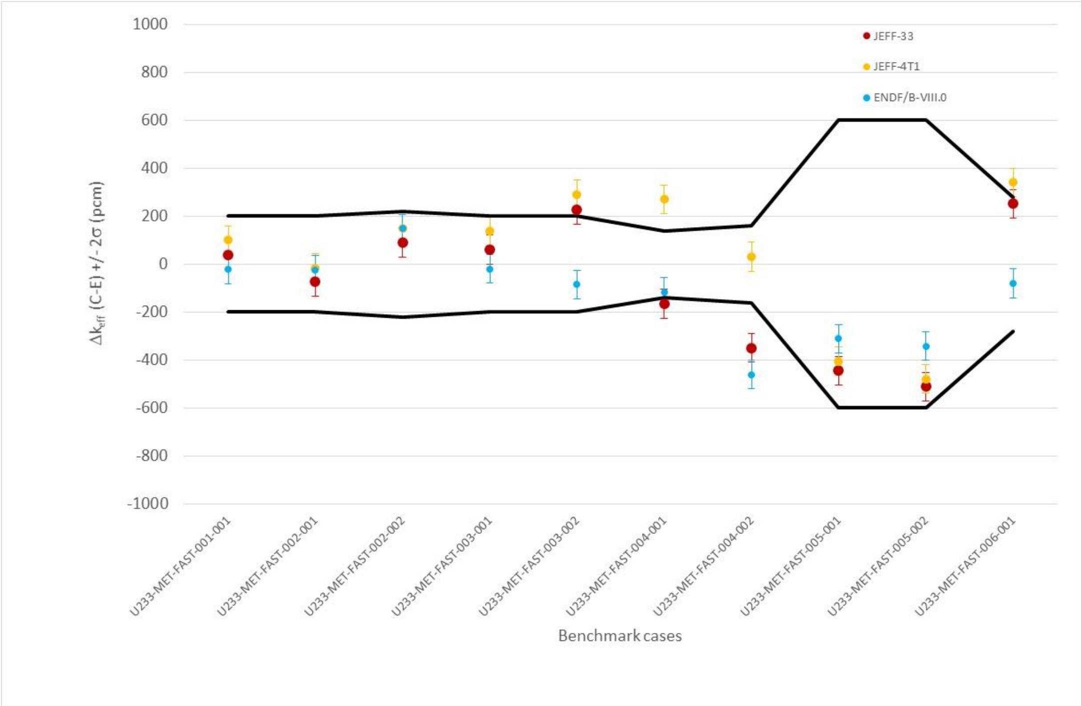

Figure 48. C-E results for experiments with U233 – FAST energy range.

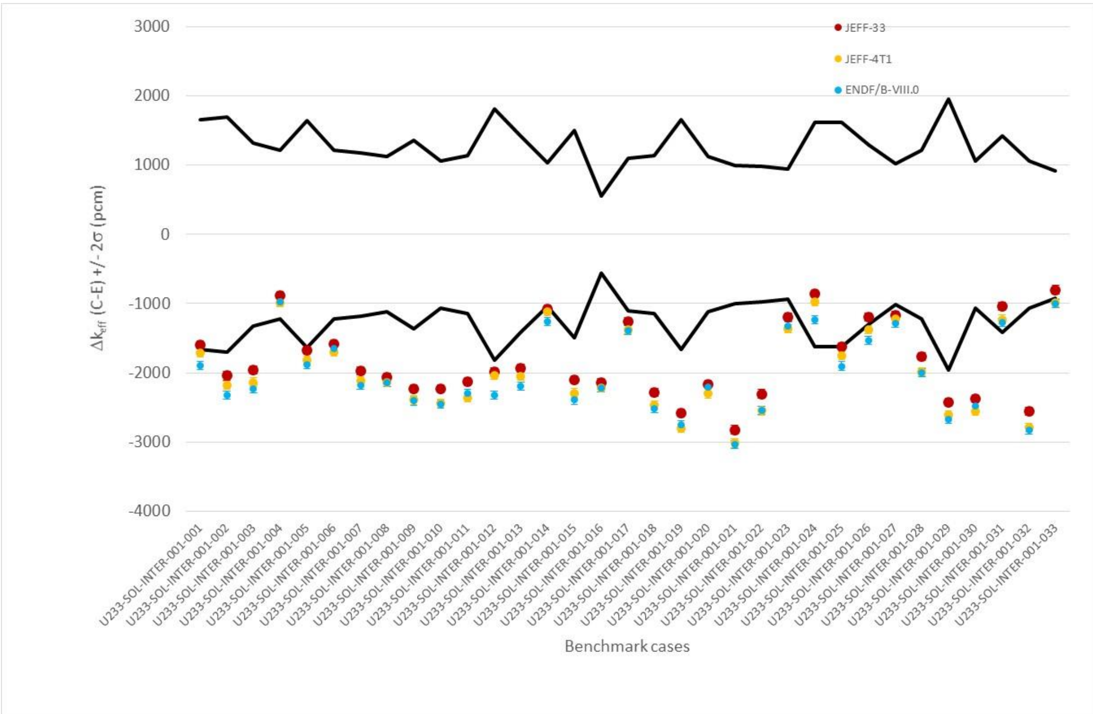

Figure 49. C-E results for experiments with U233 – EPITHERMAL energy range.

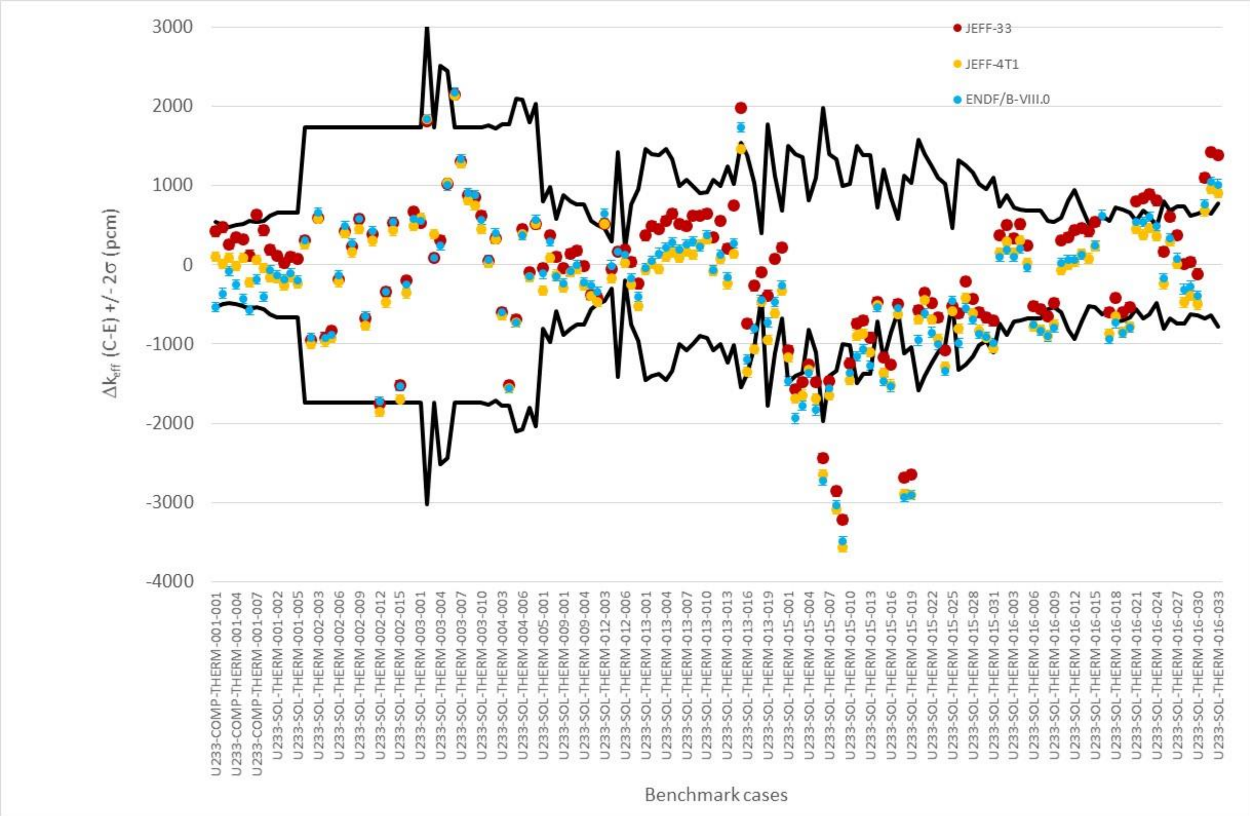

Figure 50. C-E results for experiments with U233 – THERMAL energy range.

5.4.2. NRG results

No NRG results are presented for this category.

5.5. Trends on reflectors (NRG)

5.5.1. Fast spectrum

There are fast spectrum benchmarks with many different reflector materials. The results for many of these benchmarks are shown in Figure 51 – Figure 60. Several comments can be made based on these results.

- HMF3, U-dep reflector, Figure 51: all libraries exhibit a trend of increasing C/E value when the depleted uranium reflector thickness increases. In almost all cases the C/E values is within, or close to, the experimental range of uncertainty. The exception is JEF-2.2, which under-predicts k_{eff} significantly.

- HMF3, Tungsten-carbide reflector, Figure 51: all libraries exhibit a trend of increasing C/E value when the depleted uranium reflector thickness increases. In almost all cases the C/E values is within, or close to, the experimental range of uncertainty. The exception is the case with the thickest (16.51 cm) WC reflector.

- HMF3, Ni reflector, Figure 51: the results vary significantly between the libraries, with JEFF-4t1 having the largest deviation. Using JEFF-4t2 k_{eff} is under-predicted, in contrast to all previous JEFF versions.

- HMF7, polyethylene moderation, Figure 52: the results for most libraries show a constant C/E for most cases of the benchmark, except for JEF-2.2, which shows a clear trend with a change in the H:U ratio.

- HMF7, Teflon moderation, Figure 52: there are three cases of hmf7 with Teflon as moderator. For these cases most libraries over-predict k_{eff} by 1000 pcm or more, and the over-prediction increases with increasing Teflon mass. The JEFF-4t2 has only a small over-prediction for these cases, due to the revised F-19 evaluation.

- HMF25, V reflector, Figure 53: the results for all libraries show a strong trend of C/E with the thickness of a vanadium reflector.

- HMF41, Be and graphite reflectors, Figure 54: all results are within, or close to, the experimental uncertainty band.

- HMF43, steel reflector, Figure 55: the results for all libraries show no trend of C/E as a function of the thickness of the steel reflector. Most results are within the experimental uncertainty band, with only the JEF-2.2 results significantly below it.

- HMF44, Al reflector, Figure 56: the results for JEFF-4t2, JEFF-3.3 and ENDF/B-VIII.0 show no significant trend of C/E as a function of the thickness of the aluminium reflector. The results for JEF-2.2 show a positive trend with increasing reflector thickness, with most results nevertheless within the experimental uncertainty range. On the other hand, JEFF-4t1 consistently over-predicts k_{eff} for this benchmark, and on top of that shows a positive trend with increasing reflector thickness.

- HMF27, 57, 64, Pb reflector, Figure 57: all libraries have a strong effect of the HEU mass in hmf57 on C/E, with higher HEU mass leading to higher C/E. However, this is not seen in the results for hmf64, where there is also a variation in the HEU mass between the three cases. The results are therefore considered inconclusive.

- HMF58, 66, Be reflector, Figure 58: for hmf58 all libraries exhibit a downwards trend of C/E with decreasing reflector thickness. Most libraries have a similar trend, but for JEF-2.2 the trend is more pronounced than for the other libraries. The results for hmf66 do not confirm the trends seen for hmf58, and thus also for Be reflectors in fast spectrum benchmarks the evidence is inconclusive.

- HMF84, Al, Be, C, Co, Cu, Fe, Mo, Ni, Polyethylene, Ti, U, W reflectors, Figure 59: the results for hmf84 depend strongly on the reflector material. The results for most reflector materials are consistent with the benchmark value and its uncertainty (except for JEF-2.2 which under-predicts most values), but k_{eff} for Co and Mo reflectors is over-predicted by most libraries. The results for Ni reflectors are mostly under-predicted. For the JEFF-4t1 library the values for Al, Ni, and Ti are significantly over-predicted.

- HMF85, Cu, Fe, Ni-Cu-Zn, Th, W reflector, Figure 60: All libraries show a significant trend of increasing C/E with increasing Cu reflector thickness, with JEF-2.2 higher the strongest trend. The results for Fe, Ni-Cu-Zn and Th reflectors are mostly within the experimental uncertainty range, with the exception of the JEF-2.2 results for Th and the JEFF-4t1 results for a Ni-Cu-Zn reflector. The latter result is due to the Ni data in JEFF-4t1, which also lead to bad results for cases of hmf3 and hmf84. The results for the W reflector are high for all libraries except JEF-2.2.

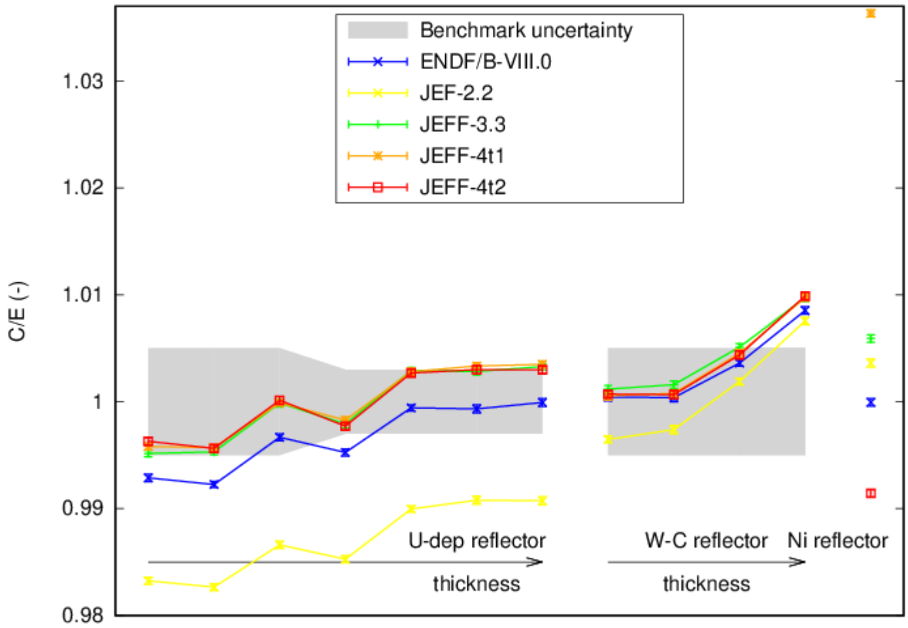

Figure 51. C/E results for hmf3, a fast spectrum benchmark with several reflector materials.

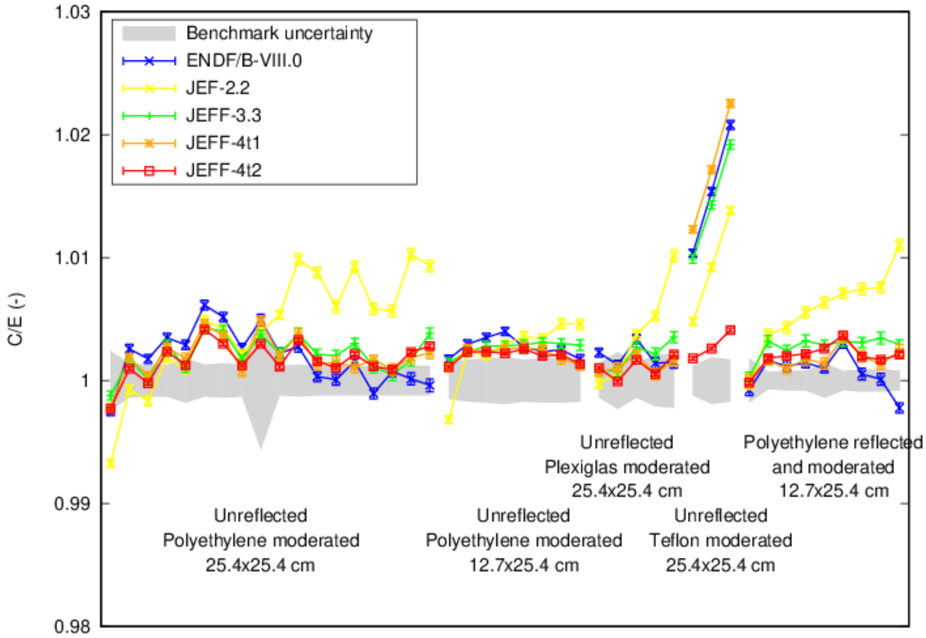

Figure 52. C/E results for hmf7, a fast spectrum benchmark with several reflector materials.

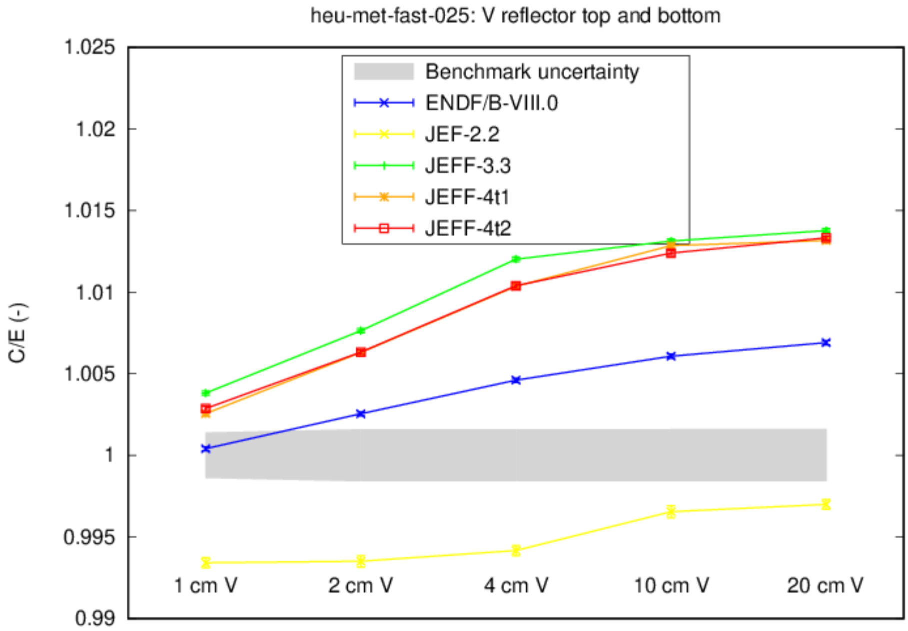

Figure 53. C/E results for hmf25, a fast spectrum benchmark with V reflector.

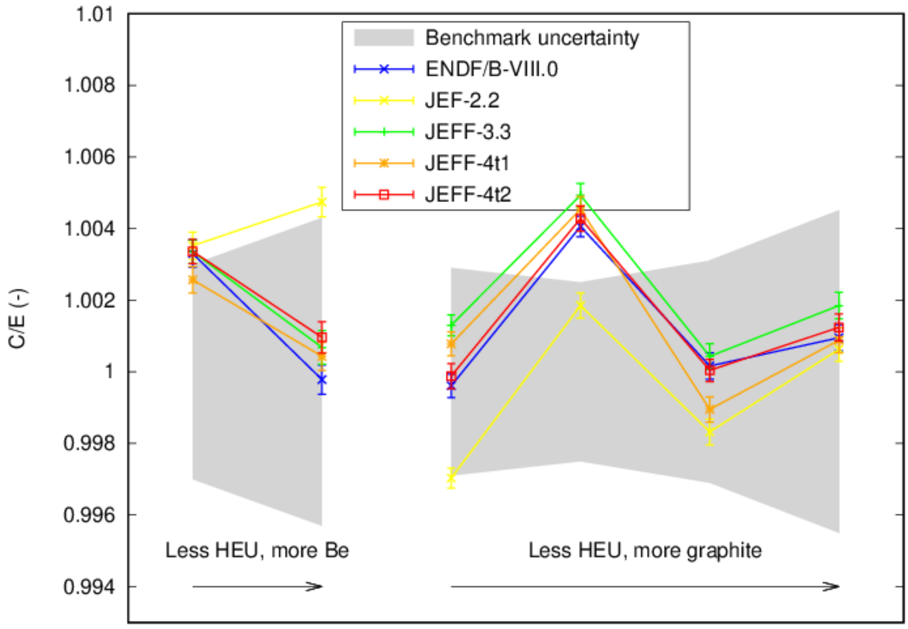

Figure 54. C/E results for hmf41, a fast spectrum benchmark with Be and graphite reflectors.

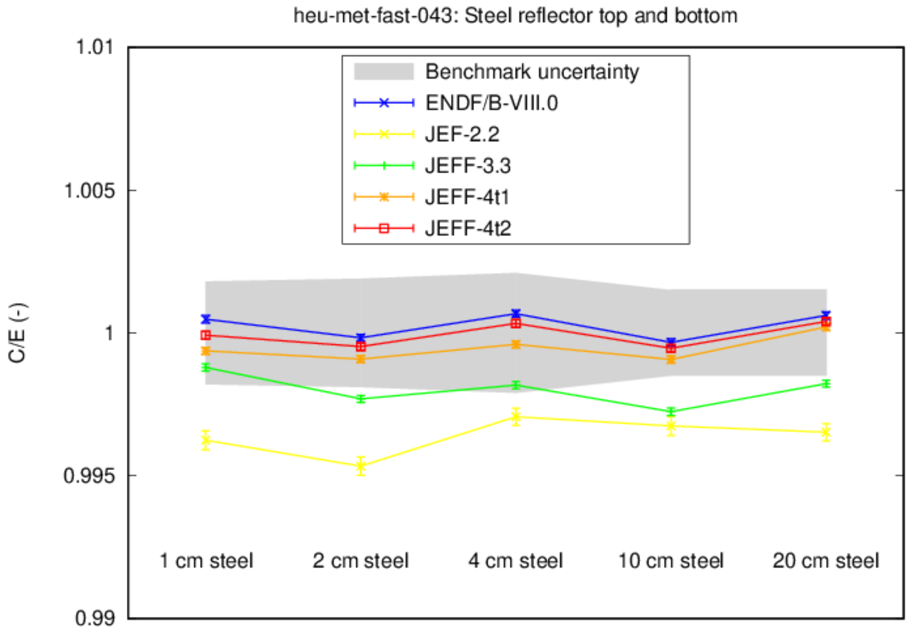

Figure 55. C/E results for hmf43, a fast spectrum benchmark with steel reflector of increasing thickness.

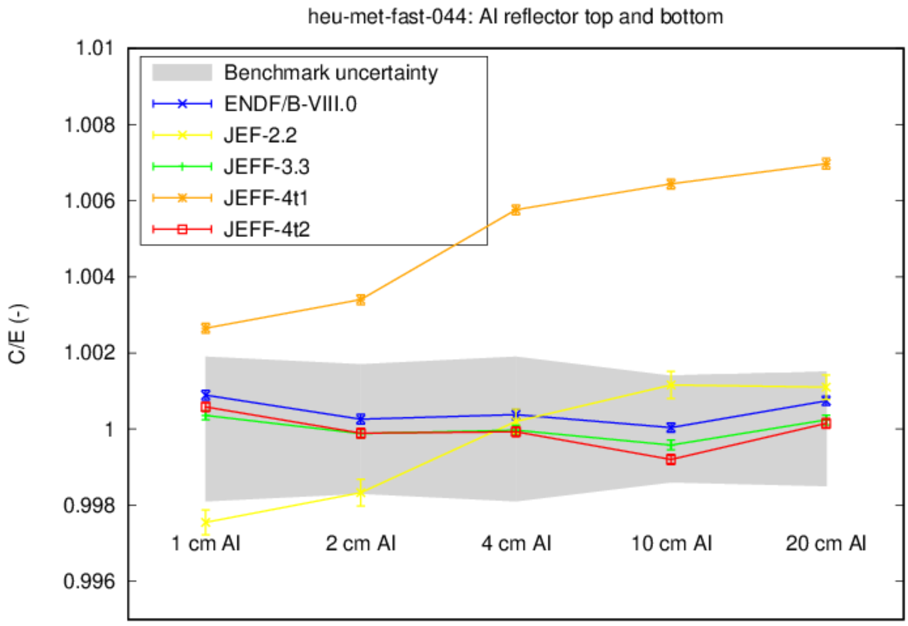

Figure 56. C/E results for hmf44, a fast spectrum benchmark with Al reflector of increasing thickness.

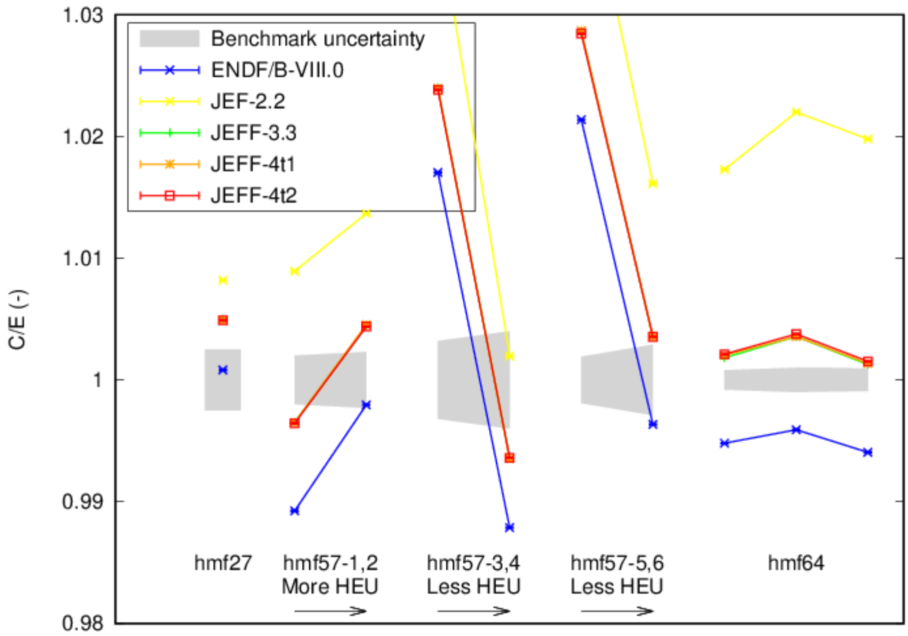

Figure 57. C/E results for fast spectrum benchmarks with lead reflectors.

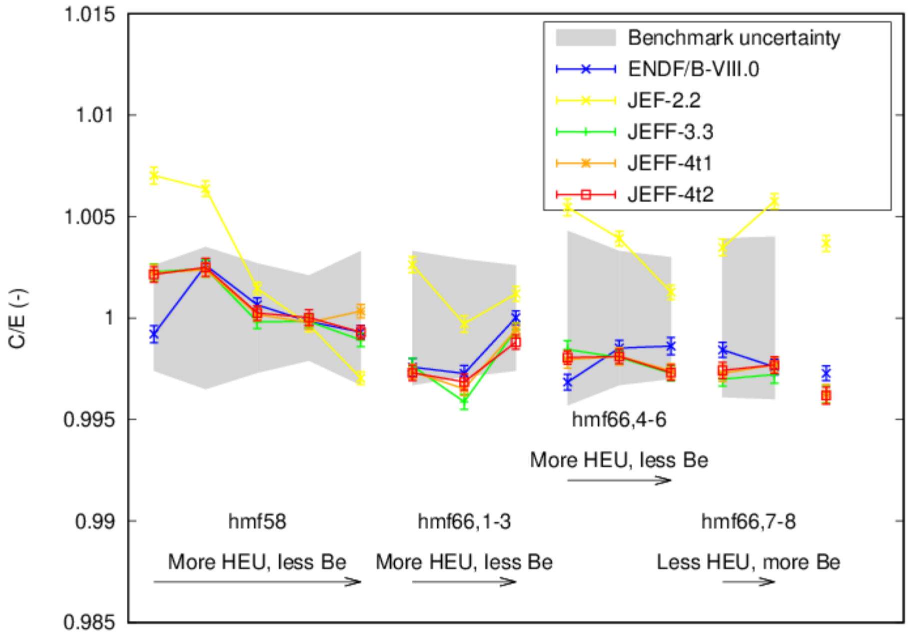

Figure 58. C/E results for fast spectrum benchmarks with Be reflectors.

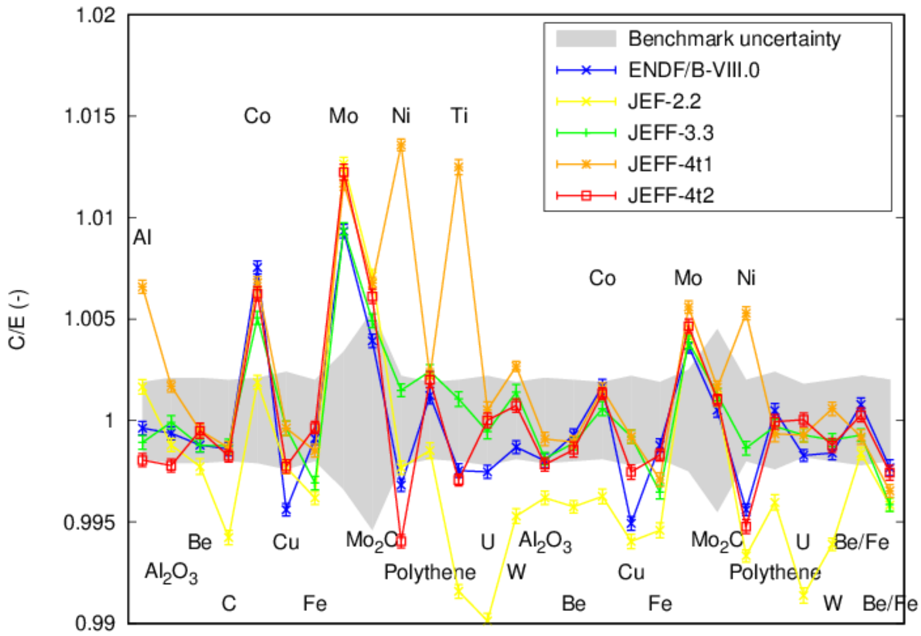

Figure 59. C/E results for hmf84, a fast spectrum benchmark with several reflector materials.

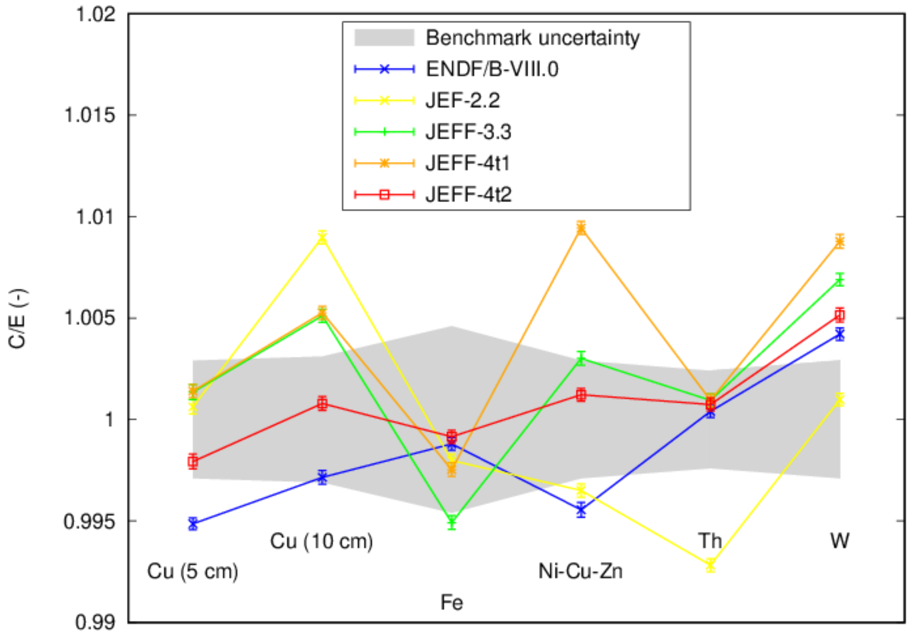

Figure 60. C/E results for hmf85, a fast spectrum benchmark with several reflector materials.

5.5.2. Thermal spectrum

- LCT43, Figure 61: This benchmark is based on experiments in the IPEN/MB01 research reactor, with on one side of the reactor core a stainless steel-304 reflector. The results in Figure 61 have no trend with the thickness of the reflector. There are differences in the value of C/E between the libraries, with only JEFF-4t1 being well outside the experimental uncertainty range.

- LCT88, Figure 62: also this benchmark is based on experiments in IPEN/MB01, now with either a carbon steel reflector or a nickel reflector. For the carbon steel reflector all libraries exhibit a modest positive trend of C/E with increasing reflector thickness. For the nickel reflector, on the other hand, most libraries exhibit a modest negative trend of C/E with increasing reflector thickness, except for JEFF-4t1, which shows a positive trend for the nickel reflector thickness. The trends are shown as a function of reflector thickness in Figure 63.

- LCT9, Figure 64: Lct9 is based on experiments with rectangular clusters of fuel rods separated by steel, boral, copper, cadmium, aluminium, or zircaloy-4 plates. The results for all cases are within the experimental uncertainty range for all libraries except JEF-2.2, in which case the values are just below it.

- LCT10, Figure 65: This benchmark consists of arrays of fuel rods reflected by two lead, uranium or steel walls. There were two values used for the pitch of the arrays, and the distance of the reflector wall to the array was varied. For both pitch values, the results for the lead reflector cases show a clear trend of C/E with the distance, see Figure 65. This holds for all libraries. For the steel and uranium reflectors most results are within or almost within the experimental uncertainty range.

- LCT16, Figure 66: Lct16 is similar to lct9, but with a lattice pitch of 2.032 cm (instead of 2.54 cm) and uranium enrichment of 2.35 wt% (instead of 4.31 wt%). Despite these differences the results are the same: all lie within the experimental uncertainty range for all libraries except JEF-2.2, in which case the values are just below it.

- LCT17, Figure 67: LCT17 is similar to lct10, but with lattice pitches of 2.032 cm and 1.684 cm (instead of 2.54 cm and 1.982 cm) and uranium enrichment of 2.35 wt% (instead of 4.31 wt%). The results presented here do not contain the uranium reflector cases. Despite the differences between lct10 and lct17, the results are the same: there is a trend of C/E with the thickness of the lead reflector, but not with the thickness of the steel reflector.

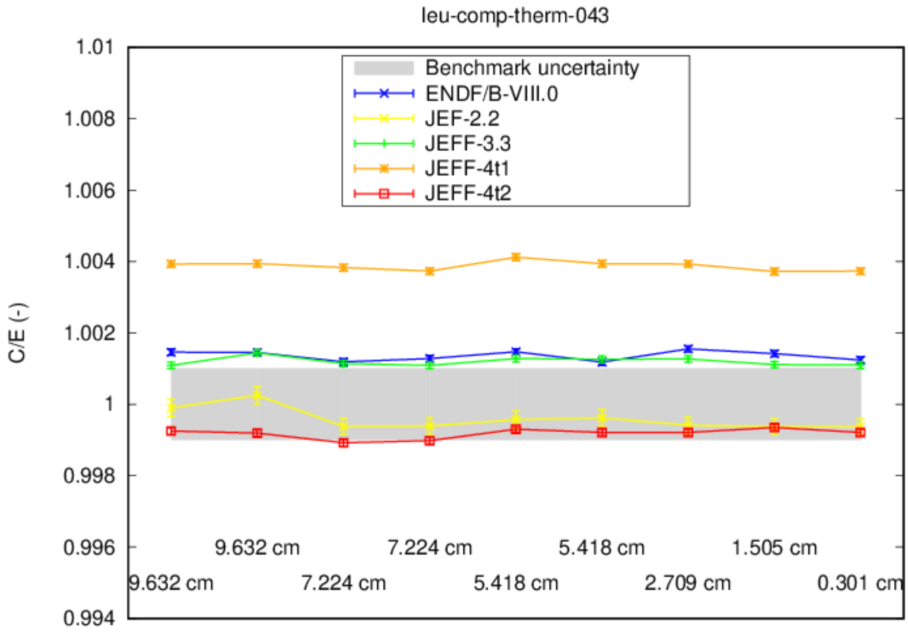

Figure 61. C/E results for lct43, a benchmark with a stainless steel 304 reflector.

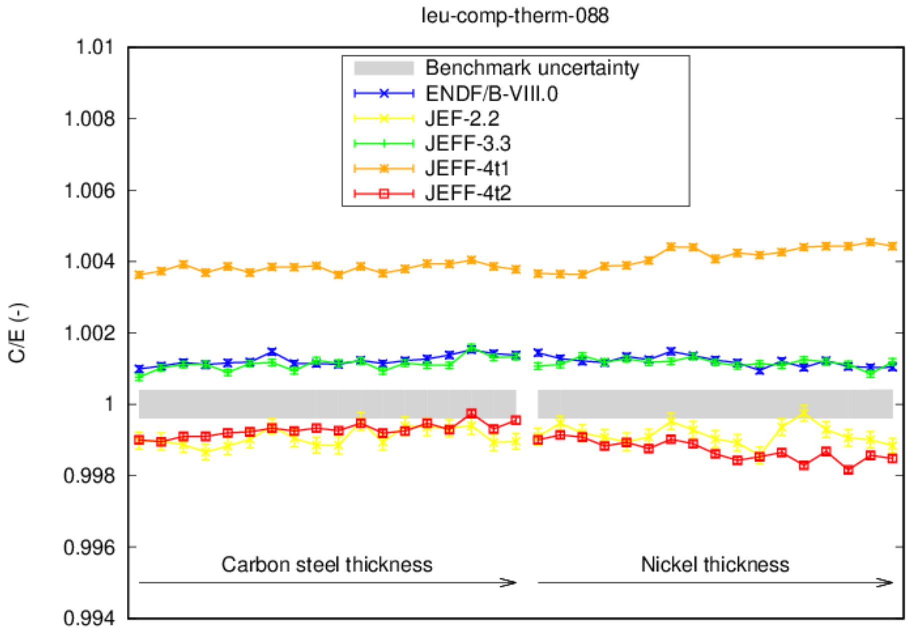

Figure 62. C/E results for lct88, a benchmark with carbon steel or nickel reflector.

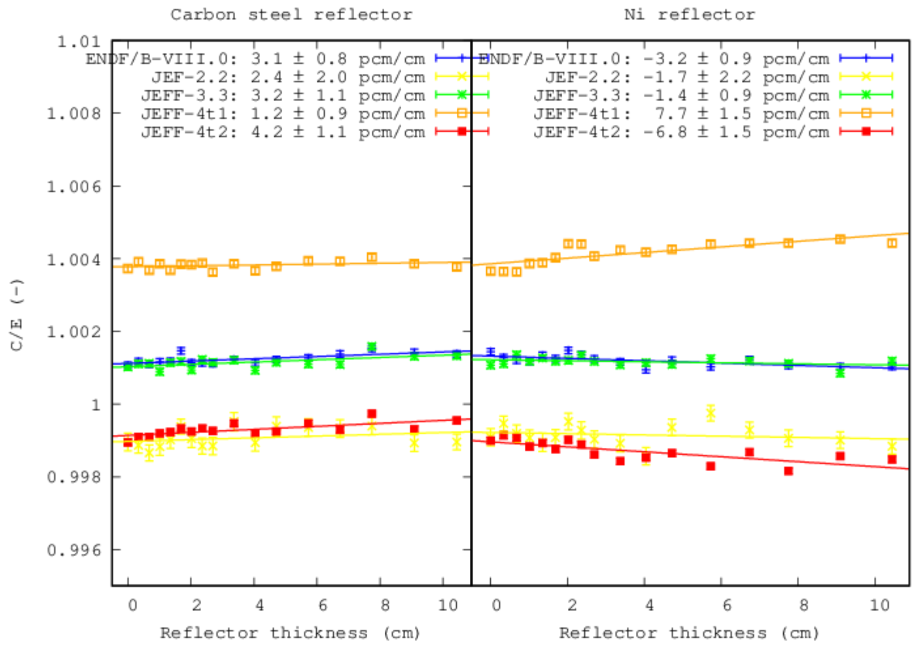

Figure 63. C/E results for lct88, plotted as a function of reflector thickness and fitted to a trend line. The value of the slope of the trend line is indicated at the top.

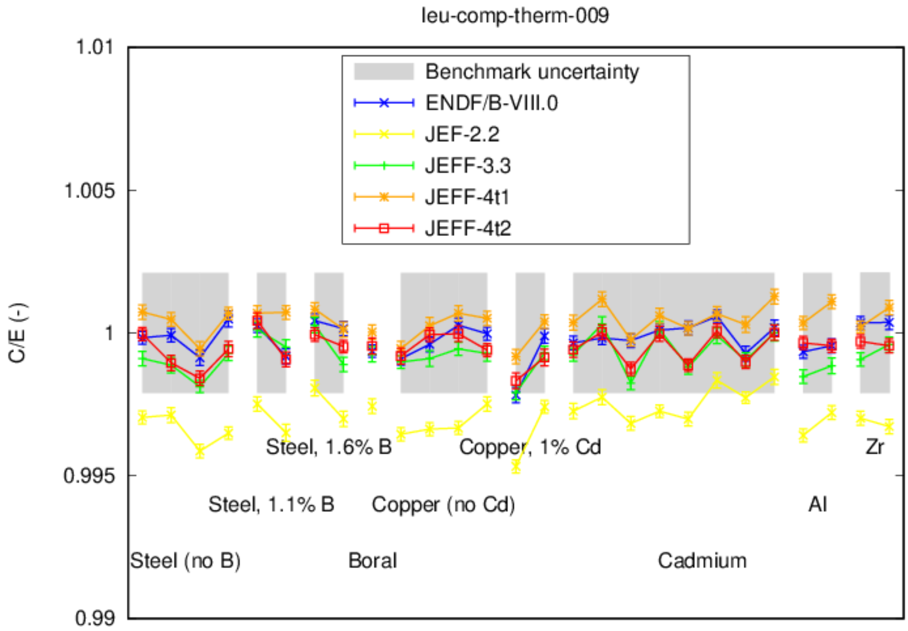

Figure 64. C/E results for lct9, a benchmark with steel, borated steel, copper, cadmium, aluminium, and zircaloy reflectors.

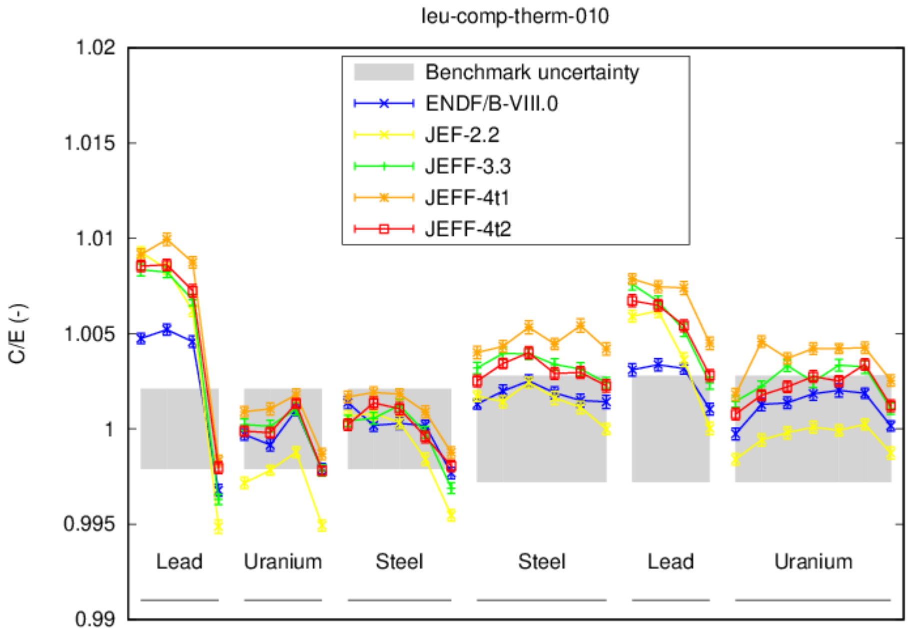

Figure 65. C/E results for lct10, a benchmark with lead, uranium and steel reflectors.

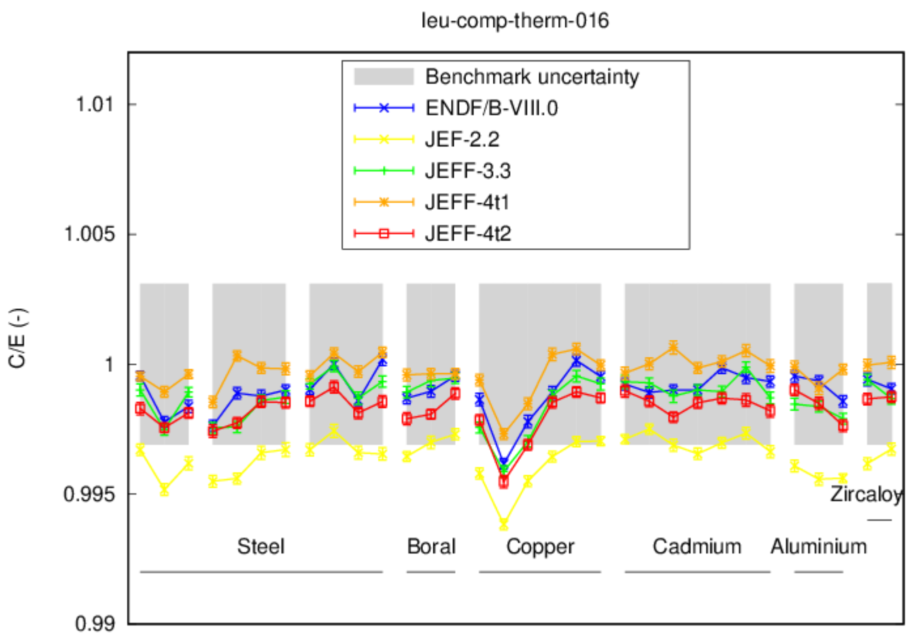

Figure 66. C/E results for lct16, a benchmark with steel, boral, copper, cadmium, aluminium, and zircaloy reflectors.

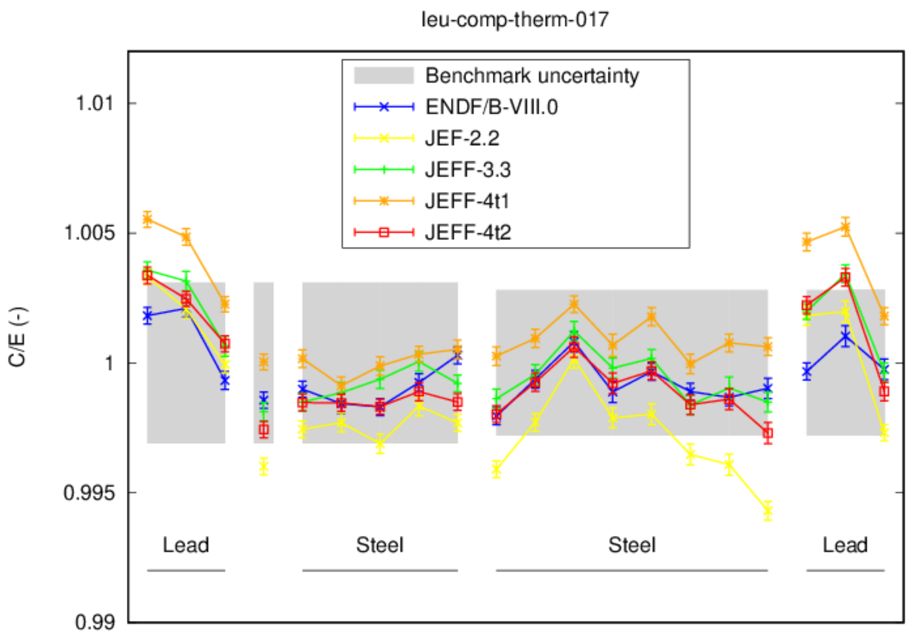

Figure 67. C/E results for lct17, a benchmark with lead and steel reflectors.

5.6. Trends on absorbers (NRG)

Several strong absorbers were investigated. In this Section results for Gd, B, and Cd are presented. Some of the cases of the relevant benchmarks also contain fission products such as Sm, Cs, Rh, and Eu. Finally, also results for a benchmark with a strong presence of F are reported.

5.6.1. Gadolinium

- HST14 – HST19, Figure 68: The benchmark series hst14 – hst19 are based on experiments in the same facility. The experiments were performed with a different uranium concentration in the solution for each of the benchmarks. Within a benchmark, the Gd concentration was varied. The results in Figure 68 show that there is a strong dependence of C/E in the Gd concentration for each of the benchmark series except hst19, or in other words, for each uranium concentration except for the highest concentration of 400 gU/liter. The sensitivity of two selected cases to the capture cross sections of ^{155}Gd and ^{157}Gd is shown in Figure 69. It is clear that there is a difference in the magnitude of the sensitivity, but also in the energy at which the sensitivity is largest.

- LCT5, Figure 70: This benchmark is with uranium fuel rods in water containing dissolved gadolinium. There are cases with several values for the lattice pitch, leading to different results for C/E. It can be observed in Figure 70 that for the largest pitch, 2.4 cm, the C/E values for JEFF-4t2 and ENDF/B-VIII.0 exhibit a downward trend with increasing Gd concentration. For a slightly lower pitch, the trend of the JEFF-4t2 and ENDF/B-VIII.0 values is smaller, and for the smallest pitch, 1.6 cm, the trend for JEFF-4t2 and ENDF/B-VIII.0 is positive. Also noteworthy are the results for the rods with higher uranium enrichment (4.31 wt% instead of 2.35 wt%): for all libraries the trend with Gd concentration is very steep (although it should also be said that for this higher enrichment there are only two cases available with the same pitch).

- LCT52, Figure 71: This benchmark is based on experiment with 4.738 wt% enriched uranium fuel rods on a hexagonal lattice. There were three hexagonal configurations with varying pitch, and three circular configurations with varying pitch. The gadolinium concentration was varied to achieve criticality at approximately the same water height in all cases. The results show an upward trend of C/E with increasing pitch (decreasing Gd concentration) for the hexagonal configurations, but a downward trend for the circular configurations, see Figure 71. The reason for these opposite trends is unclear, as the spectra in the fuel regions was checked to be very similar for these cases.

- Leu-misc-therm-006, Figure 72: This benchmark contains 5% enriched fuel rods in 6% enriched uranyl nitrate solutions with gadolinium. There are five cases with a water reflector and five cases without reflector. Both with and without reflector, the C/E results have a decreasing trend with increasing Gd concentration.

For most of the above benchmarks, hst14–hst19, lct52, and leu-misc-therm-006, the trends in C/E are similar for all libraries. Only the results for lct5 are different for the various libraries. In all cases the results for C/E are not independent of the Gd concentration.

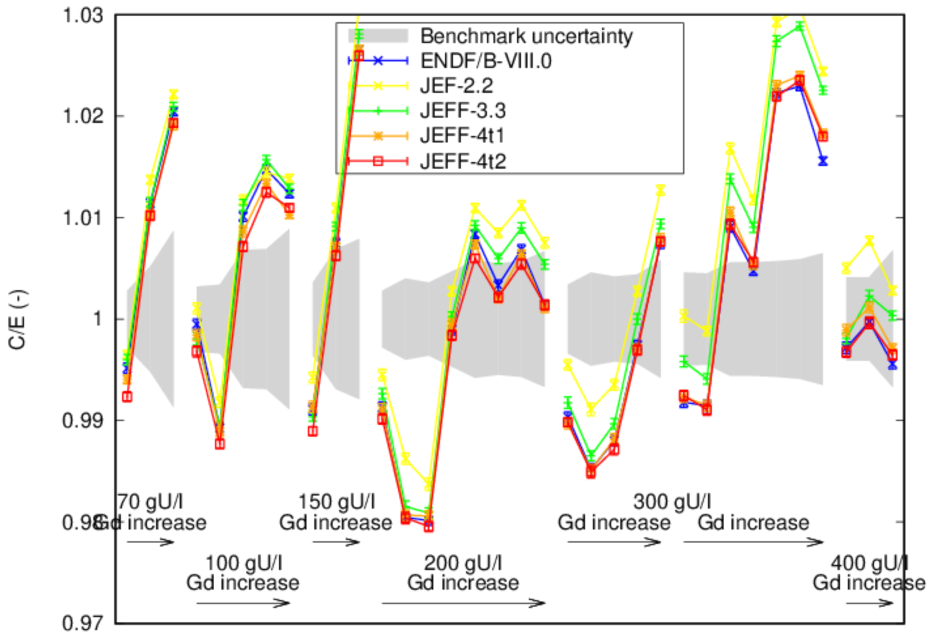

Figure 68. C/E results for hst14 – hst19, benchmarks with Gd absorber in solution.

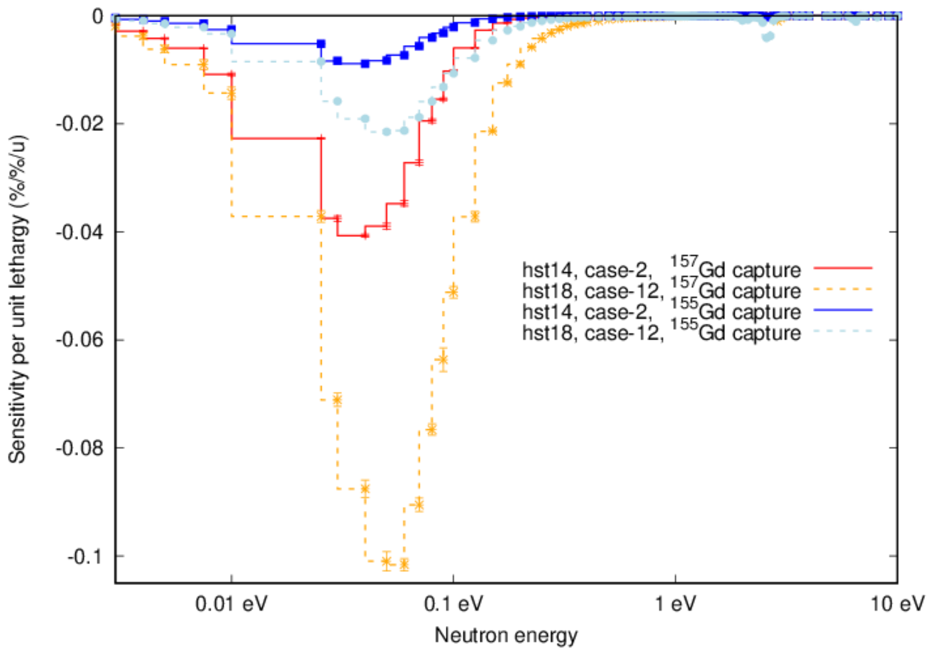

Figure 69. The sensitivity of hst14, case-2 and hst18, case-12 to the capture cross sections of ^{155}Gd and ^{157}Gd.

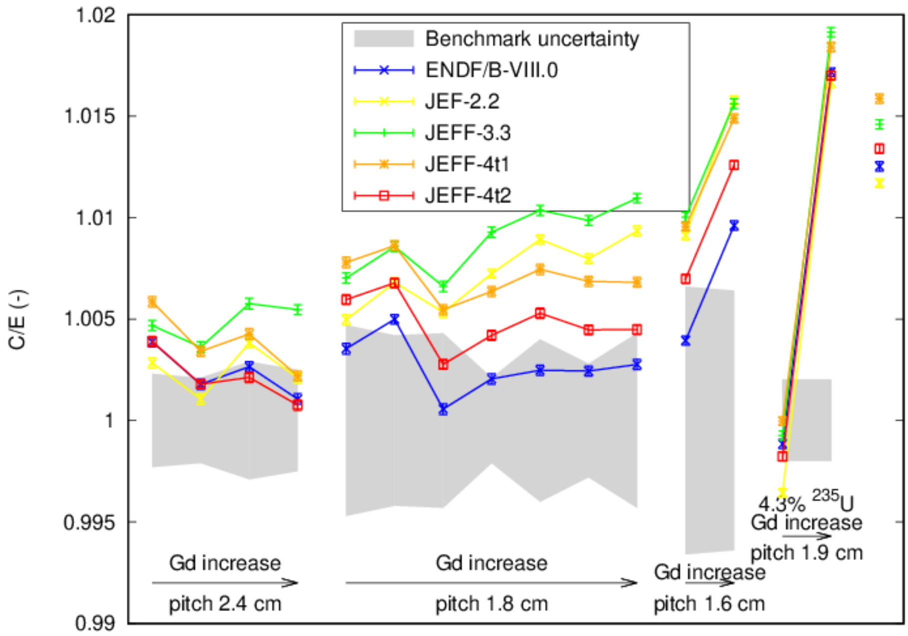

Figure 70. C/E results for lct5, a benchmark with Gd absorber in solution.

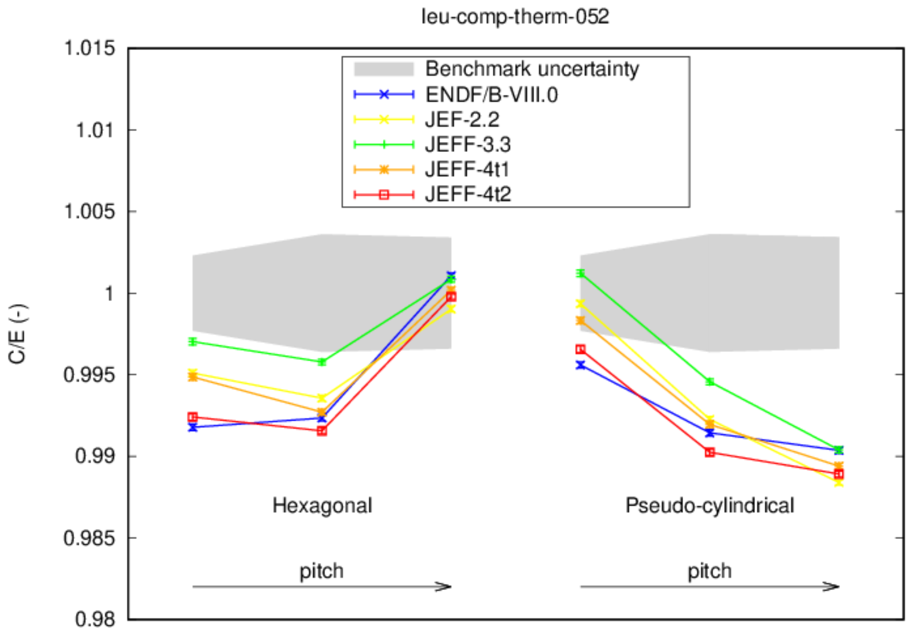

Figure 71. C/E results for lct52, a benchmark with Gd absorber in solution.

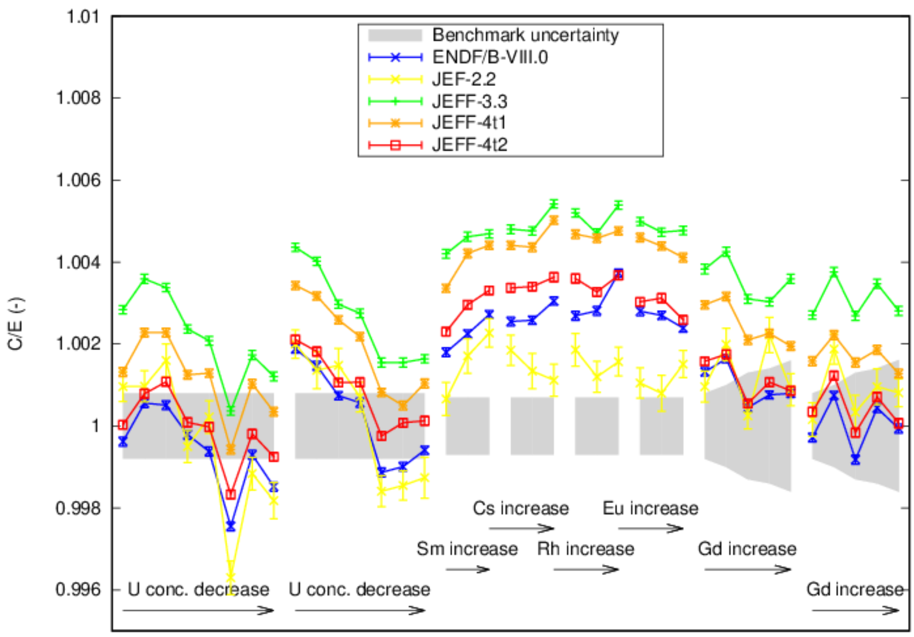

Figure 72. C/E results for leu-misc-therm-003, 5, and 6, benchmarks with several strong absorbers in solution.

5.6.2. Boron

- HST6, Figure 73: This benchmark contains a uranyl nitrate solution with and without water reflector. The uranyl nitrate was poisoned with enriched boric acid, and for some of the cases the reflector water was borated. There were seven levels of boron concentration in the uranyl nitrate solution. For each of the boron levels, there were cases with and without water reflector, and cases with and without a nickel sleeve in between the solution vessel and the reflector vessel. The C/E results are not sensitive to these variations. However, the C/E results do correlate clearly with the boron level: for low boron concentration, i.e. up to 2.33 gB/liter, the C/E values increase with the boron concentration. At larger concentrations there is no further increase, but even a small decrease in C/E values.

- HCT21, Figure 74: Hct21 has arrays of uranium and thorium oxide with water moderation and reflection. There are many cases, varying both the pitch of the lattice, the boron level, and the number of fuel rods. The water level was varied to reach criticality. It is clear from Figure 74 that for all libraries the C/E values are rather sensitive to the boron level, and that within each boron level they are also sensitive to the number of fuel rods (and hence the varying water height and the corresponding spectrum shift). Also, the pitch influences the C/E results noticeably.

- LCT50, Figure 75: This benchmark has an array of fuel rods, in the middle of which a solution tank was placed. This tank was filled with a solution that included either B or Sm. As can be seen from Figure 75 the C/E values have a positive trend with increasing boron levels. This is true for all libraries. The sensitivity of two cases to the capture cross section of ^{10}B is shown in Figure 76. An interesting feature is that the maximum sensitivity for the case with the higher boron concentration, case 5, is not higher than for case 3. Instead, the sensitivity is shifted upward in energy, with a strong tail in the epithermal region.

- LCT62, Figure 77: Lct62 consists of a rectangular array of fuel rods with a steel plate next to it. There are three steel plate types: one without boron and two plates with different levels of boron. The results for this benchmark are for all libraries only weakly dependent on the level of boron.

- LCT65, Figure 78: Experiments similar to lct62 were performed with two arrays of fuel rods, with two steel plates in between the two arrays in a symmetrical configuration. The C/E values are slightly more sensitive to the boron level in the plates than in lct62, but the effect is still relatively small.

In summary, the results for benchmarks containing boron are quite dependent on the level of boron when it is present in a watery solution (hst6, hct21, lct50), but less so when boron is present in borated steel.

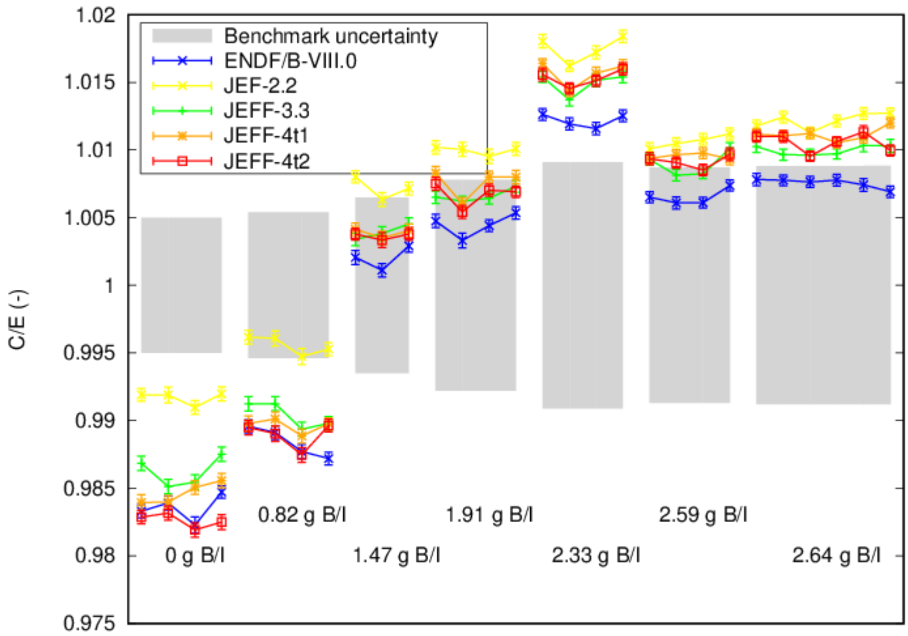

Figure 73. C/E results for hst6, a benchmark with B absorber in solution.

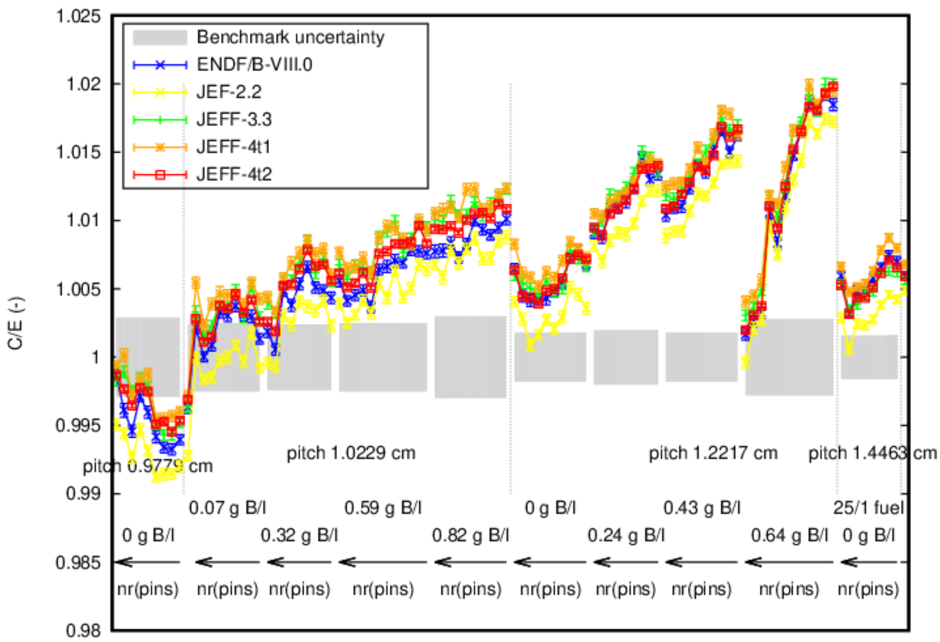

Figure 74. C/E results for hct21, a benchmark with B absorber in solution.

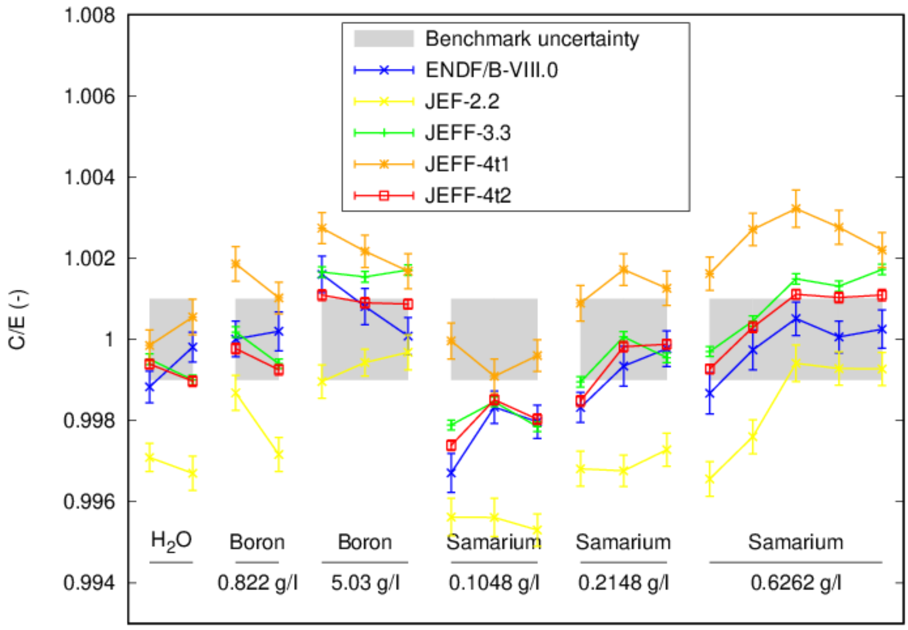

Figure 75. C/E results for lct50, a benchmark with B or Sm absorber in solution.

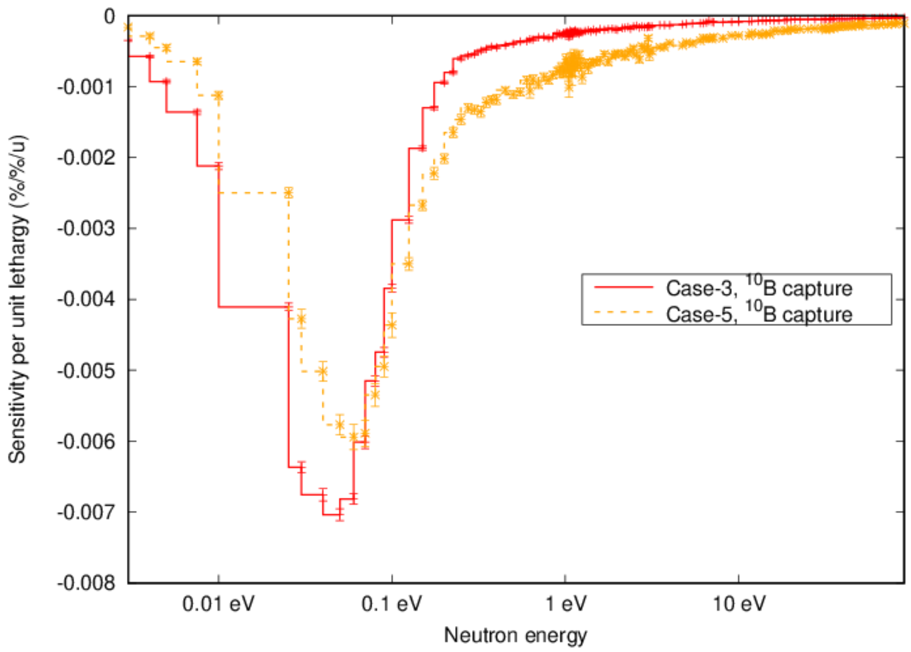

Figure 76. The sensitivity of lct50, cases 3 and 5 to the capture cross section of ^{10}B.

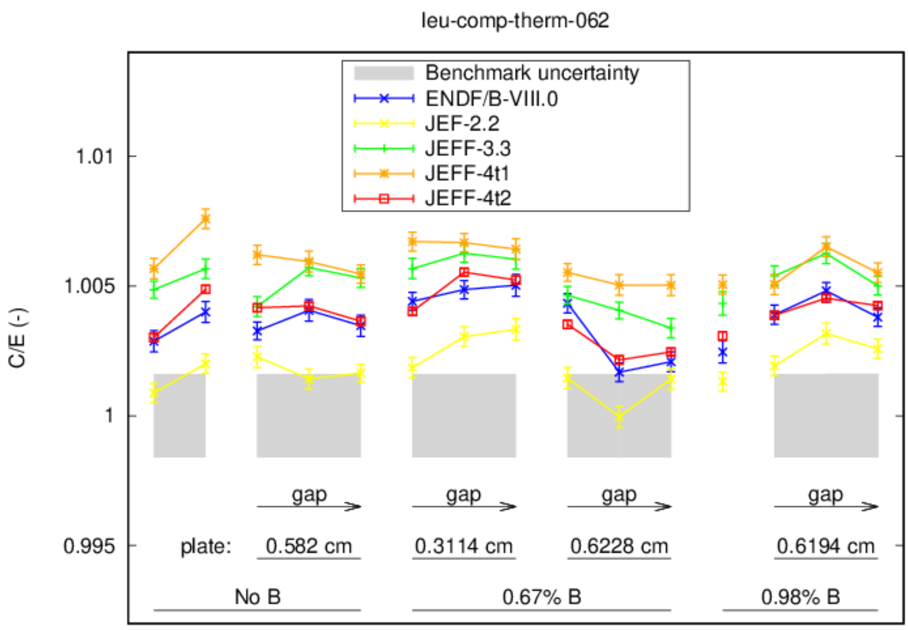

Figure 77. C/E results for lct62, a benchmark with B absorber.

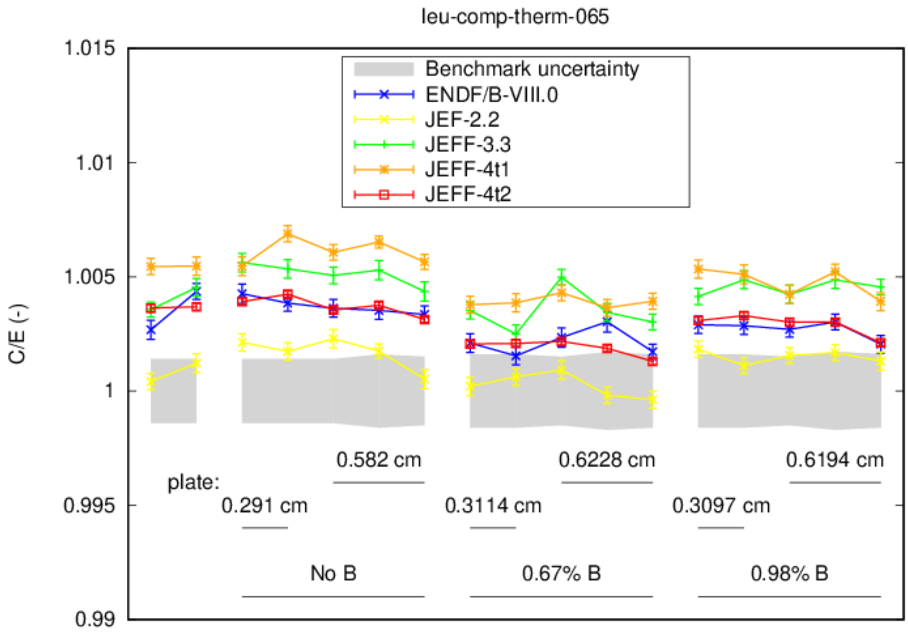

Figure 78. C/E results for lct65, a benchmark with B absorber.

5.6.3. Cadmium

Heu-sol-therm-049 is based on experiments using two cylindrical vessels with uranyl nitrate solutions containing soluble cadmium nitrate absorber. Water with and without cadmium nitrate was used as reflector. The results for both vessels, shown in Figure 79, have a strong trend of C/E on the Cd concentration in the solution. This is the case for all libraries; only for JEF2-2 the trend is less severe.

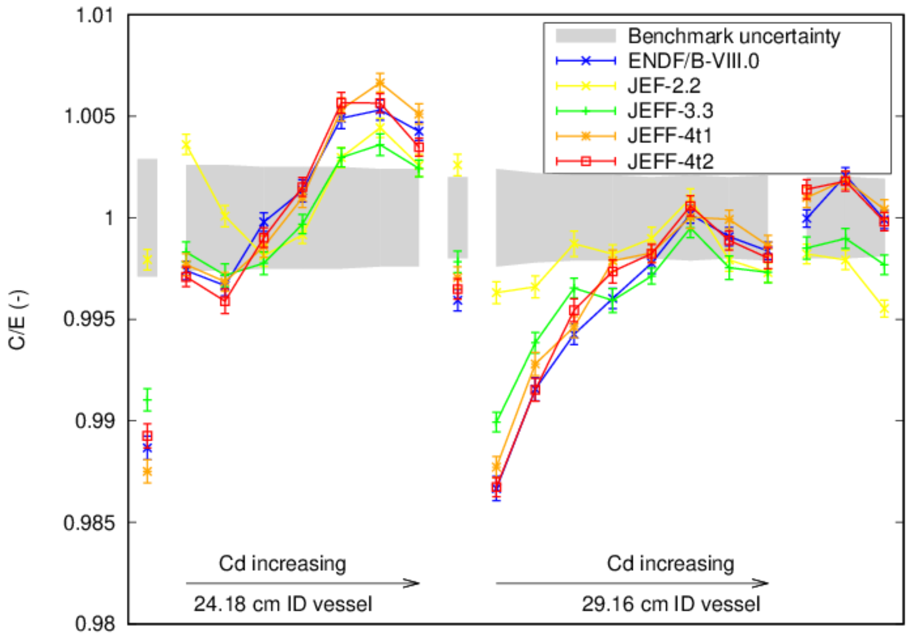

Figure 79. C/E results for hst49, a benchmark with Cd absorber in solution.

5.6.4. Fission products Sm, Cs, Rh, and Eu

- Leu-misc-therm-005, Figure 72: The benchmark leu-misc-therm-005 is similar to leu-misc-therm-006: both benchmarks contain 5% enriched fuel rods in 6% enriched uranyl nitrate solutions, but leu-misc-therm-005 has fission products dissolved in the uranyl nitrate solution (instead of gadolinium in the case of leu-misc-therm-006). The fission products used are (natural) Sm, Cs, Rh, and Eu. For the various libraries there are different trends visible in Figure 72 for each of the fission products. For instance, for JEFF-4t2, there is an upward trend of C/E for increasing Sm concentration, and a downward trend for increasing Eu concentration. For Cs and Rh, the JEFF-4t2 results exhibit almost no trend. Some examples of the sensitivity to these fission products are given in Figure 80. For ^{149}Sm the sensitivity is mainly in the thermal region, while for ^{133}Cs there is also sensitivity to resonances in the epithermal region.

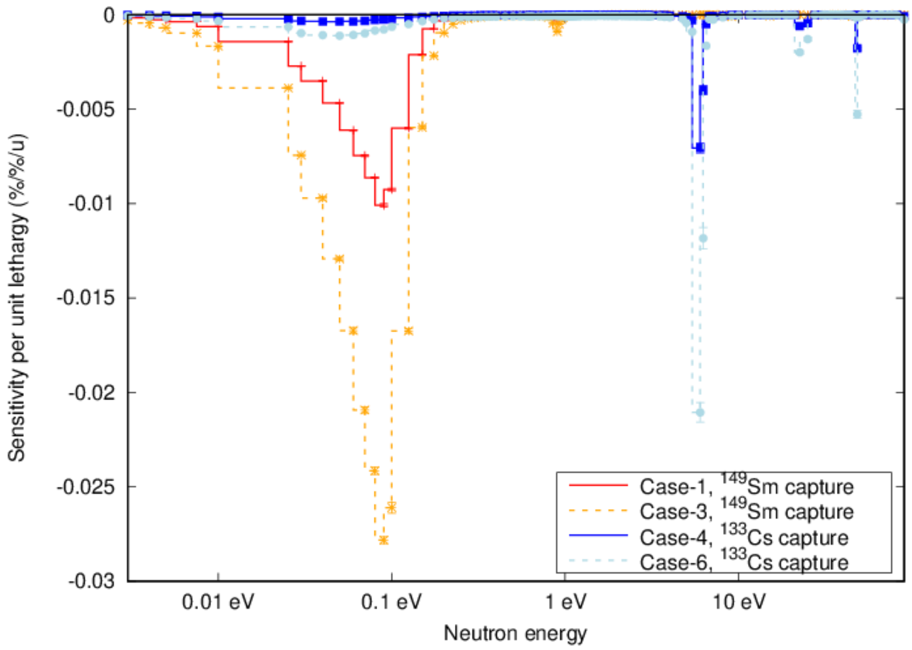

Figure 80. The sensitivity of four cases of leu-misc-therm-005 to the capture cross section of ^{149}Sm and ^{133}Cs.

- LCT50, Figure 75: This benchmark has an array of fuel rods, in the middle of which a solution tank was placed. This tank was filled with a solution that included either enriched B or enriched Sm. As can be seen from Figure 75 the C/E values have a positive trend with increasing Sm levels. This is true for all libraries.

5.6.5. Fluorine

LCT33, Figure 81, is a benchmark with rectangular stacks of uranium fluoride dispersed in paraffin. There are cases without reflector, and cases with paraffin or polyethylene as reflector. There were eight mixtures of UF_4 in paraffin, with two uranium enrichments (2 wt% and 3 wt%). In Figure 81 it is shown that the results are different for the various libraries. For most libraries there is also quite a difference in results for the different mixtures. But most striking is the difference between the results for 2 wt% and 3 wt% enriched uranium. These differences are smaller for JEFF-4t2.

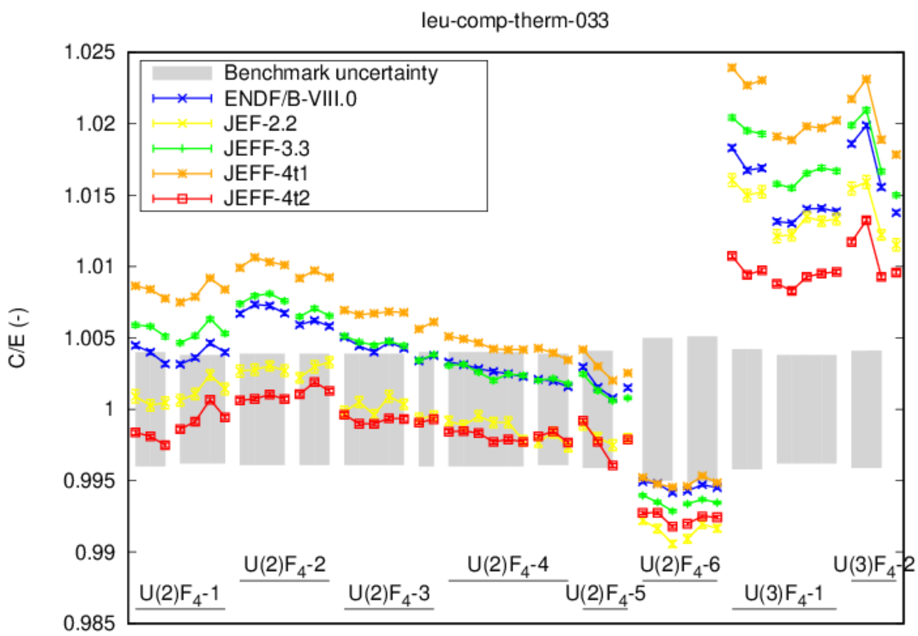

Figure 81. C/E results for lct33, a benchmark with uranium fluoride (UF_4) dispersed in paraffin.

6. Comparison between NRG and IRSN cases

The benchmarks have been modelled independently by IRSN with the MORET code and by NRG with the MCNP code. Some benchmark cases are common to the two selections made by IRSN and NRG. For a purpose of consistency in the tendencies put forward by the two authors, it was checked that for the same libraries, k_{eff} results of IRSN were consistent with those provided by NRG. Potential differences could be attributed either to the processing of nuclear data that is different between IRSN and NRG, to the potential physical models implemented in the two codes or to a modelling effect (interpretation of benchmark). The k_{eff} differences between MORET (IRSN) and MCNP (NRG) for the JEFF-33 and JEFF-4T1 nuclear data evaluations are displayed on Figure 82. The combined Monte Carlo standard deviation stands in black line. Most k_{eff} differences are comprised within this standard deviation. For hcm1 series, discrepant results could be explained by the difference in modelling the TSL for hydrogen bound to oxygen or to carbon. IRSN used TSL of polyethylene and water whereas NRG used TSL of lucite.

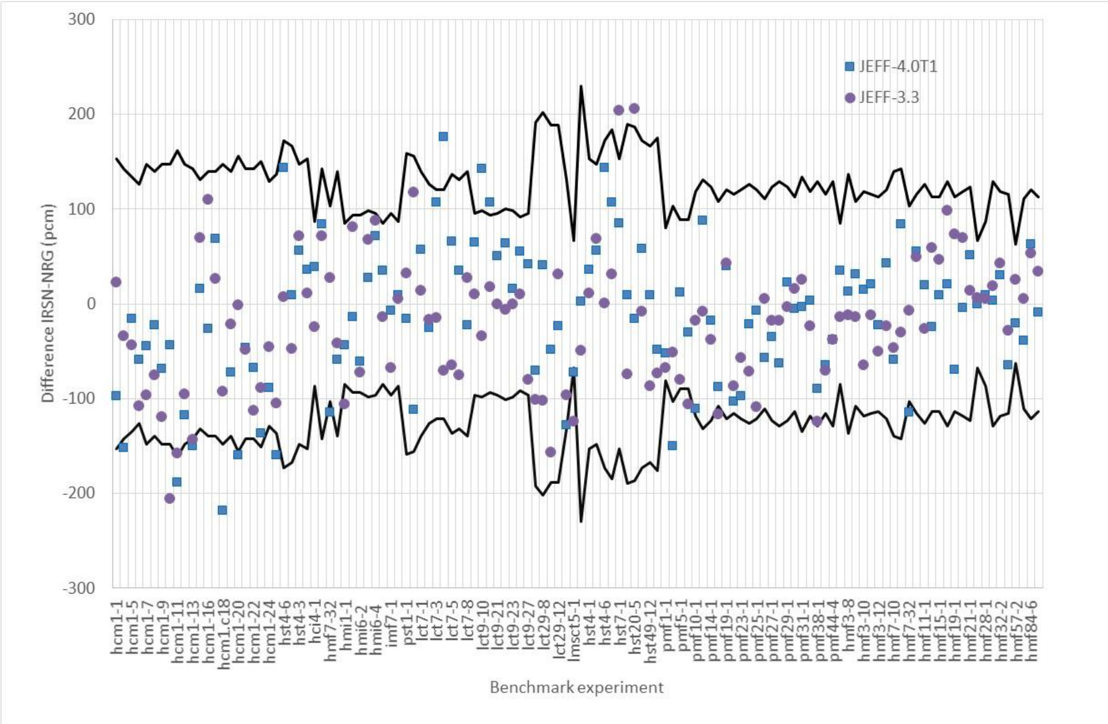

Figure 82. k_{eff} difference for JEFF-3.3 and JEFF-4.0T1 libraries between MORET (IRSN) and MCNP (NRG) results.

7. Trends with temperature (IRSN)

To evaluate nuclear data at reactor temperatures, the KRITZ-LWR-RESR-004 benchmark from the IRPhe Handbook was used. This benchmark simulates a light water moderated zero power reactor in Studsvik (Sweden) which was operated from 1969 to 1975. The objective was to obtain material buckling versus temperature coefficients and other reactor data. The rods were designed for Markiven BWR reactor. Criticality at stable, isothermal conditions was obtained by adjusting the water level. Boric acid was dissolved in the moderator as a design variable. The content in boron of the borated water varied between 0.6 µg/g and 175 µg/g. The 1.35 % 235U-enriched UO2 rods of the lattice were arranged with a 1.8-cm square pitch and located partly in water and partly in steam (upper part). Steam in the upper part of the assembly was at saturation point.

The simplified model showing a bias up to 500 pcm was modelled with the MORET 5 code (IRSN). The total uncertainties of the benchmark were lower than 150 pcm at the 1σ level. All in all, 37 cases were calculated with the temperature varying between 20.4 °C and 245.8 °C. Various quantity were measured (keff, reactivity coefficients…) but we focus in this section on the keff results. A cross scut view of the benchmark model in provided in Figure 83.

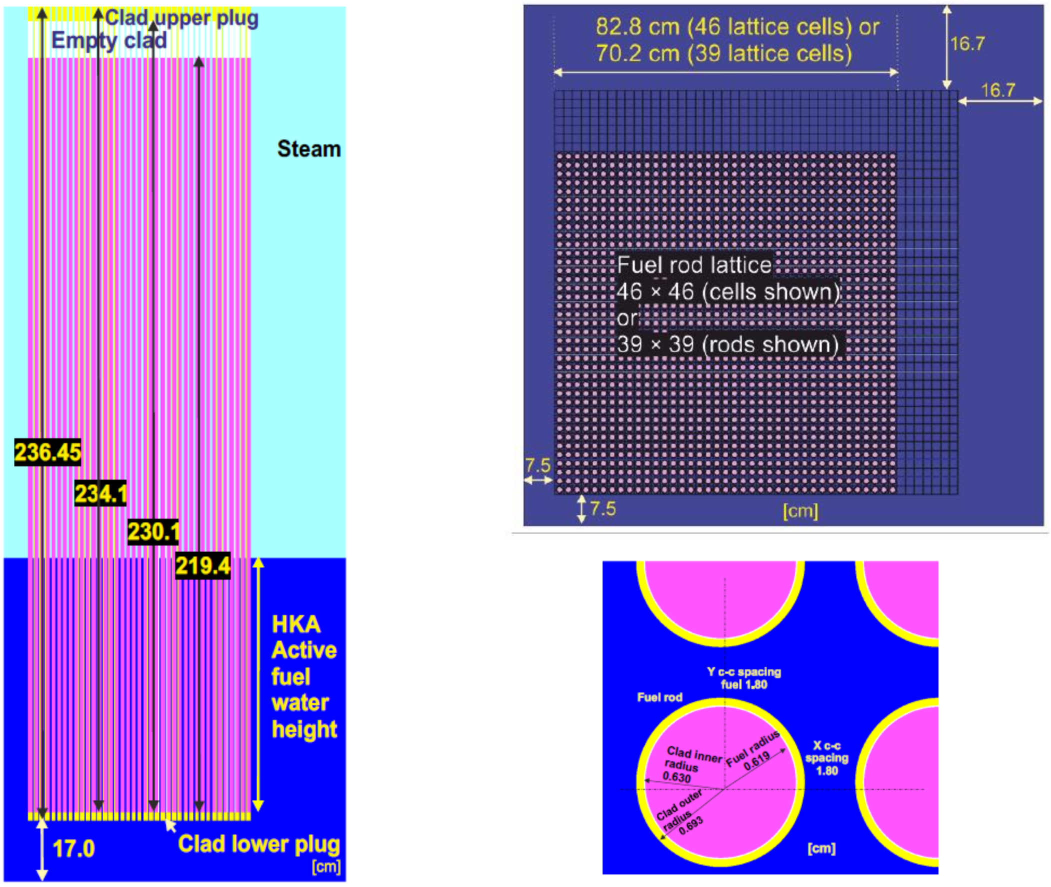

Figure 83. Cross cut view of KRITZ-LWR-RESR-004 benchmark.

7.1. Analysis of results for KRITZ benchmark

The k_{eff} results calculated with the MORET 5 Monte Carlo code for the JEFF-3.3, JEFF-4.0t1 and ENDF/B-VIII.0 evaluations of nuclear data are reported for the KRITZ benchmark on Figure 84. One can see that there is an under-estimation of k_{eff} results with the ENDF/B-VIII.0 evaluation of nuclear data and that there is better agreement with the benchmark k_{eff} using the JEFF-33 or JEFF-4.0t1 evaluations of nuclear data. A tendency to increase k_{eff} with temperature can also be pointed out for the JEFF-3.3 evaluation of nuclear data. Moreover, it has been checked that there is no clear tendency with the boron concentration in water; that is why the cases are not gathered as a function of their boron content.

Temperature reactivity coefficients are given in Table 8 for the MORET 5 calculations.

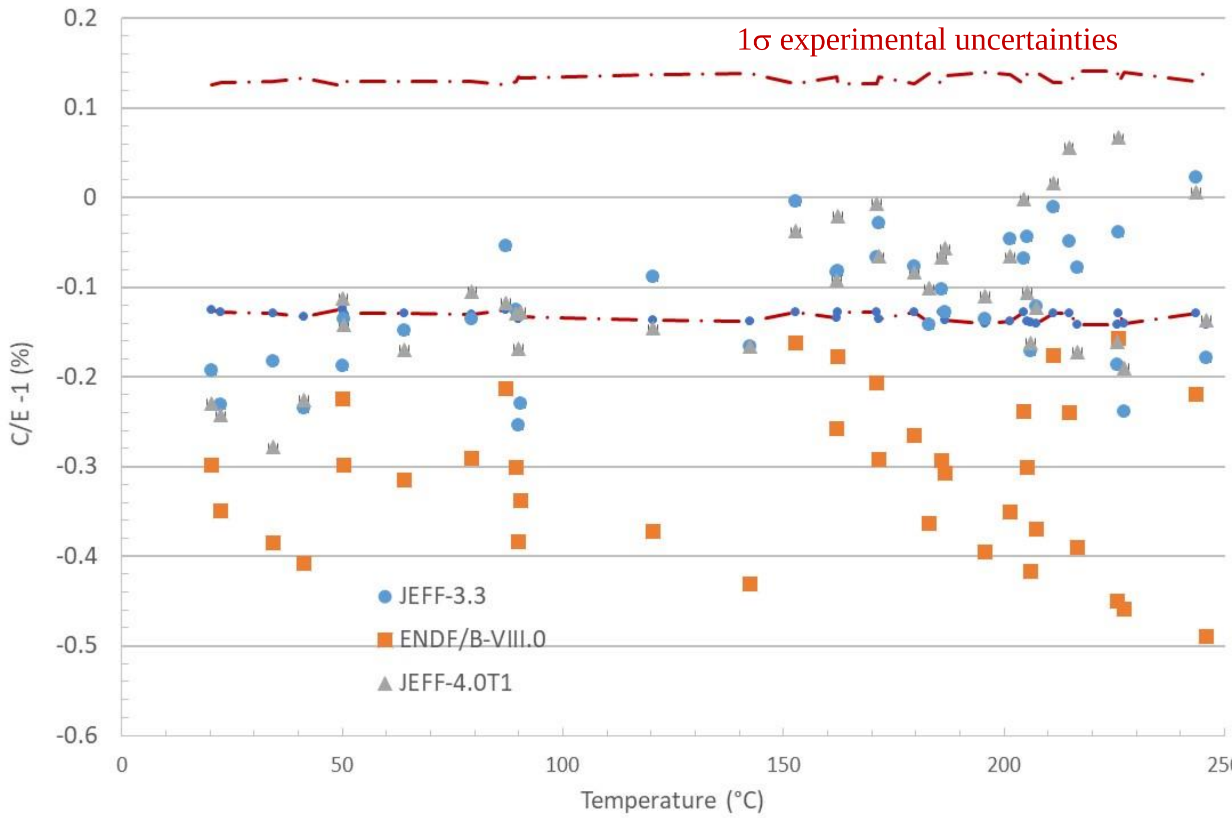

Figure 84. C/E -1 results for KRITZ benchmark.

Table 7. Results for KRITZ 4 benchmark with MORET 5.

Results for the trend in $\Delta\rho = \rho_c - \rho_m$	JEFF-4t1 (pcm/°C)	JEFF-3.3 (pcm/°C)	ENDF/B-VIII.0 (pcm/°C)
Kritz-4, UO_2 (1.35%), 39x39, 0.8 μgB/g	0.353	0.266	-0.222
Kritz-4, UO_2 (1.35%), 46x46, 46.3 μgB/g	-0.058	0.334	-0.978
Kritz-4, UO_2 (1.35%), 46x46, 175. μgB/g	0.755	1.028	0.268
Kritz-4, UO_2 (1.35%), 39x39, 0.2 μgB/g	1.057	0.972	0.358

The benchmarks kritz-lwr-resr-001, 002, 003, and 004 were also analysed with MCNP-6.2, using detailed models for the benchmark cases. The results for JEFF-3.3 confirm the above result that the JEFF-3.3 calculations show an increasing trend with temperature: it can be seen in Table 8 and Figure 85 that for three of the four configurations of the kritz4 benchmark, the JEFF-3.3 calculated trend is significantly greater than zero. This trend is also present in the JEFF-4t1 results, but less so in the ENDF/B-VIII.0 results. For the kritz1 – kritz3 benchmarks it is difficult to draw conclusions because there are only two temperature data points in each of these benchmarks, and for kritz2 and kritz3 moreover the boron concentration is different for the low and high temperature case.

Table 8. Results for the fitted trend of C-E reactivity values for kritz-lwr-resr-001, 002, 003, and 004.

Results for the trend in $\Delta\rho = \rho_c - \rho_m$	JEFF-4t1 (pcm/°C)	JEFF-3.3 (pcm/°C)	ENDF/B-VIII.0 (pcm/°C)
Kritz-1, PuO_2-UO_2, 25x24, 5 μgB/g	0.57	−1.29	0.42
Kritz-2, UO_2 (1.86%), 44x44, 218 & 26 μgB/g	−0.19	−0.22	−0.51
Kritz-3, UO_2 (1.86%), 44x40, 452 & 280 μgB/g	−0.04	−0.06	−0.75
Kritz-4, UO_2 (1.35%), 39x39, 0.8 μgB/g	0.59 ± 0.07	0.42 ± 0.08	0.07 ± 0.08
Kritz-4, UO_2 (1.35%), 46x46, 46.3 μgB/g	0.02 ± 0.13	0.00 ± 0.19	−0.54 ± 0.24
Kritz-4, UO_2 (1.35%), 46x46, 175. μgB/g	0.73 ± 0.14	0.74 ± 0.13	0.29 ± 0.15
Kritz-4, UO_2 (1.35%), 39x39, 0.2 μgB/g	0.95 ± 0.12	0.99 ± 0.10	0.35 ± 0.10

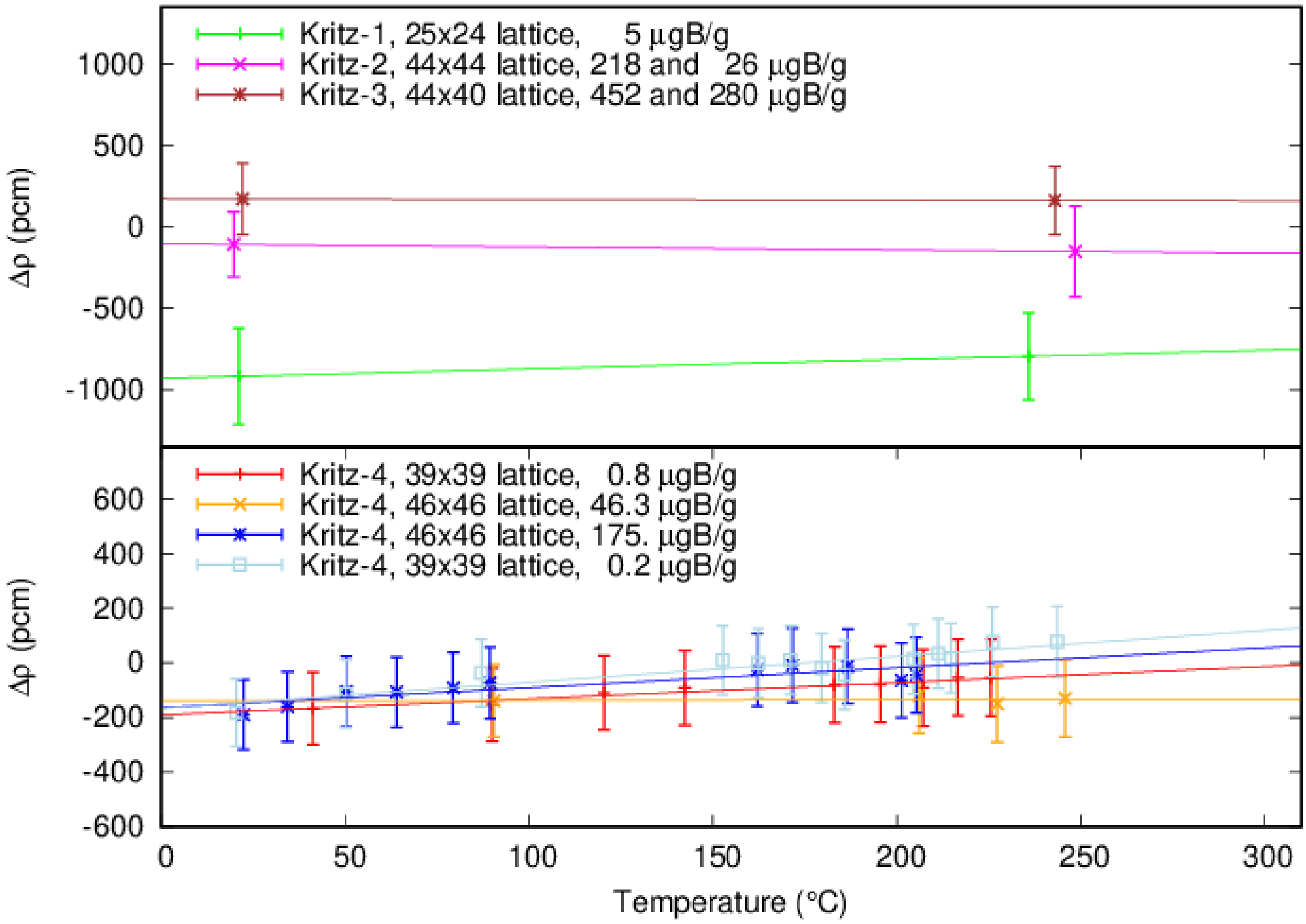

Figure 85. JEFF-3.3 results for kritz-lwr-resr-001, 002, 003, and 004.

7.2. Analysis of results for CREOLE benchmark (NRG)

Results were also generated for the creole-pwr-exp-001 benchmark, see Table 9**Erreur ! Source du renvoi introuvable.**, based on MCNP-6.2 detailed models of the benchmark. The Table shows the trends of C-E with temperature, resulting from a linear fit to the data. In all cases the trend is small, less than or equal to 0.24 pcm/°C in absolute value in all cases. For JEFF-4t1 the results are also shown in Figure 86.

Table 9. Results for the fitted trend of C-E reactivity values for creole-pwr-exp-001.

Results for the trend in $\Delta\rho = \rho_c - \rho_m$	JEFF-4t1 (pcm/°C)	JEFF-3.3 (pcm/°C)	ENDF/B-VIII.0 (pcm/°C)
Core 1: UO_2 (3.1%) with clean water	0.04 ± 0.02	0.07 ± 0.02	0.13 ± 0.02
Core 2: same but with borated water	-0.07 ± 0.03	0.24 ± 0.02	0.15 ± 0.02
Core 3: UO_2-PuO_2	-0.18 ± 0.02	0.08 ± 0.03	0.13 ± 0.02
Core 4: same with empty lattice positions	-0.22 ± 0.02	0.00 ± 0.03	0.11 ± 0.03

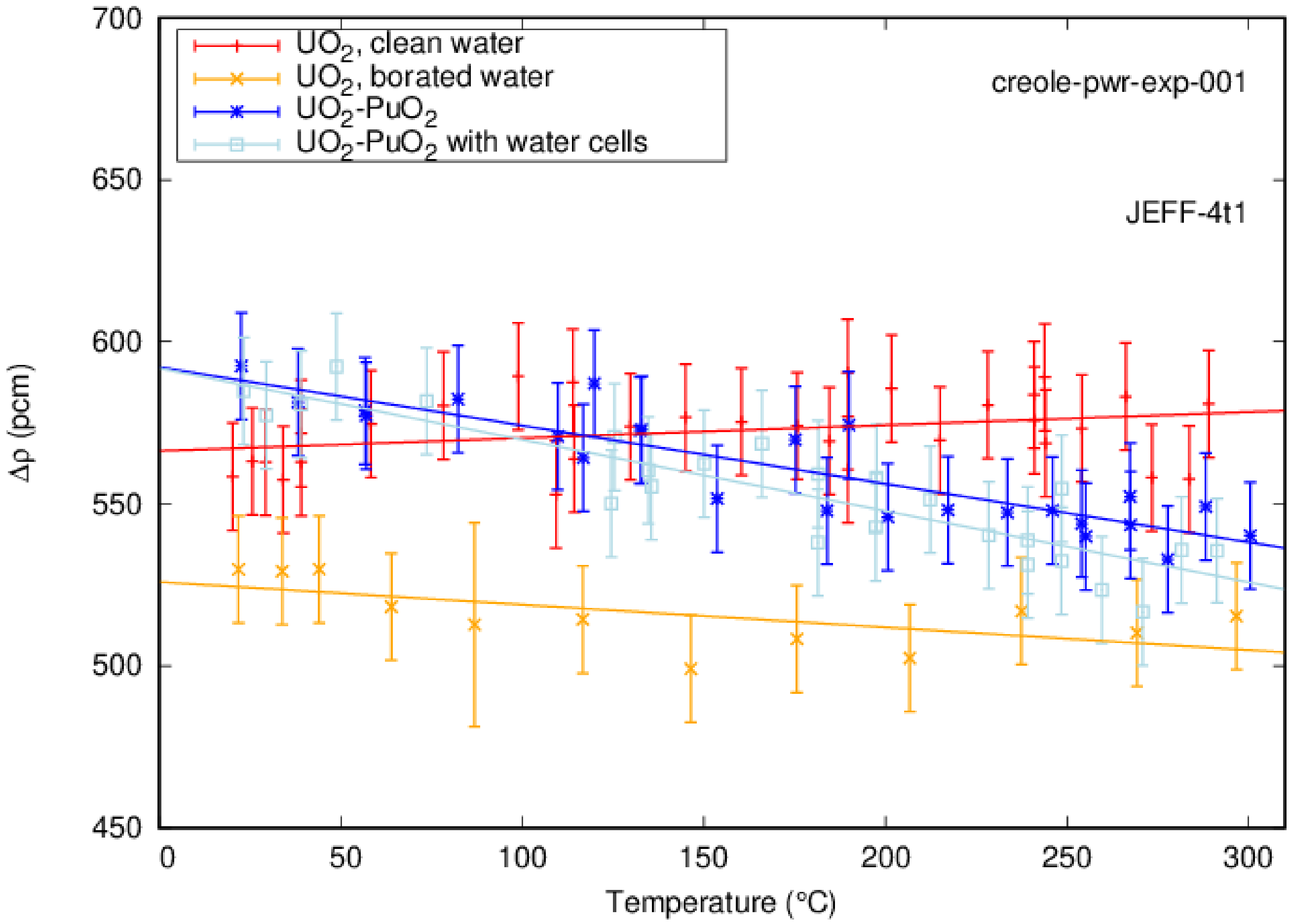

Figure 86. JEFF-4t1 results for creole-pwr-exp-001.

8. Conclusion

A selection of benchmark experiments was done by IRSN and NRG with the aim to test recent nuclear data evaluations. IRSN selected 182 benchmarks cases that are assumed to be representative of its validation database. NRG selected 576 benchmark cases. 120 benchmark cases are common to both selections. No significant k_{eff} discrepancies were put forward between MORET 5 (IRSN) and MCNP (NRG) for the same nuclear data evaluations, validating the description of benchmarks and the models used by the codes for the transport of neutrons.

The comparison of benchmark k_{eff} and calculated ones with the MORET 5 code using recent evaluations of nuclear data shows that:

- K_{eff} results with recent evaluations are generally in good agreement with the benchmark taking into account experimental uncertainty margins,
- New evaluations of ^{16}O, ^{235}U and ^{238}U, TSL of water can explain discrepancies between the JEFF-3.3 and ENDF/B-VIII.0 evaluations of nuclear data in thermal energy range,
- New evaluation of nickel in JEFF-4T1 leads to strong overestimation of k_{eff} that are not realistic,
- The evaluations of ^{56}Fe in the epithermal energy range with JEFF3.3 and JEFF-4T1 lead to k_{eff} values that are further from the benchmark k_{eff} compared with the ENDF/B-VIII.0 evaluation of ^{56}Fe,
- The JEFF-3.3 evaluation of ^{63}Cu, ^{65}Cu and ^{235}U, ^{238}U tend to improve k_{eff} results for the ZEUS experiments compared with ENDF/B-VIII.0,
- A tendency to overestimate k_{eff} values with temperature has been observed on the KRITZ benchmark for the JEFF-3.3 evaluation of nuclear data.

The comparison of MCNP-6.2 calculated results with benchmark values yields the following conclusions:

- For fast spectrum benchmarks with (almost) only uranium, the performance of JEFF-4t2 is similar to that of JEFF-3.3, JEFF-4t1 and ENDF/B-VIII.0, while the results of JEF-2.2 are systematically lower (except for ieu-met-fast-007, 'Big Ten') and further from the benchmark values. For a number of HEU benchmarks there appears to be a subtle trend of C/E values with the energy of the average lethargy causing fission (EALF). It is unclear whether this trend, which is shared by all libraries, is due to the benchmarks or due to nuclear data.
- The results for thermal spectrum benchmarks with (almost) only uranium and water are in good agreement with the benchmark values taking into account the uncertainty margins. In cases where there is a slight trend of the C/E values as a function of the pitch of the lattice (or another parameter that influences the neutron spectrum), the trend for JEFF-4t2 is smaller than for JEFF-3.3 (e.g. Figure 17, Figure 32) or similar to JEFF-3.3 (e.g. Figure 25, Figure 35).
- Fast spectrum benchmarks with specific reflector materials show that the JEFF-4t1 data for several such materials were not good. This was the case for Al, V, Ti, and Ni. For Al, Ti, and Ni this has been remedied in JEFF-4t2. For V the trend of C/E values with increasing reflector thickness is roughly equal for all libraries (Figure 53). For other materials, e.g. beryllium, graphite, depleted uranium, etc., the results are in good agreement with the benchmark values taking into account the uncertainty margins.
- The results for thermal spectrum benchmarks with specific reflector materials are generally in good agreement with the benchmark values taking into account the uncertainty margins. For one benchmark a slight trend of C/E with increasing steel or nickel reflector thickness can be quantified, see Figure 63. For lead reflectors, there are two benchmarks that show an influence of the distance between the reflector and the fuel array on C/E results (Figure 65, Figure 67).
- For several benchmarks with strong neutron absorbers in solution the results exhibit a trend with the concentration of the absorber element. This is shown for gadolinium (e.g. Figure 68, Figure 70), boron (e.g. Figure 73, Figure 75) and cadmium (Figure 79). These trends are present in the results for all libraries.
- The JEFF-4t2 data for fluorine lead to a strong improvement in the results for heu-met-fast-007 (cases 32–34, Figure 52) and leu-comp-therm-033 (Figure 81).
- The results for fast spectrum plutonium benchmarks are in good agreement with the benchmark values taking into account the uncertainty margins. Insofar as there are cases for which this is not the case, the deviation can be attributed to the nuclear data of the reflector material (aluminium and nickel in JEFF-4t1).

MCNP-6.2 results for Kritz-4 confirm the MORET 5 results mentioned above, i.e. there is a positive trend of C-E for JEFF-3.3 with increasing temperature, up to almost 1 pcm/°C. This trend is similar in JEFF-4t1 results, but smaller in ENDF/B-VIII.0 results. Results for Creole show significantly smaller trends, the absolute values of which are smaller than 0.25 pcm/°C for all libraries for all four core configurations of Creole.

9. References

[Haeck 2015] W. Haeck *et al.*, *GAIA User's Manual - Version 1.0.0*, IRSN Report PSN-EXP/SNC/2015-165, Institut de Radioprotection et de Sûreté Nucléaire, France (2015).

[Entringer 2022] A. Entringer, A. Bardelay, S. Lahaye, J.C. Trama, O. Petit, C. Carmouze, A. Peron, CRISTALV2: Improvements Overview of the CRISTALV2.0.3 Criticality Calculation Package, Proceedings Nuclear Criticality Safety Division Topical Meeting (NCSD 2022) Anaheim, CA, June 12-16, 2022,356-365.

[Monange 2022] W. Monange, A. Bardelay, New capabilities of the MORET 6 Monte Carlo neutron transport code, International conference on physics of reactors PHYSOR 2022, Pittburgh, USA

[Jinaphanh 2016] A. Jinaphanh *et al.*, *Continuous-Energy Sensitivity Coefficients in the MORET Code*. Nuclear Science and Engineering 184 (2016) 53-68.

[Jinaphanh 2017] A. Jinaphanh, *Implementation of the CLUTCH method in the MORET code*. In M&C 2017, Jeju (Korea) 16-20 April 2017.

[Haeck 2015] W. Haeck *et al.*, *GAIA User's Manual - Version 1.0.0*, IRSN Report PSN-EXP/SNC/2015-165, Institut de Radioprotection et de Sûreté Nucléaire, France (2015).

[Goorley 2012] T. Goorley (Ed.), *Special issue on the initial release of MCNP-6*, Nuclear Technology **180** (2012) 297—455

[Werner 2018] Werner et al., *MCNP Version 6.2 - Release notes*, LANL Report LA-UR-18-20808, 2018

[MacFarlane 2010] R.E. MacFarlane and A.C. Kahler, *Methods for processing ENDF/B-VII with NJOY*, Nuclear Data Sheets **111** (2010) 2739–2890

[Muir 2018] D.W. Muir, R.M. Boicourt, A.C. Kahler (Ed.), J.L. Conlin, W. Haeck, *The NJOY nuclear data processing system, Version 2016*, LANL Report LA-UR-17-20093 (2018)

[Kiedrowski 2009] B.C. Kiedrowksi, *Adjoint weighting for continuous-energy Monte Carlo radiation transport*, PhD Thesis, University of Wisconsin-Madison (2009)

[Kiedrowski 2012] B.C. Kiedrowski, F.B. Brown, *Continuous-energy sensitivity coefficient capability in MCNP6*, Trans. ANS Winter Meeting, 11–15 November 2012, 601–604

Annex 1.